

Copyright
by
Samira Gian Moorjani
2010

**The Dissertation Committee for Samira Gian Moorjani Certifies that this is the
approved version of the following dissertation:**

Directing Cell Migration by Dynamic Control of Laminar Streams

Committee:

Jason B. Shear, Supervisor

Richard Morrisett

John X.J. Zhang

Richard W. Aldrich

Muhammad Zaman

Directing Cell Migration by Dynamic Control of Laminar Streams

by

Samira Gian Moorjani, B.E., M.S.

Dissertation

Presented to the Faculty of the Graduate School of

The University of Texas at Austin

in Partial Fulfillment

of the Requirements

for the Degree of

Doctor of Philosophy

The University of Texas at Austin

December, 2010

Dedication

To Jatin Sonavane

From whom I have learned so much and continue to everyday

Acknowledgements

My debts are great and widely spread. First and foremost, I would like to thank my advisor, Jason Shear, for his help and support. His critiques of my work have helped me hone my research and writing skills. He has also been patient and forgiving when I was headstrong, for which I am grateful.

I would like to thank my committee members, Dr. Richard Aldrich, Dr. John Zhang, Dr. Richard Morrisett, and Dr. Muhammad Zaman, for their time and consideration. My interactions with them have always been very enjoyable. Special thanks go to Dr. Richard Morrisett for his advice and enthusiasm. And, to Dr. Wolfgang Frey and Dr. Krishnendu Roy for their guidance and support.

I would like to thank my labmates, past and present. In particular, Dr. Rex Nielson, who taught me the many *ins* and *outs* of cell dosing. I would also like to thank Dr. Stephanie Seidlits and Dr. Eric Ritschdorff for generously sharing their vast amount of knowledge with me. Maryam Ali, Michelle Fox, Jodi Connell, and Stephanie Seidlits proof-read parts for this dissertation, often at short notices, and I am very appreciative of that. I owe many thanks to the two undergraduate students, Jonathan Rice and Xinming Chang, who worked with me on this project.

I would like to thank Tim Hooper for assisting me with the integration and computer control of valves, pinch clamps, and pressure sensors used in the flow devices

described in this dissertation. Without him, some of the work discussed here may have been too ambitious to attempt.

Many thanks to Sepideh Khoshnevis for her friendship and our lunches together. I will miss her.

I owe many thanks to my parents, Gian and Neena Moorjani, who taught me the importance of education and encouraged me at every step of the way. Even though my father is not with me today, I know that he would have been very proud. I am very grateful to my sister, Priya Moorjani, and my uncle and aunt, Dr. Kishin Moorjani and Dr. Angela Moorjani. I could not have done all this work without the boundless love, encouragement, and support of my family.

Finally, I am very grateful to my husband, Jatin Sonavane, for years of friendship and love. And, for the many research discussions we had over coffee and cake. He has proof-read my work on multiple occasions and assisted with numerous graphics. This dissertation wouldn't have been possible without his utmost emotional and intellectual support.

Financial support for this work was provided by the National Institutes of Health and the Robert A. Welch Foundation.

Directing Cell Migration by Dynamic Control of Laminar Streams

Publication No. _____

Samira Gian Moorjani, Ph.D.

The University of Texas at Austin, 2010

Supervisor: Jason B. Shear

Interactions of cells with their chemical microenvironments are critical to many polarized processes, including differentiation, migration, and pathfinding. To investigate such cellular events, tools are required that can rapidly reshape the microscopic chemical landscapes presented to cultured cells. Existing chemical dosing technologies rely on use of pre-fabricated chemical gradients, thus offering “static” cell-reagent interactions. Such interactions are particularly limiting for studying migration and chemotaxis, during which cells undergo rapid changes in position, morphology, and intracellular signaling. This dissertation describes the use of laminar streams, containing cellular effector molecules, for precise delivery of effectors to selected subcellular regions. In this approach, cells are grown on an ultra-thin polymer membrane that serves as a barrier to an underlying reagent reservoir. By using a tightly-focused pulsed laser beam, micron-diameter pores can be ablated in the membrane upstream of desired subcellular dosing sites. Emerging through these pores are well-defined reagent streams, which dose the targeted regions. Multiple pores can be ablated to allow parallel delivery of effector molecules to an arbitrary number of targets. Importantly, both the directionality and the composition of the reagent streams can be changed on-the-fly under a second to present dynamically

changing chemical signals to cells undergoing migration. These methods are applied to study the chemotactic responses of neutrophil precursor cells. The subcellular localization of the chemical signals emerging through pores is found to influence the morphological evolution of these motile cells as they polarize and migrate in response to rapidly altered effector gradients.

Table of Contents

List of Tables	xii
List of Figures	xiii
Chapter 1: Micro-Engineered Tools for Investigation of Cellular Behavior	1
1.1 Introduction.....	1
1.2 Common Methods for Localized Chemical Dosing in Culture	3
1.3 Laminar-Flow Approaches for Localized Chemical Dosing	5
1.4 Laser-Induced Microfabrication	13
1.4.1 Multiphoton excitation-assisted additive microfabrication	13
1.4.2 Subtractive microfabrication for ablation of pores in polymer membranes	15
1.5 Neutrophil Signaling and Chemotaxis	22
1.6 Preview of Content	26
1.7 References.....	28
Chapter 2: Steering Laminar Streams for Precise Chemical Targeting of Cells	37
2.1 Introduction.....	37
2.2 Experimental Methods.....	40
2.2.1 Device design and fabrication.....	40
2.2.1.1 Alternate device configuration.....	47
2.2.2 Chemicals and reagents.....	48
2.2.3 Cell culture.....	48
2.2.3.1 Cell loading	49
2.2.4 Membrane ablation	50
2.2.5 Microscopy	53
2.3 Results and Discussion	54
2.3.1 Controlling orientation of dosing streams.....	54
2.3.2 Speed of switching stream orientation.....	62
2.3.3 Application to neutrophil cultures	67

2.4 Conclusion	72
2.5 References	75
Chapter 3: Directing Cell Migration by Dynamic Repositioning of Chemotactic Laminar Streams	80
3.1 Introduction	80
3.2 Experimental Methods	83
3.3 Results and Discussion	84
3.4 Conclusion	95
3.5 References	97
Chapter 4: Changing Reagent Stream Directionality in a Continuous Manner	102
4.1 Introduction	102
4.2 Experimental Methods	106
4.2.1 Design and fabrication of the cell-dosing chamber	106
4.2.2 Chemicals and reagents	110
4.3 Results and Discussion	111
4.4 Conclusion	121
4.5 References	123
Chapter 5: Multiple Dosing Agents within Laminar Flow Devices	127
5.1 Introduction	127
5.2 Experimental Methods	129
5.2.1 Device design and fabrication	129
5.2.2 Chemicals and reagents	136
5.2.3 Cell culture	136
5.2.4 Membrane ablation	136
5.3 Results and Discussion	139
5.3.1 Rapid switching between two chemical species	139
5.3.2 Simultaneous dosing of cells with two different chemical species	143
5.4 Conclusion	149
5.5 References	152

Appendix: List of Abbreviations	155
Bibliography	157
Vita	175

List of Tables

Table 3.1:	Cellular responses to fMLP gradient switches.....	90
Table 3.2:	Sites of new pseudopods developed during fMLP gradient switches.....	91

List of Figures

Figure 1.1: Cell-environment interactions during migration and chemotaxis	2
Figure 1.2: Localized chemical dosing using multiple parallel laminar streams.....	7
Figure 1.3: Laminar-flow chemical dosing strategy reported by Nielson and Shear..	10
Figure 1.4: Subcellular dosing using laminar flow streams..	12
Figure 1.5: Excitation of chromophores by absorption of photons	14
Figure 1.6: Schematic of the Nd:YAG (neodymium yttrium aluminum garnet) laser setup used for creation of micron-sized pores in polymer membranes	17
Figure 1.7: SEM of a pore created in 2.5 μm thick Mylar membrane by Nielson and Shear using a Ti:S (titanium-sapphire) laser	21
Figure 1.8: Differentiated HL-60 cells on fibronectin-coated Mylar membrane.....	25
Figure 2.1: Strategy for controlling stream orientation	42
Figure 2.2: Valve schematic for changing flow direction inside a cross cell-dosing chamber	47
Figure 2.3: Controlling stream directionality in the cell-dosing chamber.....	58
Figure 2.4: Deviation in stream directionality as a function of pore location.....	60
Figure 2.5: Reproducibility of stream directionality	61
Figure 2.6: Rapid switching of stream directionality	64
Figure 2.7: Millisecond dosing of HL-60 cells..	66
Figure 2.8: Reducing background fluorescence during MitoTracker labeling experiments	68
Figure 2.9: Selective labeling of HL-60 cells.....	70
Figure 2.10: Laminar flow dosing of HL-60 cells.....	71

Figure 2.11: Targeting leading and trailing edges of motile cells	72
Figure 3.1: Controlling polarization and motility of HL-60 cells using streams of a chemotactic peptide..	85
Figure 3.2: HL-60 cell reorientation by formation of pseudopod at a new site..	87
Figure 3.3: HL-60 cell reorientation via polarity reversal.....	88
Figure 3.4: HL-60 cell reorientation via gradual turning..	89
Figure 3.5: Steering an HL-60 cell through a 90° arc..	94
Figure 4.1: Steering chemotactic laminar flow streams in an asterisk-shaped microfluidic chamber directs chemotaxis of motile cells.	104
Figure 4.2: Reagent stream orientations obtained by opening two adjacent valves simultaneously..	105
Figure 4.3: Strategy for controlling stream orientation in a continuous manner.....	108
Figure 4.4: Motorized pinch clamp..	109
Figure 4.5: Controlling stream directionality in the cross cell-dosing chamber using solenoid pinch valves	112
Figure 4.6: Changing stream directionality in a continuous manner.....	115
Figure 4.7: Structure of a proportional-integral-derivative (PID) Controller....	118
Figure 4.8: Changing orientation of a 3% BSA stream by incremental closing using PID..	120
Figure 5.1: Multi-stream reagent flow cells..	131
Figure 5.2: Valve schematic for cell-dosing and reagent flow chambers..	134
Figure 5.3: Valve schematic for rapid switching between chemical species.. ..	135
Figure 5.4: Switching orientation and composition of laminar streams.....	140
Figure 5.5: Subsecond switching of composition of reagent streams..	142
Figure 5.6: Parallel dosing of subcellular sites of an HL-60 cell	144

Figure 5.7: Dosing distinct subcellular microdomains with different chemical species..	147
Figure 5.8: Moving interfaces between laminar flow streams..	148

Chapter 1: Micro-Engineered Tools for Investigation of Cellular Behavior

1.1 INTRODUCTION

Cells receive cues from the environment that trigger intracellular signaling cascades responsible for regulating various processes, including cell differentiation, growth, activity, and cell death (**Figure 1.1**). Although these cues can be of different types (*e.g.*, electrical, chemical, mechanical, topographical) [1-10], chemical cues in particular are ubiquitous and perhaps the most important inputs in the microenvironment of cells with implications in an array of cellular processes [11-18]. Chemical dosing of cells in culture is, therefore, an indispensable tool in the study of cell function and differentiation.

Traditional chemical dosing methods involve exposing entire culture dishes of cells to desired reagents. Although these methods are commonly employed by the biological community, there is a growing need to exert greater spatio-temporal control over interactions between cells and chemical agents. This is particularly relevant in the study of polarized cellular events, such as differentiation [12], chemotaxis [13, 19, 20], and axonal pathfinding [14, 15], in which spatial heterogeneity in cell signaling is observed at the subcellular level in response to chemical gradients, underscoring the need for creating controlled gradients in culture. To address this need, the Shear laboratory and others have developed tools for introducing chemical agents into culture with subcellular resolution [13, 14, 21-29]. Two approaches for subcellular localization of chemical

dosing have been adopted as routine tools by the biological community. These include puffer pipet spritzing and photolytic cleavage of caged cellular effectors.

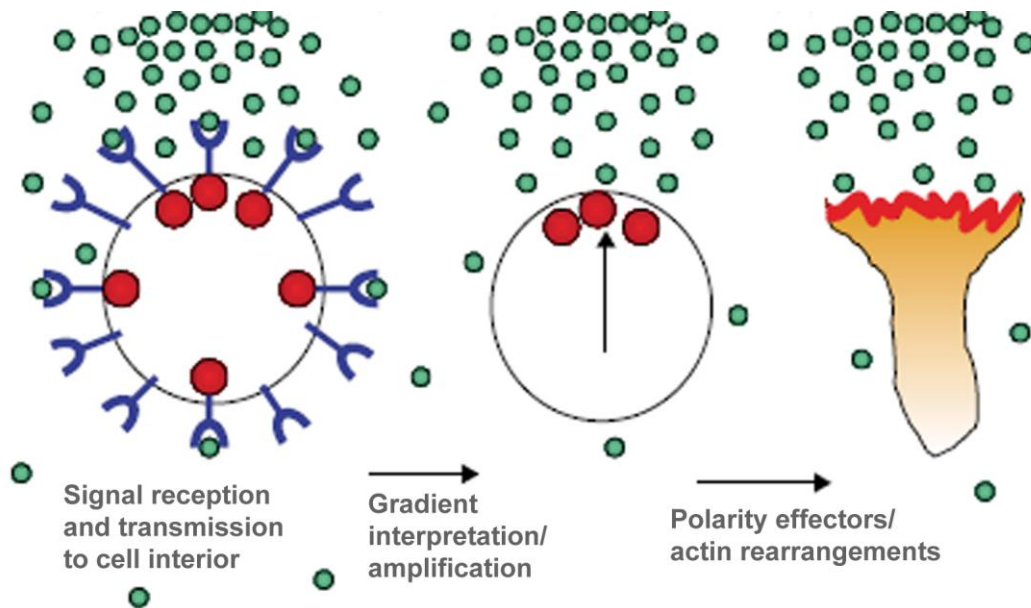


Figure 1.1: Cell-environment interactions during migration and chemotaxis. To respond appropriately to chemical signals, cells contain membrane-bound receptors (blue) that bind with the chemical input (green spheres) and transmit this information to the interior of the cell (red spheres). This triggers a variety of intracellular pathways that lead to signal interpretation and amplification, and in turn drive downstream processes, such as actin reorganization and polarity development, ultimately regulating cell migration. Adapted from [18].

1.2 COMMON METHODS FOR LOCALIZED CHEMICAL DOSING IN CULTURE

Application of chemical dosants via a pulled glass pipette is commonly used for “micro-puffing” of small solution volumes, ranging from nanoliters to picoliters, at desired subcellular coordinates using high resolution micropositioners. This approach has been commonly employed in neuroscience for applications ranging from growth cone redirection [14] to localized cellular stimulation with neurotransmitters [30, 31]. Bourne and coworkers have also used this method for studying neutrophil polarization and chemotaxis [13, 19]. Some of the important advantages of this technique include the use of very small reagent volumes for dosing cells and few restrictions on the type of reagent that can be delivered, which could range from inorganic ions (Na^+ , K^+ , Ca^{2+}) to small molecules, such as cyclic adenosine monophosphate (cAMP), to large biological compounds, such as hyaluronic acid.

Despite these advantages, puffer pipet expulsion suffers from important limitations. Parallel dosing of more than a few cellular sites is usually not feasible as it requires tandem positioning of bulky micromanipulators. Also, accessing new sites of interest requires repositioning the pipet, which cannot be achieved rapidly, leading to low temporal resolution. Lastly, the dosant gradients created using this method are typically shallow and hard to maintain for extended periods.

A second approach relies on the use of light for photolytic cleavage of caged cellular effectors [21-23]. Here, absorption of a photon initiates a photochemical process which leads to the release of the effector molecule (from a photocleavable group). Release of the effector can be rapid, generally occurring within microseconds to

milliseconds after photon absorption. Also, two-photon excitation using pulsed lasers can be used to confine the reaction bolus to dosant volumes as small as 1 fL [32]. In addition, because uncaging is initiated in a (caged) reagent that bathes the entire culture, the use of fast laser scanning systems allow release to be coordinated in multiple positions, either in parallel (using multiple lasers) or in rapid succession, thus eliminating some of the temporal resolution issues associated with puffer pipets.

The applicability of photolytic cleavage is limited mainly by the availability of caged precursor molecules. For every new dosant to be examined, a caged precursor has to be synthesized, which is often challenging and time-consuming. Moreover, synthesis of precursors becomes particularly challenging in case of large molecules, such as proteins, which may have multiple active sites requiring determination of the location of these sites and synthesis of multiple cages for masking activity. Protein folding and unfolding are other factors to consider while designing cages. Also, the attachment of photocleavable groups to the signaling molecule can often lead to reduced biological activity after uncaging. These limitations have resulted in development of only a few caged proteins (*e.g.*, G-actin, myosin, thrombin) [33, 34], thus restricting the reagents that cells can be dosed with using this method. Finally, unintended dosing of cells due to thermal (*i.e.*, non-photochemical) release of effectors is another limitation of using this approach [35], and as with puffer pipets, it typically is not feasible to generate sharp gradients that can be maintained for extended periods in culture.

To combat some of the limitations of puffer pipets and photolytic cleavage, recent advances have exploited laminar flow streams inside microfluidic environments for subcellular chemical dosing [24-28], a topic examined in the following section.

1.3 LAMINAR-FLOW APPROACHES FOR LOCALIZED CHEMICAL DOSING

Microfluidics deals with the behavior and precise manipulation of very small volumes of fluids, typically ranging from nanoliters to femtoliters. One of the important properties of fluids in the “micro” domain are their low Reynolds numbers (usually less than 5), leading to a laminar regime in which two parallel fluid streams can flow next to each other without significant mixing. Multiple laminar flow systems have been used extensively in capillary electrophoresis for separation of ionic species [36-38] and in sensors [39]. The use of microfluidics became particularly popular following advances in micro-electromechanical systems (MEMS) that came about in the early 1980s, which in turn were fueled by strides in the semiconductor industry [40-43]. Whitesides and coworkers in 1999 published a paper in *Science* extending the application of laminar streams for fabrication of microstructures inside capillaries [44], a technique that was subsequently adopted for patterning cells and their microenvironments [45, 46]. In another report that followed soon after, the Whitesides laboratory used multiple parallel laminar streams to create stable concentration gradients [47]. Combined with the use of small solution volumes in microfabricated systems, which is particularly attractive for dosing cells with culture-grade reagents that are often very expensive, this has become a successful platform for localized chemical dosing in culture.

The Whitesides’ method uses multiple inlet channels to deliver solutions to a main channel (**Figure 1.2**). The microfluidic device is fabricated using standard PDMS (polydimethylsiloxane) molding processes. In this approach, an elastomeric stamp is made by casting a prepolymer of PDMS against a master that is fabricated using microlithographic techniques. Heating the prepolymer allows curing and production of

the elastomeric stamp with a negative relief pattern compared to the master. The patterned stamp is then sealed irreversibly to glass to complete the flow chamber.

Due to the laminar flow conditions inside the main channel, sharp boundaries are formed at the interface between the flowing solutions with mixing limited to the small amount of diffusional transport. These interfaces can be targeted to selected subcellular regions by adjusting the relative amounts of fluid flowing through each inlet, thus allowing delivery of membrane-permeable effector molecules to selected microdomains (**Figure 1.2**) [24, 25]. Moreover, stable concentration gradients ranging from linear to more complex profiles, such as periodic, exponential and parabolic, have been generated using this technique by flowing multiple fluid streams, each carrying a different concentration of a chemical species, adjacent to each other [48, 49], and the generated gradients have been used for studying the migration of neutrophils and cancer cells in response to chemoattractant molecules [26, 27, 50, 51].

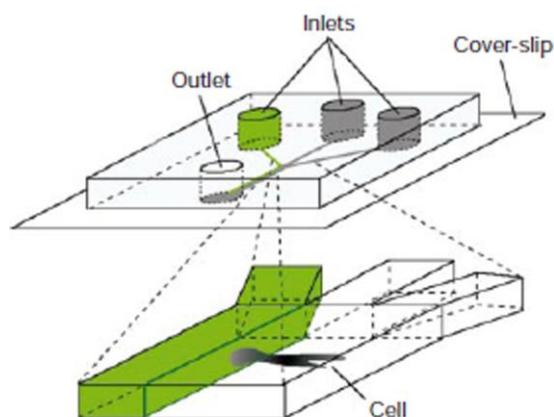


Figure 1.2: Localized chemical dosing using multiple parallel laminar streams. Experimental set-up showing a close-up of the point at which the inlet channels combine into one main channel inside a microfluidic device. Due to the laminar flow conditions inside the main channel, the three streams flow next to each other without any significant mixing. The interfaces generated at the boundaries of the streams can be targeted to specific subcellular regions. Adapted from [24].

Despite its high resolution, the Whitesides' dosing approach is significantly constrained by the pre-determined design of the microfluidic device. This makes dosing more than a few independent cellular sites and dynamic targeting of individual subcellular features challenging because the method relies on the compatibility between the positions of cells and dosant streams. The flexibility to dynamically change dosing sites is vital in experiments with motile cells, especially over extended periods and with multiple reagents. Even though chemical gradients may be stable over the experimental duration when using pre-fabricated devices, multiple chemical dosings combined with parallel targeting of specific “non-stationary” cells throughout the experiment will require rapid manipulation of flow streams, a capability that is difficult with a pre-determined

setup. The transient times reported for building and switching concentration profiles with this method are on the order of minutes [47-49], which is much slower than the timescale at which many intracellular signaling events transpire. Furthermore, although complex microfluidic devices can be fabricated using PDMS molding processes, changes in device design requires fabrication of new masters, which is often a time-consuming and expensive process.

More recently, attempts have been made to generate dynamically changing gradient signals in microfluidic chambers. Poznansky and coworkers were able to toggle between gradient profiles in ~5 s by incorporating microstructured membranes in their system to serve as valves for switching between two microfluidic gradient generators [52]. Beta and coworkers used a combination of two dosing methods, photolytic cleavage and microfluidics, to generate a variety of concentration profiles within a second [53]. Despite this high temporal resolution, this method can be used only with reagents for which caged precursors are available, as discussed in the previous section.

Furthermore, since the flow direction using this approach is pre-defined (*i.e.*, oriented along the channel's longitudinal axis), access to certain cellular targets whose positions and orientations are parallel with the pre-set geometry of dosing streams may not be possible. For example, a neurite growing longitudinally in a channel would have to be dosed along its entire length or not at all. An ability to change the flow direction would also be advantageous for probing dynamic cellular events such as chemotaxis and axonal pathfinding.

Lastly, the closed fluidic nature of this system does not allow for insertion of additional experimental apparatus, such as patch electrodes, thus limiting the range of cellular assays that can be performed on cultures under study.

In a previous publication, the Shear laboratory reported a cell dosing strategy for overcoming some of the limitations of existing methods [28]. In this approach, cells were cultured on an ultra-thin polymer membrane that separated two stacked laminar flow chambers: one containing the cell culture and the other containing the reagent. By focusing a pulsed laser beam onto one or more selected polymer-membrane positions, micron-diameter pores could be ablated upstream of desired cellular targets. Drain pressures in the two chambers were pre-adjusted to direct stable reagent streams into the culture chamber through the ablated pores for dosing targeted regions (**Figure 1.3**). Pores could be ablated in direct proximity to a cellular feature, thus making the dosing of dendrites, growth cones, or cell bodies possible without dosing unwanted upstream features. The dosing of downstream sites could be minimized by tuning laminar flow velocities (to change the width of the reagent streams for reducing unintentional dosing) and through appropriate selection of ablation sites. Importantly, reagent streams could be shut off by photofabricating a protein plug over selected pores. Plugged pores could also be opened for re-initiating dosing at the same site. In contrast to other cell dosing techniques, this approach is amenable to creation of an arbitrary number of reagent flow streams for dosing multiple cellular regions in parallel as well as termination of reagent flow through selected pores when needed, permitting distinct cellular regions to be targeted with a chemical species for differing times.

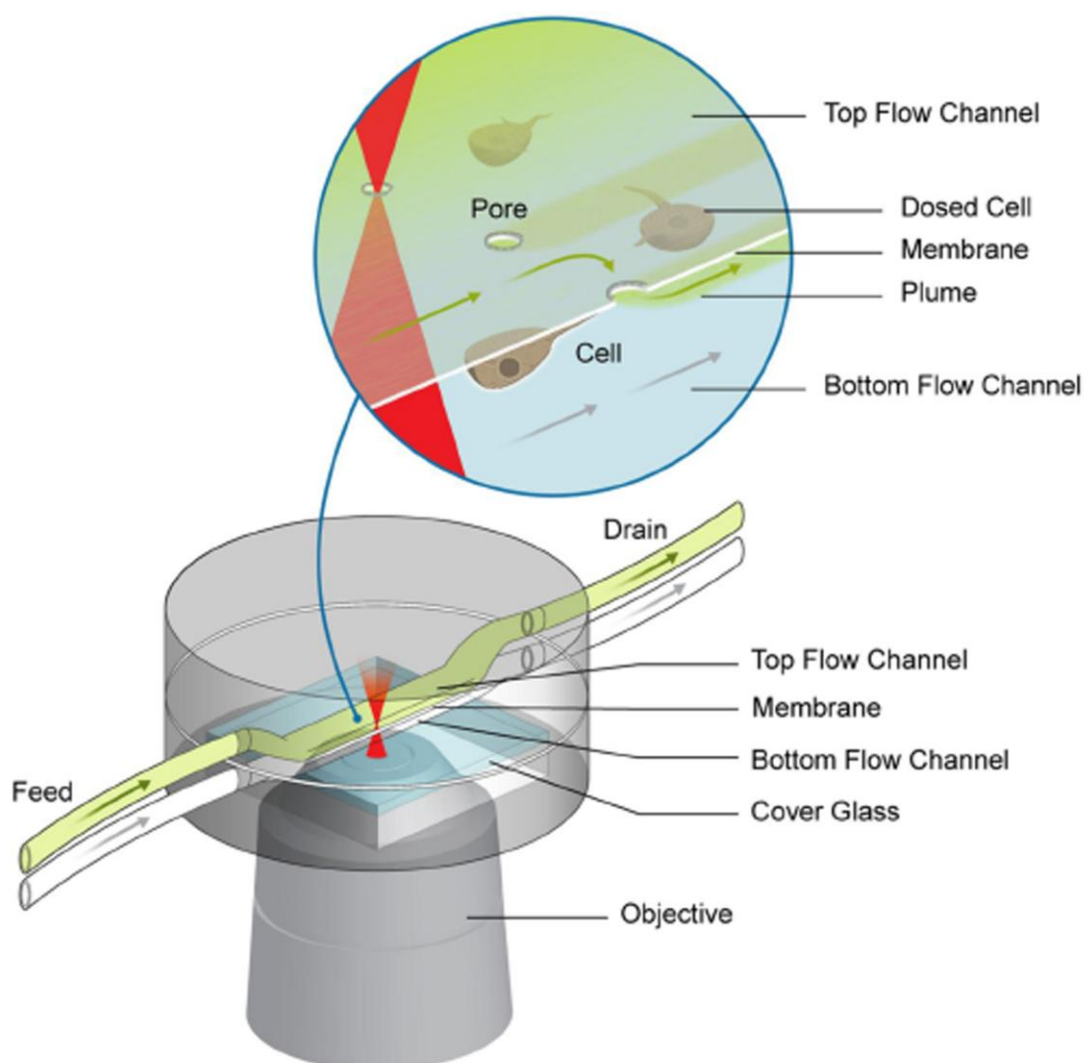


Figure 1.3: Laminar-flow chemical dosing strategy reported by Nielson and Shear. This method uses photo-induced membrane ablation for creating micron-sized pores in an ultra-thin polymer membrane with cells attached to it. Production of a pore provides an entry route for a reagent on the opposing side of the membrane, which emerges as a well-defined laminar stream (green plume) inside the culture chamber dosing selected cellular regions. In this stacked-chamber configuration, cells were attached on the underside of the membrane and the reagent was flowed in the upper chamber. Adapted from [28].

Figure 1.4a demonstrates the utility of this device for labeling specific subcellular regions in fibroblasts using a lipophilic fluorescence dye, 3,3'-dihexyloxacarbocyanine iodide (DIOC₆). Although this dye is weakly fluorescent in water, its fluorescence is significantly enhanced when incorporated into organelles such as the mitochondria, nuclear membrane, and endoplasmic reticulum [54]. Because visualization of the dye relies on the continued functioning of cellular metabolic components and on a reasonably leak-free plasma membrane, use of this dye also serves the additional role of probing the viability of the labeled cells downstream of the ablated pores [55, 56].

The width of the reagent streams emerging from the ablated pores is a function of the volumetric flow rate in the cell-dosing chamber, which can be varied to manipulate the reagent gradient—created at the borders of the reagent streams and bulk medium—to influence cell activity.

Lastly, **Figure 1.4b** illustrates chemotactic guidance of motile human promyelocytic leukemia (HL-60) cells, a neutrophil precursor cell line, using low concentrations of a chemotactic peptide, *N*-formyl-methionyl-leucyl-phenylalanine (fMLP).

This chemical dosing approach makes dual use of lasers; firstly, for creation of micron-sized pores at selected membrane locations, and secondly, for fabrication of protein plugs to terminate flow through the ablated pores. The next section provides a brief overview of the mechanisms involved in these laser-induced processes.

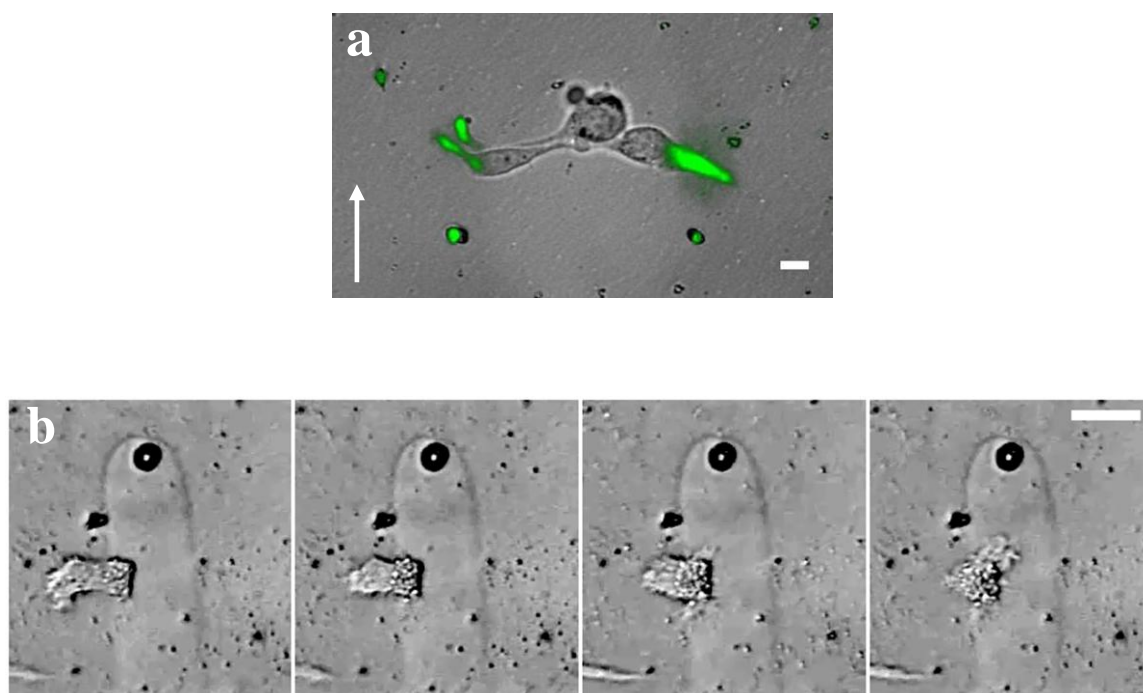


Figure 1.4: Subcellular dosing using laminar flow streams. (a) Selective fluorescence labeling of subcellular features in 3T3 fibroblast cells with 1 μM DIOC_6 (3,3'-dihexyloxacarbocyanine iodide) by ablation of two pores upstream of the cells. The figure is a processed overlay of bright-field and fluorescence images acquired sequentially. Arrow indicates direction of flow in the dosing chamber. Scale bar, 10 μm . (b) Guiding motile cells using chemotactic laminar streams. Shown is a human promyelocytic leukemia (HL-60) cell dosed with a 100 nM fMLP (*N*-formyl-methionyl-leucyl-phenylalanine) stream. Upon intersection with the fMLP stream, the cell changes its polarization, then gradually moves into the gradient. Scale bar, 20 μm . Bovine serum albumin (BSA) was added to fMLP for visualization of reagent streams inside the cell-dosing chamber.

1.4 LASER-INDUCED MICROFABRICATION

1.4.1 Multiphoton excitation-assisted additive microfabrication

Multiphoton excitation (MPE) is a photon absorption process that was first suggested by Maria Göppert-Mayer in her doctoral thesis in 1931 [57], but was not observed experimentally until the invention of lasers in 1961 [58]. In single-photon excitation, the energy of the absorbed photons must equal the energy gap between the ground and excited states of the chromophore. However, the same excitation can be achieved by the near simultaneous absorption of two (or more) relatively low-energy photons. Absorption of the two photons is a sequential process in which the absorption of the first photon excites the chromophore to a virtual (or superposition) state which persists over femtosecond timescales, a time frame within which the second photon must be absorbed (**Figure 1.5**). Otherwise, the molecule relaxes back to the ground state, typically via elastic light scattering. Very high photon fluxes are needed to achieve MPE, a requirement often met through the use of femtosecond pulsed laser sources, such as the titanium-sapphire oscillator (Ti:S; 80 MHz). Due to the low duty cycle (defined as the fraction of time that the laser light is produced) of such pulsed laser sources, photons are concentrated into discrete temporal packets providing high instantaneous intensities at low average powers when the laser beam is tightly focused using high numerical aperture (NA) diffraction-limited optics [59].

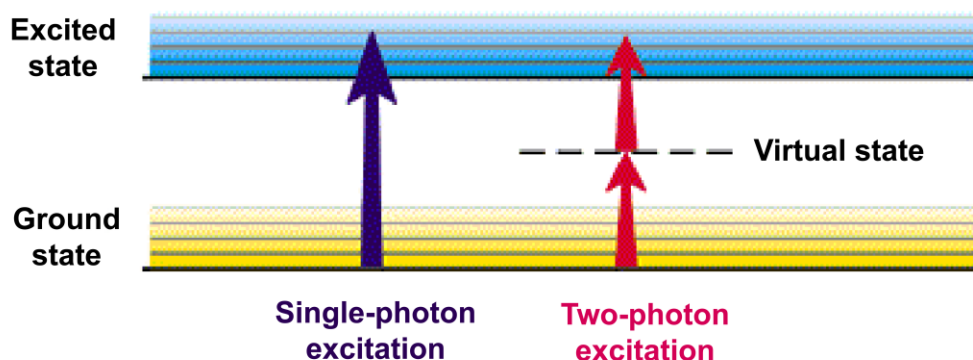


Figure 1.5: Excitation of chromophores by absorption of photons. In single-photon excitation, the absorption of one photon elevates the chromophore to the excited state. In two-photon absorption, the chromophore goes from the ground to the excited state by absorption of two photons separated by a virtual (or superposition) state. Adapted from [60].

Both single and multiphoton absorption processes can be related in terms of a chemical reaction [60]:



Here, M and M^* are the ground and excited states of the chromophore, respectively. $h\nu$ is a photon and n is the number of absorbed photons needed to reach the excited state. The reaction rate for formation of M^* can be stated in terms of reactant concentrations:

$$d[M^*]/dt = k[h\nu]^n [M] = \delta I^n [M] \quad (1.2)$$

Where, k is the forward rate constant, I is the instantaneous intensity and δ is the excitation cross section.

As seen from **Equation 1.2**, the excitation rate $d[M^*]/dt$ is proportional to I^n . This implies that for single-photon excitation ($n = 1$), the excitation is proportional to the intensity, whereas a quadratic dependence exists for multiphoton processes. This makes

MPE a non-linear absorption process in which excitation events dominate in planes nearest to the focal point producing femtoliter-sized reaction volumes (or voxels). MPE has been used to spatially define reaction chemistries to highly localized 3D coordinates for applications such as multiphoton fluorescence microscopy [60, 61], photolytic cleavage [32], and photocrosslinking (*e.g.*, for fabricating protein plugs to occlude flow through pores) [10, 62, 63]. An important advantage of MPE is the reduced likelihood of damage from heating (due to the small voxel size), an important consideration for its use in live cell cultures.

Microfabrication of plugs can be described as an additive process which occurs by focusing laser light into a concentrated protein solution resulting in the formation of a solid matrix whose size can be restricted to the submicron dimensions of the focal volume. By scanning the laser focus in the protein solution, elaborate 3D microstructures can also be fabricated, details of which are discussed elsewhere [10, 28, 62, 63]. The next section summarizes the processes involved in laser-induced ablation of pores in polymer membranes.

1.4.2 Subtractive microfabrication for ablation of pores in polymer membranes

Ablation of pores can be described as subtractive microfabrication. In this case, the laser beam is focused into a polymer membrane used as a substrate for attachment of cells and as a barrier between the stacked laminar flow chambers (**Figure 1.3**). The membrane is ionized at the laser focus resulting in heating, followed by melting, cavitation, and removal of material. The resulting micron-sized pore is used as a conduit for introduction of the reagent into the cell-dosing chamber.

All ablation studies described in the subsequent chapters were conducted using a frequency-doubled (532 nm), diode-pumped, Q-switched Nd:YAG (neodymium yttrium aluminum garnet) laser (JDS Uniphase, NG-10320-110[†]), which has a pulse frequency of 7.7 kHz and a pulse duration of 600 ps. The laser dimensions are ~3 cm x 4 cm x 15 cm (height x width x length), and the lasing system, including the power supply, is available for ~\$5K. Although previous membrane ablation studies in the Shear laboratory [28] were done using a femtosecond Ti:S laser, this dissertation explored the use of Nd:YAG for production of pores in polymer membranes. Femtosecond pulsed laser sources, such as the Ti:S, remain cost-prohibitive (\$150 – 200K) for most potential users in the biosciences, motivating the use of cheaper, less bulky sources for pore ablation. Ease of operation of YAG lasers is another attractive feature. Note that even though the Nd:YAG is a picosecond laser source, it produces sufficiently high instantaneous intensities (comparable to intensities produced by the Ti:S) to allow production of pores in cellular environments. Pore ablation using YAG lasers is explored in this dissertation to allow for easier dissemination of the laminar dosing technology.

Laser powers ranging from 10 – 15 mW were typically used for ablation of pores in 2.5 μm thick Mylar membrane, a polymer membrane often employed in the studies described in this dissertation. The laser output was directed by mirrors into a half-wave plate and beam-splitting cube, used for controlling the average power of the laser beam. A pair of lenses in the path of the laser output served as a telescope to expand and collimate the beam. The beam was then directed onto a dichroic mirror mounted inside a

[†]Teem Photonics acquired this line of MicroChip lasers from JDS Uniphase in August, 2005.

microscope, which aligned the laser with the microscope's optical train. The microscope and its attached CCD (charge-coupled device) camera were used to observe and record events at the focal plane of the objective (**Figure 1.6**).

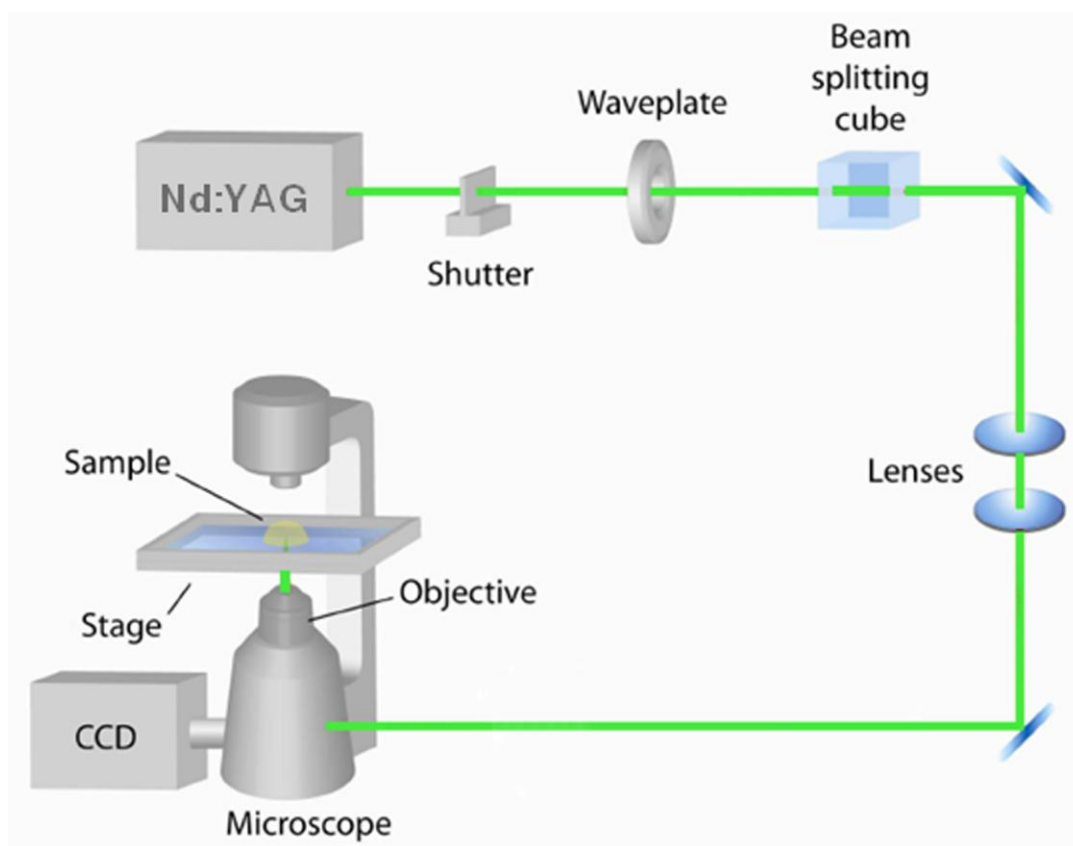


Figure 1.6: Schematic of the Nd:YAG (neodymium yttrium aluminum garnet) laser setup used for creation of micron-sized pores in polymer membranes.

Assuming a Gaussian laser beam profile and a constant power during laser pulses, corresponding peak intensities at the focal point of the laser were calculated to range from $0.7 - 1.0 \text{ TW cm}^{-2}$ using the following equation:

$$I_0 = 2 P_0 / \omega_0^2 \pi \quad (1.3)$$

Where, I_0 is the peak intensity, P_0 is the peak power, and ω_0 is the beam waist. ω_0 for a diffraction-limited focus can be described using the following equation:

$$\omega_0 = 0.61 \lambda / \text{NA} \quad (1.4)$$

Here, λ is the wavelength of the laser and NA is the numerical aperture of the objective used to focus the laser beam.

The other parameter necessary to estimate the intensity is the incident power of a laser pulse, also known as the peak power P_0 , which can be described using the equation below.

$$P_0 = P_{avg} \phi / \tau \omega \quad (1.5)$$

Here, P_{avg} is the average power measured at the back aperture of the objective, ϕ is the throughput of the objective (at 532 nm), τ is the laser pulse width, and ω is the pulse repetition rate. Typical functions describing the temporal variation of power during a laser pulse do not vary largely from the assumption of constant power during a square pulse [64]. Therefore, for simplicity, it is assumed here that the power is constant during a pulse, and the above equations are not written explicitly as functions of time.

Non-linear or multiphoton ionization typically occurs during subtractive microfabrication, processes that are essentially the same as MPE except the molecules are ionized instead of being electronically excited. Ionization processes often require higher transition energy than MPE, which implies a larger number of instantaneously absorbed

photons. During the application of an intense laser pulse into a thin polymer membrane, such as Mylar, the material typically undergoes dielectric breakdown, and develops a conduction band of free electrons. These free electrons play an important role in deposition of laser energy into materials through avalanche ionization, a process in which the free electrons absorb photons and gain enough energy to promote a valence electron into the conduction band. Repetition of this event leads to an exponential growth of free electrons. Avalanche ionization operates on “seed” electrons already in the conduction band, most likely produced by photoionization [65]. Inverse bremsstrahlung may also be involved in which radiation is absorbed by a free electron when it collides with a heavier particle [66]. In this manner, electrons can gain enough energy to ionize atoms during collisions leading to rapid multiplication of ionized electrons, and generation of a plasma in the region of the laser focus [67].

Whether photoionization or avalanche ionization plays a larger role in generation of the free electrons depends on the laser conditions. Pulses more than a few picoseconds in length (such as in case of the YAG laser used in this study) allow time for exponential growth of free electrons through avalanche ionization, making it the dominant process in dielectric breakdown of the material [68-71].

For high energy laser interactions, another mechanism of breakdown involves heat produced when the energy carried by free electrons is transferred to the medium. The result is damage to the substrate, known as optical or laser-induced breakdown [72]. The series of events involved include heating of the substrate, explosive expansion, and emission of a shock wave [67].

In the studies described in this dissertation, pores were typically ablated in 2.5 μm thick Mylar membranes by the brief application of a train of focused laser pulses with extended delay between pulses. Insertion of delays provided an opportunity for the ablation site to dissipate heat between periods of brief and intense irradiation resulting in more regularly sized pores than were obtained using an unbroken train of laser pulses.

With the Ti:S laser, there was a threshold for apparent damage to the membrane, with intensities below 1.0 TW cm^{-2} not damaging the membrane under typical experimental conditions. This allowed for direct-writing of protein structures at laser intensities less than 1.0 TW cm^{-2} (and thereby, fabrication of protein plugs to terminate flow through the pores). It was not feasible to do so with the Nd:YAG laser in which damaged occurred to the membrane even at very low average powers. While the bulk optical properties of Mylar membranes are transparent at visible wavelengths, for packaging purposes they are coated with inorganic particles of proprietary composition. If these particles easily ionize at 532 nm, it would greatly enhance breakdown of the material by providing seed electrons for avalanche ionization, possibly the reason for absence of threshold [65].

The events observed during pore formation include a visible flash and the formation of a small gas bubble. Finished pores were characterized using scanning electron microscopy (SEM) and optical microscopy. SEM is a type of microscopy where the sample surface is imaged by scanning it with a high-energy beam of electrons in a raster scan pattern. The electrons interact with the atoms that make up the sample, producing signals that contain information about the sample's surface topography, composition, and other properties such as electrical conductivity [73].

SEM analysis of pores ablated in Mylar using a femtosecond Ti:S laser tuned to 750 nm in previous studies showed pore diameters of 3 – 4 μm [28]. Analysis of the pores made with the Nd:YAG and Ti:S lasers using optical microscopy indicated that they had similar morphologies, consisting of a 3 – 4 μm diameter aperture rimmed with a raised burr of material (**Figure 1.7**). Notably, the diameter of the pore was much larger than the beam waist (= 433 nm, calculated using **Equation 1.4**), which indicates a transport of energy outwards from the region of highest intensity. A burr surrounding the pore implies that melting and resolidification had occurred. These features indicate that the ablation process likely involves both dielectric breakdown and an accompanying thermal process [74-77], with the primary mechanism possibly being the deposition of thermalized energy through avalanche ionization, which leads to melting and ablation of the polymer membrane.

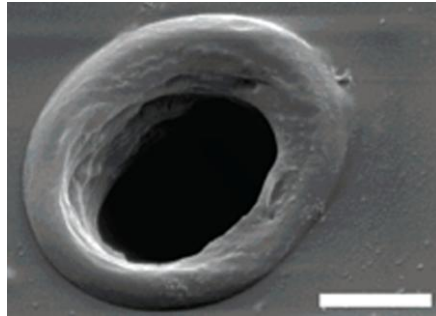


Figure 1.7: SEM of a pore created in 2.5 μm thick Mylar membrane by Nielson and Shear using a Ti:S (titanium-sapphire) laser. Scale bar, 2 μm . Adapted from [28].

This dissertation focuses on extending the capabilities of the above described chemical dosing approach [28], primarily on increasing its spatio-temporal resolution and on incorporation of multiple reagents, to enhance control over cell-dosant interactions. The power of this enhanced dosing methodology to specifically influence cellular behavior is demonstrated by guidance of motile HL-60 cells, a neutrophil precursor cell line, through extended migration paths specified using different effector molecules in an attempt to understanding neutrophil migration and chemotaxis. A brief discussion of neutrophil signaling and migration is warranted at this point before presenting a preview of the chapters in this dissertation.

1.5 NEUTROPHIL SIGNALING AND CHEMOTAXIS

Neutrophils are a type of white blood cell involved in inflammatory response. They constitute approximately two-thirds of all white blood cells, and are one of the fastest migratory cells in the human body moving at speeds of $10 - 20 \mu\text{m min}^{-1}$ on glass, which is 5 – 10 times faster than the rate of crawling of keratocytes and macrophages, and almost 50 times faster than the rate at which fibroblasts move [78, 79]. These cells survive for 24 – 48 hours inside the human body. They travel passively through the blood stream until they sense the chemical traces of invading bacteria. At that point, they leave the blood stream, crawl through the vessel endothelial cell barrier to the site of inflammation, and digest the intruder. This is achieved by sensing gradients of chemotactic molecules and moving up the gradient (*i.e.*, towards its highest concentration), a process called chemotaxis [20, 80, 81]. In addition to neutrophils, chemotaxis is exhibited by fibroblasts [82, 83] and keratocytes [84, 85] as well as by

other organisms, such as bacteria [86] and slime molds [87, 88], for detection of toxins, hunting for food, and mating.

The migration of neutrophils is directed by a number of chemotactic factors, such as bacterially-derived N-formylated peptides (*e.g.*, fMLP), and host-derived products, such as interleukin-8 (IL-8) and leukotriene-B₄ (LTB₄) [89, 90]. Neutrophils are capable of detecting very shallow chemoattractant gradients, in many cases less than 1% concentration difference across its cell length [78].

Chemotaxis is a complex process that involves morphological changes in a cell in response to a chemoattractant gradient and concomitant intracellular signaling [91]. When presented with a chemoattractant gradient, neutrophils respond with highly oriented polarity with their leading edges pointed towards the highest chemoattractant concentration across its body followed by directed migration up the chemical gradient [81]. G-protein-coupled receptors are responsible for transmitting the signal from the extracellular environment of a cell to its interior [20]. Activation of these receptors leads to an accumulation of phosphatidylinositol 3-kinase (PI3K) lipid products, such as phosphatidylinositol 3,4,5-triphosphate (PIP₃), at the edge of the cell nearest to the chemoattractant [13, 92]. PIP₃ activates Rho GTPases, such as Cdc42 and Rac [93]. The activated forms of these molecules are implicated in bringing about an extension of the lamellipodia (or the leading edge) and polymerization of actin filaments [19, 94], which in turn activate a positive feedback loop, causing further production of PIP₃ [95-97]. In addition, certain inhibitory mechanisms restrict the spatial pattern of PI3K activity and ruffling during chemotaxis to the leading edge of the cell. Negative regulators of PIP₃ accumulation, such as 3' lipid phosphatase and 5' lipid phosphatase, are considered

possible candidates for this inhibition [96]. Overall, this process, which involves changes in cellular morphology and signaling pathways, acts as a chemical compass allowing cells to effectively navigate themselves inside chemoattractant gradients.

Researchers study neutrophil signaling by exposing cells to various effector molecules that promote (*e.g.*, chemoattractants such as fMLP and IL-8) or inhibit (*e.g.*, Clostridium difficile toxin B and wortmannin) chemotaxis. Use of some of these effector molecules is explored in this dissertation.

In the absence of chemotactic factors or in the presence of uniform concentration of the chemoattractant molecules, neutrophils continue to sense their environment and exhibit random migration, during which they fail to develop and/or sustain highly polarized geometries, but still exhibit ruffling at the leading edges. Directed migration is absent, as expected.

In the experiments presented in this dissertation, HL-60 cells were used to demonstrate the utility of the improved laminar flow dosing technology. Differentiated HL-60 (dHL-60) cells (**Figure 1.8**), a neutrophil-like cell line, are considered a valid model system for studying neutrophil migration and chemotaxis. Chemotactic peptides, such as fMLP, have been found to induce a front-tail polarity in these cells comparable to that seen in primary neutrophils. It has also been reported that chemokinetic and chemotactic responses to chemotactic peptides are similar in both cell types, with respect to the mean speed of migration, the fraction of migrated cells, and the concentration of stimulus optimal for activation [98-100]. This cell line is a convenient alternative to the use of primary neutrophils, obtained from human blood, since in the case of the latter the

cell isolation procedure typically takes ~3 hours and the cells only survive for 4 – 6 hours following isolation.

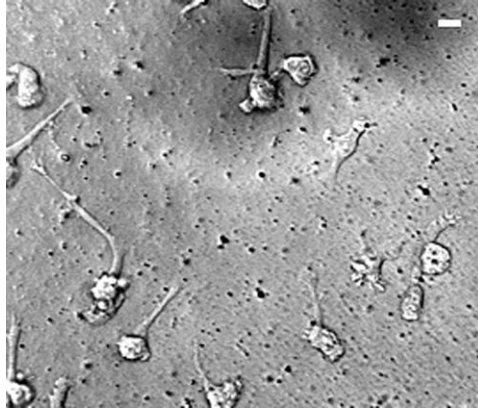


Figure 1.8: Differentiated HL-60 cells on fibronectin-coated Mylar membrane. The Mylar membrane was oxygen plasma-etched, then coated with 0.1 mg mL^{-1} fibronectin. Gey's medium[†] with 0.5% BSA was flowed in the cell-dosing chamber. Scale bar, $10 \text{ }\mu\text{m}$.

[†]6 mM KCl, 138 mM NaCl, 5 mM glucose, 1 mM Na_2HPO_4 , 20 mM HEPES, 1 mM MgCl_2 and 1 mM CaCl_2 , pH 7.4

1.6 PREVIEW OF CONTENT

This chapter provides an introduction to the techniques and concepts that have been described in this dissertation. It also outlines the motivation behind the work.

In the configuration reported by Nielson and Shear (**Figure 1.3**) [28], and as seen with most laminar-flow dosing approaches, the flow direction is pre-defined, making it impossible to target many subcellular features without also dosing regions upstream from the site of interest. This pre-assignment of flow direction also means that the position of a chemical signal originating from a given pore is fixed, making it difficult to investigate dynamic cellular behaviors, such as polarization and migration. Chapter 2 reports a strategy for rapid control of reagent stream directionality along discrete angles, the applicability of which is demonstrated by millisecond dosing of HL-60 cells.

In Chapter 3, the ability to dynamically modify the chemical microenvironment of cells is used to specifically influence cell activity by exposing HL-60 cells to fast chemoattractant gradient switches and studying the reorientation mechanisms adopted by motile cells during such chemical events.

In Chapter 2, the directionality of laminar flow streams can only be changed along pre-defined angles, making it difficult to guide cells along extended migration paths. Chapter 4 describes improved methods for changing stream directionality along arbitrary angles to truly offer dynamic control over reorientation of chemical gradients.

Incorporation of multiple reagents is the topic of Chapter 5, which would permit site-specific cellular dosing with multiple chemical species (or varying concentrations of the same species). The methods considered in this chapter allow targeting of selected subcellular regions with two dosing reagents, introduced in rapid succession, or present

simultaneously to allow parallel dosing with distinct dosing solutions on the same cell or on two different cells.

1.7 REFERENCES

- [1] Brown MJ, Loew LM. Electric field-directed fibroblast locomotion involves cell surface molecular reorganization and is calcium independent. *Journal of Cell Biology*. 1994;127:117-28.
- [2] Nishimura KY, Isseroff RR, Nuccitelli R. Human keratinocytes migrate to the negative pole in direct current electric fields comparable to those measured in mammalian wounds. *Journal of Cell Science*. 1996;109:199-207.
- [3] Stump RF, Robinson KR. *Xenopus* neural crest cell migration in an applied electrical field. *Journal of Cell Biology*. 1983;97:1226-33.
- [4] Zhao M, Song B, Pu J, Wada T, Reid B, Tai G, Wang F, Guo A, Walczysko P, Gu Y. Electrical signals control wound healing through phosphatidylinositol-3-OH kinase and PTEN. *Nature*. 2006;442:457-60.
- [5] Ingber DE. Mechanical signaling and the cellular response to extracellular matrix in angiogenesis and cardiovascular physiology. *Circulation Research*. 2002;91:877-87.
- [6] Ingber DE. Mechanosensation through integrins: cells act locally but think globally. *Proceedings of the National Academy of Sciences of the United States of America*. 2003;100:1472-4.
- [7] Clark P, Connolly P, Curtis AS, Dow JA, Wilkinson CD. Topographical control of cell behaviour. I. Simple step cues. *Development*. 1987;99:439-48.
- [8] Clark P, Connolly P, Curtis AS, Dow JA, Wilkinson CD. Cell guidance by ultrafine topography in vitro. *Journal of Cell Science*. 1991;99:73-7.
- [9] Miller C, Jeftinija S, Mallapragada S. Micropatterned Schwann cell-seeded biodegradable polymer substrates significantly enhance neurite alignment and outgrowth. *Tissue Engineering*. 2001;7:705-15.
- [10] Kaehr B, Allen R, Javier DJ, Currie J, Shear JB. Guiding neuronal development with in situ microfabrication. *Proceedings of the National Academy of Sciences of the United States of America*. 2004;101:16104-8.
- [11] Contestabile A, Ciani E. Role of nitric oxide in the regulation of neuronal proliferation, survival and differentiation. *Neurochemistry International*. 2004;45:903-14.

- [12] Phung YT, Bekker JM, Hallmark OG, Black SM. Both neuronal NO synthase and nitric oxide are required for PC12 cell differentiation: a cGMP independent pathway. *Molecular Brain Research*. 1999;64:165-78.
- [13] Wang F, Herzmark P, Weiner OD, Srinivasan S, Servant G, Bourne HR. Lipid products of PI(3)Ks maintain persistent cell polarity and directed motility in neutrophils. *Nature Cell Biology*. 2002;4:513-8.
- [14] Wang GX, Poo M. Requirement of TRPC channels in netrin-1-induced chemotropic turning of nerve growth cones. *Nature*. 2005;434:898-904.
- [15] Song H, Poo M. Signal transduction underlying growth cone guidance by diffusible factors. *Current Opinion in Neurobiology*. 1999;9:355-63.
- [16] Beg AA, Baltimore D. An essential role for NF-kappa B in preventing TNF-alpha-induced cell death. *Science*. 1996;274:782-4.
- [17] Ito H, Nomoto H, Furukawa Y, Furukawa S. Neurotrophins facilitate synthesis of choline acetyltransferase and tyrosine hydroxylase in cultured mouse neural stem cells independently of their neuronal differentiation. *Neuroscience Letters*. 2003;339:231-4.
- [18] Weiner OD, Servant G, Parent CA, Devreotes PN, Bourne HR. Cell polarity in response to chemoattractants. In: Drubin DG, editor. *Cell Polarity: Frontiers in Molecular Biology*. Oxford University Press; Oxford: 2000. p. 201-39.
- [19] Weiner OD, Servant G, Welch MD, Mitchison TJ, Sedat JW, Bourne HR. Spatial control of actin polymerization during neutrophil chemotaxis. *Nature Cell Biology*. 1999;1:75-81.
- [20] Servant G, Weiner OD, Herzmark P, Balla T, Sedat JW, Bourne HR. Polarization of chemoattractant receptor signaling during neutrophil chemotaxis. *Science*. 2000;287:1037-40.
- [21] Matsuzaki M, Ellis-Davies GCR, Nemoto T, Miyashita Y, Iino M, Kasai H. Dendritic spine geometry is critical for AMPA receptor expression in hippocampal CA1 pyramidal neurons. *Nature Neuroscience*. 2001;4:1086-92.
- [22] Callaway EM, Yuste R. Stimulating neurons with light. *Current Opinions in Neurobiology*. 2002;12:587-92.
- [23] Boucsein C, Nawrot M, Rotter S, Aertsen A, Heck D. Controlling synaptic input patterns in vitro by dynamic photo stimulation. *Journal of Neurophysiology*. 2005;94:2948-58.

- [24] Takayama S, Ostuni E, LeDuc P, Naruse K, Ingber DE, Whitesides GM. Laminar flows: Subcellular positioning of small molecules. *Nature*. 2001;411:1016.
- [25] Takayama S, Ostuni E, LeDuc P, Naruse K, Ingber DE, Whitesides GM. Selective chemical treatment of cellular microdomains using multiple laminar streams. *Chemistry & Biology*. 2003;10:123-30.
- [26] Jeon NL, Baskaran H, Dertinger SKW, Whitesides GM, Van de Water L, Toner M. Neutrophil chemotaxis in linear and complex gradients of interleukin-8 formed in a microfabricated device. *Nature Biotechnology*. 2002;20:826-30.
- [27] Saadi W, Wang SJ, Lin F, Jeon NL. A parallel-gradient microfluidic chamber for quantitative analysis of breast cancer cell chemotaxis. *Biomedical Microdevices*. 2006;8:109-18.
- [28] Nielson R, Shear JB. Parallel chemical dosing of subcellular targets. *Analytical Chemistry*. 2006;78:5987-93.
- [29] Moorjani S, Nielson R, Chang XA, Shear JB. Dynamic remodeling of subcellular chemical gradients using a multi-directional flow device. *Lab on a Chip*. 2010;10:2139-46.
- [30] Ji D, Lape R, Dani JA. Timing and location of nicotinic activity enhances or depresses hippocampal synaptic plasticity. *Neuron*. 2001;31:131-41.
- [31] Latour I, Gee CE, Robitaille R, Lacaille JC. Differential mechanisms of Ca^{2+} responses in glial cells evoked by exogenous and endogenous glutamate in rat hippocampus. *Hippocampus*. 2001;11:132-45.
- [32] Brown EB, Shear JB, Adams SR, Tsien RY, Webb WW. Photolysis of caged calcium in femtoliter volumes using two-photon excitation. *Biophysical Journal*. 1999;76:489-99.
- [33] Pirrung MC, Drabik SJ, Ahamed J, Ali H. Caged chemotactic peptides. *Bioconjugate Chemistry*. 2000;11:679-81.
- [34] Shigeri Y, Tatsu Y, Yumoto N. Synthesis and application of caged peptides and proteins. *Pharmacology & Therapeutics*. 2001;91:85-92.
- [35] Furuta T, Noguchi K. Controlling cellular systems with Bhc-caged compounds. *Trends in Analytical Chemistry*. 2004;23:511-9.
- [36] Burgi DS, Chien RL. Optimization in sample stacking for high-performance capillary electrophoresis. *Analytical Chemistry*. 1991;63:2042-7.

- [37] Burgreen D, Nakache FR. Electrokinetic Flow in Ultrafine Capillary Slits. *Journal of Physical Chemistry*. 1964;68:1084-91.
- [38] Kinzer JA, Olesik JW, Olesik SV. Effect of laminar flow in capillary electrophoresis: model and experimental results on controlling analysis time and resolution with inductively coupled plasma mass spectrometry detection. *Analytical Chemistry*. 1996;68:3250-7.
- [39] Weigl BH, Yager P. Microfluidics: microfluidic diffusion-based separation and detection. *Science*. 1999;283:346-7.
- [40] Petersen KE. Silicon as a mechanical material. *Proceedings of the IEEE*. 1982;70:420-57.
- [41] Wise KD. Integrated sensors, MEMS, and microsystems: Reflections on a fantastic voyage. *Sensors and Actuators A: Physical*. 2007;136:39-50.
- [42] Greenwood J. Silicon in mechanical sensors. *Journal of Physics E: Scientific Instruments*. 1988;21:1114-28.
- [43] Ho CM, Tai YC. Micro-electro-mechanical-systems (MEMS) and fluid flows. *Annual Review of Fluid Mechanics*. 1998;30:579-612.
- [44] Kenis PJA, Ismagilov RF, Whitesides GM. Microfabrication inside capillaries using multiphase laminar flow patterning. *Science*. 1999;285:83-5.
- [45] Takayama S, Ostuni E, Qian X, McDonald JC, Jiang X, LeDuc P, Wu MH, Ingber DE, Whitesides GM. Topographical micropatterning of poly (dimethylsiloxane) using laminar flows of liquids in capillaries. *Advanced Materials*. 2001;13:570-4.
- [46] Takayama S, McDonald JC, Ostuni E, Liang MN, Kenis PJA, Ismagilov RF, Whitesides GM. Patterning cells and their environments using multiple laminar fluid flows in capillary networks. *Proceedings of the National Academy of Sciences of the United States of America*. 1999;96:5545-8.
- [47] Jeon NL, Dertinger SKW, Chiu DT, Choi IS, Stroock AD, Whitesides GM. Generation of solution and surface gradients using microfluidic systems. *Langmuir*. 2000;16:8311-6.
- [48] Dertinger SKW, Chiu DT, Jeon NL, Whitesides GM. Generation of gradients having complex shapes using microfluidic networks. *Analytical Chemistry*. 2001;73:1240-6.

- [49] Irimia D, Geba DA, Toner M. Universal microfluidic gradient generator. *Analytical Chemistry*. 2006;78:3472–7.
- [50] Lin F, Nguyen CMC, Wang SJ, Saadi W, Gross SP, Jeon NL. Effective neutrophil chemotaxis is strongly influenced by mean IL-8 concentration. *Biochemical and Biophysical Research Communications*. 2004;319:576-81.
- [51] Lin F, Nguyen CMC, Wang SJ, Saadi W, Gross SP, Jeon NL. Neutrophil migration in opposing chemoattractant gradients using microfluidic chemotaxis devices. *Annals of Biomedical Engineering*. 2005;33:475-82.
- [52] Irimia D, Liu SY, Tharp WG, Samadani A, Toner M, Poznansky MC. Microfluidic system for measuring neutrophil migratory responses to fast switches of chemical gradients. *Lab on a Chip*. 2006;6:191-8.
- [53] Beta C, Wyatt D, Rappel WJ, Bodenschatz E. Flow photolysis for spatiotemporal stimulation of single cells. *Analytical Chemistry*. 2007;79:3940-4.
- [54] Koning AJ, Lum PY, Williams JM, Wright R. DiOC6 staining reveals organelle structure and dynamics in living yeast cells. *Cell Motility and the Cytoskeleton*. 1993;25:111-28.
- [55] Kataoka M, Fukura Y, Shinohara Y, Baba Y. Analysis of mitochondrial membrane potential in the cells by microchip flow cytometry. *Electrophoresis*. 2005;26:3025-31.
- [56] Lecoeur H, Melki MT, Saïdi H, Gougeon ML. Analysis of Apoptotic Pathways by Multiparametric Flow Cytometry: Application to HIV Infection. *Methods in Enzymology*. 2008;442:51-82.
- [57] Göppert-Mayer M. Elementary processes with two quantum jumps. In: *Annalen der Physik*. Berlin, Germany. 1931;9. p. 273-94.
- [58] Kaiser W, Garrett CGB. Two-Photon Excitation in $\text{CaF}_2:\text{Eu}^{2+}$. *Physical Review Letters*. 1961;7:229-31.
- [59] Zipfel WR, Williams RM, Webb WW. Nonlinear magic: multiphoton microscopy in the biosciences. *Nature Biotechnology*. 2003;21:1369-77.
- [60] Shear JB. Multiphoton-excited fluorescence in bioanalytical chemistry. *Analytical Chemistry*. 1999;71:598-605.
- [61] Xu C, Zipfel W, Shear JB, Williams RM, Webb WW. Multiphoton fluorescence excitation: new spectral windows for biological nonlinear microscopy.

- Proceedings of the National Academy of Sciences of the United States of America.* 1996;93:10763-8.
- [62] Allen R, Nielson R, Wise D, Shear JB. Catalytic three-dimensional protein architectures. *Analytical Chemistry* 2005;77:5089-95.
 - [63] Hill R, Lyon J, Allen R, Stevenson K, Shear JB. Microfabrication of three-dimensional bioelectronic architectures. *Journal of the American Chemical Society.* 2005;127:10707-11.
 - [64] Birge RR. One-photon and two-photon excitation spectroscopy. In: Kliger DS, editor. *Ultrasensitive Laser Spectroscopy*. Academic Press; New York: 1983. p. 109-74.
 - [65] Schaffer CB, Brodeur A, Mazur E. Laser-induced breakdown and damage in bulk transparent materials induced by tightly focused femtosecond laser pulses. *Measurement Science and Technology.* 2001;12:1784.-94
 - [66] Haug E, Nakel W. In: *The Elementary Process of Bremsstrahlung*. World Scientific; Singapore: 2004.
 - [67] Shen YR. In: *The Principles of Nonlinear Optics*. Wiley; New York: 1984.
 - [68] Cremers DA, Radziemski LJ. In: *Handbook of Laser-Induced Breakdown Spectroscopy*. John Wiley & Sons Ltd; London: 2006.
 - [69] Nahen K, Vogel A. Plasma formation in water by picosecond and nanosecond Nd:YAG laser pulses. II. Transmission, scattering, and reflection. *IEEE Journal of Selected Topics in Quantum Electronics.* 1996;2:861-71.
 - [70] Noack J, Vogel A. Laser-induced plasma formation in water at nanosecond to femtosecond time scales: calculation of thresholds, absorption coefficients, and energy density. *IEEE Journal of Quantum Electronics.* 1999;35:1156-67.
 - [71] Tien AC, Backus S, Kapteyn H, Murnane M, Mourou G. Short-pulse laser damage in transparent materials as a function of pulse duration. *Physical Review Letters.* 1999;82:3883-6.
 - [72] Stuart BC, Feit MD, Rubenchik AM, Shore BW, Perry MD. Laser-induced damage in dielectrics with nanosecond to subpicosecond pulses. *Physical Review Letters.* 1995;74:2248-51.
 - [73] Oatley CW, Nixon WC, Pease RFW. Scanning electron microscopy. *Advances in Electronics and Electron Physics.* 1966;21:181-247.

- [74] Shirk MD, Molian PA. A review of ultrashort pulsed laser ablation of materials. *Journal of Laser Applications*. 1998;10:18-28.
- [75] Schaffer CB, Jamison AO, Garcia JF, Mazur E. Structural changes induced in transparent materials with ultrashort laser pulses. In: Sucha G, editor. *Ultrafast Lasers*. Marcel Dekker, Inc.; New York: 2003. p. 395-418.
- [76] Chichkov BN, Momma C, Nolte S, Von Alvensleben F, Tünnermann A. Femtosecond, picosecond and nanosecond laser ablation of solids. *Applied Physics A: Materials Science & Processing*. 1996;63:109-15.
- [77] Joglekar AP, Liu H, Spooner GJ, Meyhöfer E, Mourou G, Hunt AJ. A study of the deterministic character of optical damage by femtosecond laser pulses and applications to nanomachining. *Applied Physics B: Lasers and Optics*. 2003;77:25-30.
- [78] Zhelev DV, Alteraifi A. Signaling in the motility responses of the human neutrophil. *Annals of Biomedical Engineering*. 2002;30:356-70.
- [79] Zigmond SH. Recent quantitative studies of actin filament turnover during cell locomotion. *Cell Motility and the Cytoskeleton*. 1993;25:309-16.
- [80] Weiner OD. Regulation of cell polarity during eukaryotic chemotaxis: the chemotactic compass. *Current Opinion in Cell Biology*. 2002;14:196-202.
- [81] Bourne HR, Weiner OD. A chemical compass. *Nature*. 2002;419:21.
- [82] Postlethwaite AE, Seyer JM, Kang AH. Chemotactic attraction of human fibroblasts to type I, II, and III collagens and collagen-derived peptides. *Proceedings of the National Academy of Sciences of the United States of America*. 1978;75:871-5.
- [83] Senior RM, Griffin GL, Huang JS, Walz DA, Deuel TF. Chemotactic activity of platelet alpha granule proteins for fibroblasts. *Journal of Cell Biology*. 1983;96:382-5.
- [84] Andresen JL, Ehlers N. Chemotaxis of human keratocytes is increased by platelet-derived growth factor-BB, epidermal growth factor, transforming growth factor-alpha, acidic fibroblast growth factor, insulin-like growth factor-I, and transforming growth factor-beta. *Current Eye Research*. 1998;17:79-87.
- [85] Andresen JL, Ledet T, Ehlers N. Keratocyte migration and peptide growth factors: the effect of PDGF, bFGF, EGF, IGF-I, aFGF and TGF- β on human keratocyte migration in a collagen gel. *Current Eye Research*. 1997;16:605-13.

- [86] Adler J. Chemotaxis in bacteria. *Science*. 1966;153:708-16.
- [87] Mato JM, Losada A, Nanjundiah V, Konijn TM. Signal input for a chemotactic response in the cellular slime mold *Dictyostelium discoideum*. *Proceedings of the National Academy of Sciences of the United States of America*. 1975;72:4991-3.
- [88] Mato JM, Konijn TM. Chemotaxis and binding of cyclic AMP in cellular slime molds. *Biochimica et Biophysica Acta-General Subjects*. 1975;385:173-9.
- [89] Foxman EF, Campbell JJ, Butcher EC. Multistep navigation and the combinatorial control of leukocyte chemotaxis. *Journal of Cell Biology*. 1997;139:1349-60.
- [90] Foxman EF, Kunkel EJ, Butcher EC. Integrating conflicting chemotactic signals. The role of memory in leukocyte navigation. *Journal of Cell Biology*. 1999;147:577-88.
- [91] Xu J, Wang F, Van Keymeulen A, Herzmark P, Straight A, Kelly K, Takuwa Y, Sugimoto N, Mitchison T, Bourne HR. Divergent signals and cytoskeletal assemblies regulate self-organizing polarity in neutrophils. *Cell*. 2003;114:201-14.
- [92] Weiner OD, Neilsen PO, Prestwich GD, Kirschner MW, Cantley LC, Bourne HR. A PtdInsP3-and Rho GTPase-mediated positive feedback loop regulates neutrophil polarity. *Nature Cell Biology*. 2002;4:509-13.
- [93] Srinivasan S, Wang F, Glavas S, Ott A, Hofmann F, Aktories K, Kalman D, Bourne HR. Rac and Cdc42 play distinct roles in regulating PI(3,4,5)P3 and polarity during neutrophil chemotaxis. *Journal of Cell Biology*. 2003;160:375-85.
- [94] Weiner OD, Marganski WA, Wu LF, Altschuler SJ, Kirschner MW. An actin-based wave generator organizes cell motility. *Public Library of Science Biology*. 2007;5:2053-63.
- [95] Wang F, Herzmark P, Weiner OD, Srinivasan S, Servant G, Bourne HR. Lipid products of PI(3)Ks maintain persistent cell polarity and directed motility in neutrophils. *Nature Cell Biology*. 2002;4:513-8.
- [96] Weiner OD. Regulation of cell polarity during eukaryotic chemotaxis: the chemotactic compass. *Current Opinion in Cell Biology*. 2002;14:196-202.
- [97] Srinivasan S, Wang F, Glavas S, Ott A, Hofmann F, Aktories K, Kalman D, Bourne HR. Rac and Cdc42 play distinct roles in regulating PI(3,4,5)P3 and polarity during neutrophil chemotaxis. *Journal of Cell Biology*. 2003;160:375-85.

- [98] Hauert AB, Martinelli S, Marone C, Niggli V. Differentiated HL-60 cells are a valid model system for the analysis of human neutrophil migration and chemotaxis. *International Journal of Biochemistry & Cell Biology*. 2002;34:838-54.
- [99] Millius A, Weiner OD. Chemotaxis in neutrophil-like HL-60 cells. In: *Methods in Molecular Biology*. New Jersey: 2009;571. p. 167-77.
- [100] Collins SJ, Ruscetti FW, Gallagher RE, Gallo RC. Normal functional characteristics of cultured human promyelocytic leukemia cells (HL-60) after induction of differentiation by dimethylsulfoxide. *Journal of Experimental Medicine*. 1979;149:969-74.

Chapter 2: Steering Laminar Streams for Precise Chemical Targeting of Cells[†]

2.1 INTRODUCTION

To elucidate mechanisms by which chemical cues regulate cellular behavior, responses to stimuli often are studied in two-dimensional culture where the levels of soluble effectors can be independently varied. Although many *in vitro* experiments are conducted without regard for the spatial and temporal distributions of solutes, cells *in vivo* experience a broad range of dynamic chemical gradients believed to play critical roles in their behavior. As a consequence, techniques have been developed for introducing chemical agents into culture with subcellular resolution, aiding efforts to study polarized cellular events such as differentiation [4, 5], chemotaxis [6-8], and axonal pathfinding [9, 10].

As discussed in Chapter 1, sub-nanoliter dosings of bioactive compounds are routinely applied to culture environments using micropositioned puffer pipets [6, 10-12], an approach capable of modulating chemical concentrations over distances of tens of micrometers. Greater spatial and temporal control of dosing is possible by photolytically activating caged reagents using focused laser light, particularly when performed using two-photon excitation [13-15]. A number of small, bioactive species (*e.g.*, ions, neurotransmitters, adenosine triphosphate) can be focally released from photolabile, inactivating chemical groups within volumes as small as ~1 fL [13], and the absence of

[†]Adapted from Moorjani et al., *Lab on a Chip*, 2010 [1].

bulky micropositioners allows release to be coordinated at multiple positions either in parallel or in rapid succession. Unfortunately, challenges in designing caged compounds limit the generality of photolytic dosing. For delivery using either micropipets or uncaging, it typically is not feasible to establish steep concentration gradients that can be maintained for extended periods.

Recent approaches for creating stable concentration gradients within cell cultures on the micrometer scale have relied on fluid-control capabilities of microfabricated systems [16-24]. In one approach, two or more laminar streams are directed into confluence, forming sharp interfacial boundaries that can be targeted to specific subcellular regions. Because the number, dimensions, and orientation of confluent streams are largely determined by the physical architecture of the microfabricated device, use of this approach generally relies on the ability to identify cultured cells whose positions and orientations are compatible with the pre-set geometry of dosing streams. In addition, the kinetics for altering chemical concentrations within laminar streams in such devices are relatively slow. In the best cases, gradient changes have required at least several seconds [25, 26], periods substantially longer than the timescales on which many intracellular signaling events take place.

In a previous publication, the Shear laboratory described a strategy for stably dosing an arbitrary number of subcellular targets in parallel that avoided restrictions on the relative position of dosing sites [20]. This strategy was discussed in Chapter 1 (Section 1.3), and is summarized here. In this approach, a focused laser beam was used to create pores in a polymer membrane that served as a substrate for cell adhesion. Production of a pore provided an entry route for a dosing reagent from a reservoir on the

opposing side of the membrane, and the reagent that crossed the membrane formed a well-defined dosing stream as a result of the laminar-flow conditions present in the culture chamber. Flow also could be terminated through one or more selected pores using a laser-induced pore-plugging method, allowing distinct cellular regions to be targeted with a chemical species for differing times.

Unfortunately, as with the other laminar-flow dosing approaches, effector streams were aligned in a single pre-determined direction, making it impossible to target many subcellular features without also dosing regions upstream from the site of interest. This pre-assignment of flow direction also meant that gradients—created at the borders of reagent streams and bulk medium—could be generated only along a fixed vector path, and could not be dynamically re-oriented to probe polarized cellular behaviors.

This chapter reports a strategy for controlling flow directionality—and thus, stream and gradient orientations—in real time with subsecond temporal resolution. Here, a cell-dosing chamber is outfitted with multiple pairs of solution sources and drains distributed along the chamber circumference. By selecting specific source/drain pairs using computer-controlled pinch valves, reagent streams can be redirected to dynamically recast the microscopic chemical landscape in which cells develop, migrate, and interact with each other. The application of this technology is demonstrated by site-specific chemical targeting of features of interest (*e.g.*, leading and trailing edges of motile cells). Furthermore, the power of this approach to specifically influence cell activity is demonstrated in Chapter 3 by sustained guidance of motile HL-60 cells, a neutrophil precursor cell line [27-29], through arbitrary migration paths using low concentrations of a chemoattractant peptide.

2.2 EXPERIMENTAL METHODS

2.2.1 Device design and fabrication

The cell-dosing device consisted of two flow chambers stacked on top of each other separated by a 2.5 μm thick Mylar membrane (SPI Supplies, catalog no. 100; West Chester, PA; **Figure 2.1a**). Each flow chamber was composed of a flow cell and its corresponding gasket. To construct flow cells, channels were cut in 0.12 mm Secure-Seal adhesive sheets (Grace Bio-Labs, SA-S-1L; Bend, OR), using a XL-12000 or X-660 laser cutter (Universal Laser Systems, Inc.; Scottsdale, AZ), available at the School of Architecture at UT Austin. The cut adhesive was aligned with Dura-Lar (0.003" thick; Grafix Plastics, P03DC0912; Cleveland, OH) or polycarbonate (0.01" thick; Grace Bio-Labs, HS3838) coverslips, with holes in them to serve as entry and exit ports for fluid flow, to complete the flow cells.

For cutting adhesive sheets, appropriate laser power, speed, pulses per inch (PPI), and air flow were input into the software-driven 120 W XL-12000 or 60 W X-660 laser system. Flow cell geometries were designed in AutoCAD (Autodesk, Inc.; San Rafael, CA), and these drawings were input to the laser system. The ratio of the laser power to the speed of the laser head determines the cut's depth. For the flow cells used in this chapter, 12 – 18 W of laser power with a speed of 4.50 inches per second were used for cutting the adhesive sheets. An intermediate number of PPI (value = 500; used to specify the spacing between laser pulses) with air flow digitally set to 750 cubic feet per minute (CFM; in XL-12000) or manually to 30 psi (in X-660) were employed. Holes were drilled in plastic (Dura-Lar or polycarbonate) coverslips to serve as entry and exit ports for fluid flow. In case of Dura-Lar coverslips, holes were often cut (vs. manually drilled)

using the XL-12000 laser system. For cutting holes in Dura-Lar, 24 W of laser power with a speed set to 11.25 inches per second, PPI of 300, and air flow of 1500 CFM were used. The diameter of the holes was set equal to the channel width.

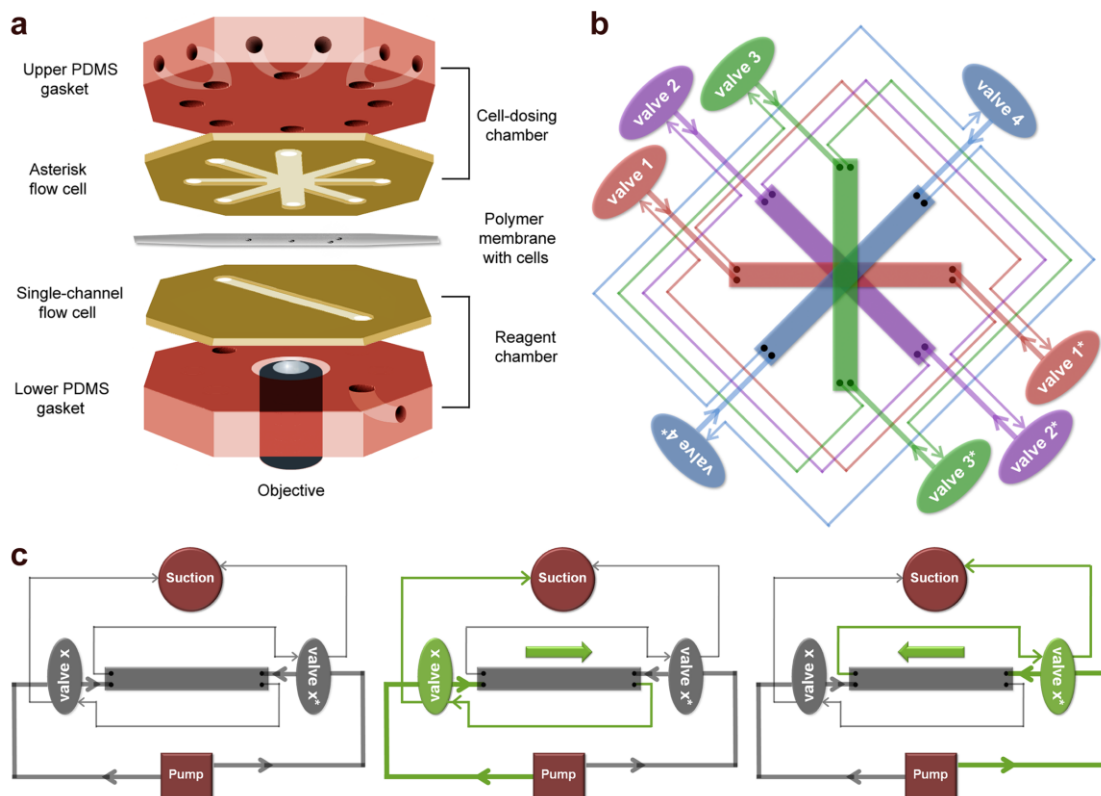


Figure 2.1: Strategy for controlling stream orientation. (a) Device design. The flow device consisted of two stacked chambers with a 2.5 μm thick Mylar membrane sandwiched between them supporting cultured cells. A pulsed Nd:YAG laser beam was focused near the top surface of the membrane to ablate pores through which the reagent could pass from the lower chamber into the cell-dosing chamber. The resultant reagent streams were used to dose selected downstream targets. (b) Valve schematic for changing flow direction. Eight solenoid pinch valves were used to change flow direction in the cell-dosing chamber. Thick solid lines denote the feed tubes and thinner lines denote drains. Each valve controlled one flow direction, yielding a total of eight possible directions. (c) Simplified valve schematic showing flow inside a single channel. The channel—one of the four channels of the asterisk flow cell that forms the cell-dosing chamber—is connected to two pinch valves, x and x^* . When both pinch valves are closed, there is no flow through the channel (left panel). When pinch valve x is open (and x^* is closed), the flow direction is towards the right (middle panel), and when x^* is open (with x closed), the flow direction is to the left (right panel).

The bottom (reagent) flow cell consisted of a single 31 mm long x 1 mm wide channel. The upper flow cell, which contained the cell medium, was composed of four intersecting channels arranged in an asterisk-like geometry. Each channel had the same dimensions as the reagent channel. Note that the height of the channels was determined by the thickness of the adhesive sheets used (0.12 mm). PDMS (GE Silicones, RTV 615; Niskayuna, NY) gaskets, containing access ports for inserting the feed and drain tubes, were used in conjunction with the flow cells to establish flow inside the channels.

Masters for the reagent gasket were created by gluing two pieces of polyurethane-coated wires (0.9-mm diameter) to the bottom of a Petri dish using cyanoacrylate (super glue) in an orientation initially normal to the surface. At a height of ~2 mm, the wires were bent parallel to the surface of the Petri dish. PDMS, mixed at a 10:1 ratio of monomer to curing agent, was poured into the Petri dish mold, and cured overnight in an oven at 60 °C. The hardened polymer was separated from its master by pulling out the wires, and the mold was cut to its final form using a razor. The gasket for the cell-dosing chamber was fabricated in a similar fashion except sixteen pieces of thicker solder wires (1.27-mm diameter) were used to create the masters.

The entire device, consisting of the membrane sandwiched between the two flow cells with their corresponding gaskets, was assembled on a microscope stage, with one of the asterisk channels aligned with the reagent channel. A plexiglass plate with two screws was used to clamp the assembly tightly onto the stage, which helped in securing the seal between the flow cells and corresponding PDMS gaskets, thus preventing leaks. Screws were further tightened during the experiment if any leaks were observed. An intermediate borosilicate glass piece was placed between the top PDMS gasket and the plexiglass plate

to prevent any compression of the PDMS gasket that may result from clamping. This process yielded two flow chambers separated by the polymer membrane (**Figure 2.1a**).

Cells were cultured on the topside of Mylar membranes (**Figure 2.1a**). Pieces of membrane, stretched taut and affixed using permanent double-sided adhesive tape (3M, 665; St. Paul, MN) to plastic frames, were washed multiple times with deionized water and ethanol, after which they were air-dried at room temperature and mounted between the two flow chambers (described above).

Feed and drain tubes were connected to both flow chambers. Solutions were supplied by syringes driven by electro-mechanical pumps (Braintree Scientific, BS-9000; Braintree, MA). Platinum-cured silicone tubing (0.8-mm inner diameter; Cole-Parmer, 95802-01; Vernon Hills, IL), recommended for use with solenoid pinch valves (described below), was used to provide fluidic connection between the chambers and syringe pumps on the feed side and on the reagent drain line. The same type of tubing with a larger inner diameter (1.6 mm; Cole-Parmer, 95802-02) was used for the drain lines from the upper (dosing) chamber, a configuration that resulted in pressure-driven transfer of the reagent into the cell-dosing chamber. In addition, a small tube (~0.4-mm outer diameter) typically was inserted at the end of the reagent drain tube to create additional pressure within the reagent chamber. Separate syringe pumps delivered cell medium to the upper chamber and desired reagent to the bottom chamber. The feed line supplying the cell medium was split into eight lines using a PDMS manifold, fabricated using standard molding processes. Similarly, all of the drain lines from the cell-dosing chamber were connected via another PDMS manifold to a syringe driven by a third pump operated in the withdrawal mode to provide suction, a modification that was found useful in

preventing leaks within the upper chamber. The push and pull rates of the supply and suction pumps of the upper (cell-dosing) chamber were set to equal values.

Eight electrically-controlled solenoid pinch valves (Bio-Chem Fluidics, 100PD2; Boonton, NJ) were used to change the flow direction in the cell-dosing flow chamber (**Figure 2.1b**). The pinch valves were interfaced with the computer using a Desktop Connector Block (National Instruments, SCB-68; Austin, TX) to control the activation of valves using LabView software (National Instruments). Each channel of the cell-dosing chamber was connected to two pinch valves to obtain two flow directions, as shown in **Figure 2.1c**, yielding a total of eight flow directions from the four channels of the asterisk chamber. As seen from the figure, both feed and drain tubes were pinched to control flow directionality. To comply with the tubing diameter specified by the supplier of the pinch valves (0.8-mm inner diameter), a small piece of the 0.8-mm tubing (used in the feed lines) was inserted in each drain tube for the pinching action.

Piezoresistive silicon pressure sensors (Freescale Semiconductor, MPVZ5010G; Austin, TX) were incorporated in the feed lines to monitor pressure in the two chambers. This was done by splitting a feed line using a PDMS T-splitter, such that one line was directed to the pressure sensor and the second to the appropriate channel. The pressure (p) inside the flow chambers can be modeled using the following equation [30]:

$$p = 12 \frac{Q\mu L}{wh^3} \quad (2.1)$$

Where, Q is the volumetric flow rate, μ is the fluid viscosity, and L , w , and h are the length, width, and height of the channel, respectively. This equation describes the pressure inside a long, wide channel; *i.e.*, for h/w (which is equal to 0.12 in this case) $\ll 1$

and h/L (equal to 0.0039) $\ll 1$. Even though the first condition was not fully met here, this equation provided a reasonable estimate of the pressure inside the flow chambers.

Using the above equation, the pressure in the two chambers was calculated to range between 0.4 – 2.7 kPa as Q varied between 0.10 – 0.50 mL min⁻¹. Note that there is a ~7-fold change in pressure between the lower and higher values with a 5-fold change in the volumetric flow rate. This calculation assumes typical experimental conditions in which a 6% (w/v) bovine serum albumin (BSA) solution is flowed in the reagent chamber with cell medium in the dosing chamber. The higher viscosity of the 6% BSA solution (1.5 cP) [31] compared to the cell medium (1 cP; assumed to be same as the viscosity of water), with all the other parameters of **Equation 2.1** remaining the same, generate the higher pressure values. Given this pressure range, sensors with pressure outputs ranging from 0 – 10 kPa were used for recording. Pressures could be monitored in near real time using LabView as a result of the fast response time of the sensors (1 ms although this resolution may be affected by processing delays arising from LabView). Flow rates in the two chambers were manipulated to change the pressure gradient between them, providing an additional means to tune laminar stream characteristics.

2.2.1.1 Alternate device configuration

A simpler cross-shaped cell-dosing chamber was employed in some experiments (as indicated in the Results). In this configuration, the flow cell consisted of two channels aligned perpendicular to each other, and was used with a gasket containing four inlet and four outlet ports. In conjunction with four solenoid pinch valves, flow could be initiated in one of the four possible directions (**Figure 2.2**). This cell-dosing chamber geometry was used in experiments where additional flow directions were not required, or in some cases, as a simplified alternative for preliminary studies. The design of the reagent chamber remained unchanged.

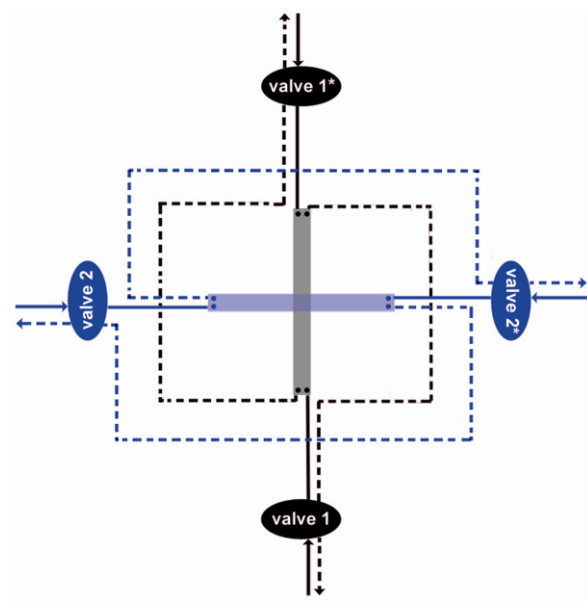


Figure 2.2: Valve schematic for changing flow direction inside a cross cell-dosing chamber. Four solenoid pinch valves were used to change flow direction in the cross cell-dosing chamber. The solid lines denote the feed tubes and the dashed lines denote drains. Each valve controlled one flow direction, yielding a total of four possible directions.

2.2.2 Chemicals and reagents

KCl (P-9541), MgCl₂ (M-8266), and fMLP (F3506) were purchased from Sigma-Aldrich (St. Louis, MO). D-Glucose (4912) and CaCl₂ (4225) were purchased from Mallinckrodt Baker, Inc. (Paris, Kentucky). HEPES sodium salt was obtained from Acros Organics (327260025; Morris Plains, NJ), Na₂HPO₄·7H₂O from EM Science (SX0715-1; Gibbstown, NJ), and NaCl was purchased from Fisher Chemicals (S271; Fair Lawn, NJ). MitoTracker Green FM dye was obtained from Invitrogen (M7514; Carlsbad, CA). All chemicals were used without additional purification.

2.2.3 Cell culture

HL-60 cells, kindly provided by Dr. O. D. Weiner (Department of Biochemistry, University of California at San Francisco), were cultured in RPMI-1640 medium (containing L-glutamine and HEPES; catalog no. 22400) supplemented with 10% (v/v) fetal bovine serum (FBS; 10082), all purchased from Invitrogen. Flasks were maintained at 37 °C in a 5% CO₂ atmosphere. These cells have a doubling time of 36 – 48 hours. To induce differentiation, 1.3% (v/v) dimethyl sulfoxide (DMSO) was added to a culture flask containing $\sim 0.1 \times 10^6$ cells mL⁻¹, and the cells were incubated for 3 – 4 days without changing the cell medium. On the day of an experiment, cells were centrifuged for 5 min at 300 x g, then washed three times in Gey's medium (6 mM KCl, 138 mM NaCl, 5 mM glucose, 1 mM Na₂HPO₄, 20 mM HEPES, 1 mM MgCl₂ and 1 mM CaCl₂, pH 7.4) containing 0.5 – 1% (w/v) BSA (Equitech-Bio, BAH64; Kerrville, TX), and resuspended in the same medium at densities ranging from $0.33 - 1.90 \times 10^6$ cells mL⁻¹. High purity grade BSA that was immunoglobulin and protease-free, obtained from Rockland

Immunochemicals, Inc. (BSA-50; Gilbertsville, PA), also was used in some experiments to eliminate the chemotactic effect of endotoxins on cell migration.

2.2.3.1 Cell loading

Cleaned 2.5 μm thick Mylar membranes were reactive-ion etched using oxygen plasma for 200 s (March Plasma, CS1701F; Concord, CA). For the etching procedure, the instrument was operated using an oxygen pressure of 100 mTorr at 25 °C and a power of 100 W. Using contact angle measurements, it was found that the etching procedure made the membranes extremely hydrophilic, decreasing their contact angles from $\sim 70^\circ$ to 6.7° . The etched membranes were mounted between the two flow chambers, and incubated with 0.05 – 0.10 mg mL^{-1} human plasma fibronectin (Calbiochem, 341635; San Diego, CA) by pipetting the protein solution into the upper chamber of the assembled device. After protein incubation for 1.5 h at room temperature, 200 μL of the cell suspension was pipetted into the chamber (which replaced the fibronectin solution). Cells were allowed to attach to the coated substrates for ~ 30 min, after which vacuum degassed Gey's medium (with or without BSA) was flowed in the chamber, starting at a low volumetric flow rate of 0.01 mL min^{-1} that was gradually increased to 0.20 mL min^{-1} over the next 30 min. Addition of 0.5% – 1% (w/v) BSA in the Gey's medium promoted cell migration by inhibiting cell spreading on the protein-coated membranes [32].

Gey's medium was vacuum degassed for 2 h before introduction into the dosing chamber to minimize formation of air bubbles. It was found that the degassing procedure reduced the concentration of dissolved oxygen in the medium from 8.3 mg L^{-1} , as measured before degassing, to 6.6 mg L^{-1} , the dissolved oxygen concentration of

degassed media coming out at the drain end after flowing through the cell-dosing chamber. An oxygen meter (YSI Inc., 550A; Yellow Springs, OH) was used for these measurements. No gross deleterious effects on cells were observed in the experiments reported here over periods of up to 6 h, as assessed from morphology, attachment, and motility, probably due to the high oxygen permeability of PDMS [33, 34] and higher tolerance of neutrophils compared to many other cell types (such as neurons) to low oxygen levels [35-37].

2.2.4 Membrane ablation

All studies described here were conducted using a frequency-doubled (532 nm), “MicroChip” Q-switched Nd:YAG laser (JDS Uniphase, NG-10320-110; San Jose, CA) with an average power output of greater than 25 mW, a pulse width of ~600 ps, and a repetition rate of 7.65 kHz. These values correspond to a laser peak power of ~7 kW and pulse energy of ~2 μ J. The laser output was attenuated to desired powers using a half-wave plate/polarizer pair, and then aligned into an Axiovert 135 inverted microscope (Carl Zeiss, Inc.; Germany). The laser beam was collimated to under-fill the back aperture of a 40x air objective (Olympus UPlanFl; Center Valley, PA) with a NA of 0.75, producing a Gaussian focus. Under-filling the back aperture made the ablation process less sensitive to where the laser was focused within the membrane, leading to creation of pores in a reproducible manner. Laser powers ranging from 10 – 15 mW (measured before the back aperture of the objective) were used for ablation of pores. Assuming a Gaussian beam profile and a constant power during laser pulses, corresponding laser peak

intensities at the focal point were calculated to range from $0.7 - 1.0 \text{ TW cm}^{-2}$ using the following equation:

$$I_0 = 2P_0 / \omega_0^2 \pi \quad (2.2)$$

Where, I_0 is the peak intensity, P_0 is the peak power, and ω_0 is the beam waist (calculated value = 433 nm).

Pores were ablated by focusing the laser beam at desired positions, typically near the top surface of Mylar membranes, and irradiating the membranes with a pulse-train consisting of 10 exposures of 5 ms each, spaced by 50 ms intervals. Insertion of these extended “dark” periods provided an opportunity for the ablation site to dissipate heat between periods of brief and intense irradiation resulting in more regularly sized pores than were obtained using an unbroken train of laser pulses. A range of ablation parameters were tested (laser powers, length of exposures and delays, and position of the laser focus within membranes), and it was found that ablations performed using the above parameters provided precise control over pore sizes (assessed using optical microscopy) with ~85% of the 60 ablated pores permitting solution flow across membranes. The average pore size in these measurements was found to be $5.5 \pm 0.8 \text{ }\mu\text{m}$ (including the surrounding burrs; mean \pm standard deviation). Laser exposure periods were controlled using a Uniblitz UHS1 shutter (Vincent Associates, VMM-T1; Rochester, NY).

The finished pores consisted of a 3 – 4 μm diameter aperture with a prominent lip around the pore. These features indicated that the ablation process likely involved both dielectric breakdown, caused by non-linear multiphoton ionization processes (discussed in Chapter 1), and an accompanying thermal process [38-41]. It has been shown that once the pulse durations exceed the low picosecond time scale (as in the case of the Nd:YAG

laser used in this study), threshold pulse energies for dielectric breakdown scale as $(\text{pulsewidth})^{1/2}$ [42].

Solution flow through pores and resultant formation of laminar flow streams were monitored either by flowing a fluorescent dye in the reagent chamber or by using solutions in the two chambers that had different refractive indices (*e.g.*, by dissolving a high concentration of a protein, such as BSA, in one solution).

Pores were typically ablated with an empty lower (reagent) chamber by focusing the laser beam at desired positions, and the reagent was introduced into the lower chamber after production of the pores. When ablations were performed with aqueous solutions in both the upper and lower chambers, gas bubbles created from the ablation process often adhered to the lip surrounding the pores, obstructing the reagent streams from entering the cell-dosing chamber. Such blockage could be avoided by performing ablations with an air-filled reagent chamber, an approach that required the lower chamber to be refilled with the dosing reagent after formation of the pore. Another approach involved ablating pores with an ethanol-filled reagent chamber. Since ethanol can dehydrate and kill cells [20, 43-46], the drain pressures in the two chambers were varied by changing chamber flow rates and/or height of the drain tubes, such that the cell-dosing chamber was at a higher pressure than the reagent chamber before ablations were performed. This prevented ethanol from entering the cell-dosing chamber. The dosing reagent was re-introduced after formation of the pores.

2.2.5 Microscopy

Light transmission photomicrographs were obtained on the Axiovert microscope using a Hamamatsu ORCA II scientific-grade CCD camera (C4742-98; Hamamatsu City, Japan) with MetaMorph software (Molecular Devices; Downingtown, PA), and processed using ImageJ (National Institutes of Health; Bethesda, MD) [47] and Adobe Photoshop (San Jose, CA).

To track laminar flow streams for assessment of stream switching times, a video CCD (Hitachi Denshi, Ltd., KP-M1U; Japan) was interfaced with the Axiovert, and a Sony video capture card with Sony Giga Pocket software was used to acquire images. Image stacks were processed using QuickTime Pro (Apple Inc.; Cupertino, CA) and Adobe ImageReady.

2.3 RESULTS AND DISCUSSION

2.3.1 Controlling orientation of dosing streams

To rapidly re-direct flow orientation, a cell-dosing chamber composed of an eight-ported asterisk flow cell and a corresponding PDMS gasket, containing eight inlet and eight outlet ports (**Figure 2.1a**), was designed. A feed line supplying cell media to the flow chamber was split using a PDMS manifold, and computer-controlled solenoid pinch valves were used to direct solution to any one of the eight inlet ports. To designate flow direction, each valve also controlled flow through a drain line from a corresponding outlet port positioned 180° from the inlet (**Figures 2.1b and 2.1c**). Thus, release of an individual pinch valve initiated flow in one of the eight possible directions.

Cells were cultured on the topside of a thin polymer (Mylar) membrane. Solutions containing dosing agents were directed through a two-port flow chamber on the underside of the membrane (**Figure 2.1a**), and could be induced by a pressure differential to pass into the cell-dosing chamber through pores ablated in the membrane positioned to target specific regions in culture.

Agents that entered the cell-dosing chamber formed narrow streams whose orientation was determined by the direction of media flow in the chamber. The mean 1/e stream radius 10 μm downstream from the pore edge was measured to be $\sim 5 \mu\text{m}$ when using a typical cell-dosing chamber flow rate of 0.20 mL min^{-1} , although streams were observed to fan out more at lower flow rates in the cell-dosing chamber [20]. The small vertical profile of the cell-dosing chamber (120 μm) created laminar flow conditions (calculated Reynolds number $\approx 3^\dagger$) [48] that minimized convective mixing, and produced

relatively high linear flow rates even at positions close to the membrane surface. At the top surface of motile HL-60 cells (measured relative to the substrate), estimated to be $\sim 3.6 \mu\text{m}$ [49], the linear flow rate (v_x) was calculated to be 4.9 mm s^{-1} when pumping solution through the cell-dosing chamber at a volumetric flow rate of 0.20 mL min^{-1} , using the following equation [30]:

$$v_x(y) = \frac{3}{2} \frac{Q}{wh} \left(1 - \frac{4y^2}{h^2} \right) \quad (2.3)$$

Where, h and w are the height and width of the channel, respectively, y is the distance from the center of the channel, and Q is the volumetric flow rate. Importantly, most motile cell types, including neutrophils, experience negligible deleterious effects under such flow conditions [50-52].

To further characterize the flow streams, the Péclet number (Pe), which is a dimensionless value that compares the typical time scale for diffusive transport to that for convective transport in a channel with a given height h , was calculated using the following equation [2]:

$$Pe = v_{avg}h/D \quad (2.4)$$

Here, v_{avg} is the average linear flow rate, and D is the diffusivity of the species of interest.

†Reynolds number, $Re = \rho v_{avg}h/\mu$, where ρ is the solution density, μ is the viscosity, v_{avg} is the average linear flow rate, and h is the height of the channel [2, 3].

For a typical cell-dosing chamber flow rate of 0.20 mL min^{-1} , which corresponds to an average linear rate of 2.8 cm s^{-1} , and $D = 6 \times 10^{-7} \text{ cm}^2 \text{ s}^{-1}$ for BSA streams [3], the calculated Péclet number is $\sim 55,000$. This large value implies that convection is the dominant mode of transport with minimal diffusive transport along the flow direction. As a result, well-defined dosant streams could be established in the cell-dosing chamber that experienced little diffusional degradation over distances of tens of microns downstream from the pore (**Figure 2.3a**).

Figure 2.3a shows an image overlay of the eight stream orientations obtained by changing flow directionality in the cell-dosing chamber. Here, streams emerged from a single central pore ablated in a $2.5 \text{ }\mu\text{m}$ thick Mylar membrane using a tightly focused Nd:YAG laser. A solution of 6% (w/v) BSA was flowed through the pore to visualize streams based on refractive index discontinuities. As shown, the nominal angle between two successive flow orientations using this approach was 45° .

To effectively target cells, it is critical that the direction of dosing streams be controlled accurately. The histogram of **Figure 2.3b** reveals the accuracy of stream directionality by showing the absolute angular difference between the expected and obtained directions in the absence of cells. Streams were switched to twenty-four positions in three separate experiments (eight distinct directions/experiment x three experiments). Each experiment was conducted on a different day using new flow cells outfitted with fresh sections of membrane. In 50% of the trials, this difference was 2° or less, and in no case did it deviate by more than 7° .

Similar results were obtained when stream directions were switched in the presence of moderate surface densities of motile HL-60 cells. In these studies, two

separate experiments were performed in which 0.33×10^6 and 0.43×10^6 cells mL^{-1} were plated on the topside of Mylar membranes mounted inside the flow-cell device (see Experimental Methods), giving densities of cells ($150 - 400$ cells mm^{-2}) comparable to those typically used in neutrophil studies (O. D. Weiner, personal communication). In 6 of the 10 trials, the accuracy of stream re-orientation was within 2° of the expected angle, and in only one instance did the deviation exceed 7° . At higher cell densities used (up to 1.9×10^6 cells mL^{-1}), deviations could be significantly larger. Since the goal of experiments performed with the multi-directional flow device was to target single cell migration, the use of moderate cell densities ($150 - 400$ cells mm^{-2}) does not pose any significant issues.

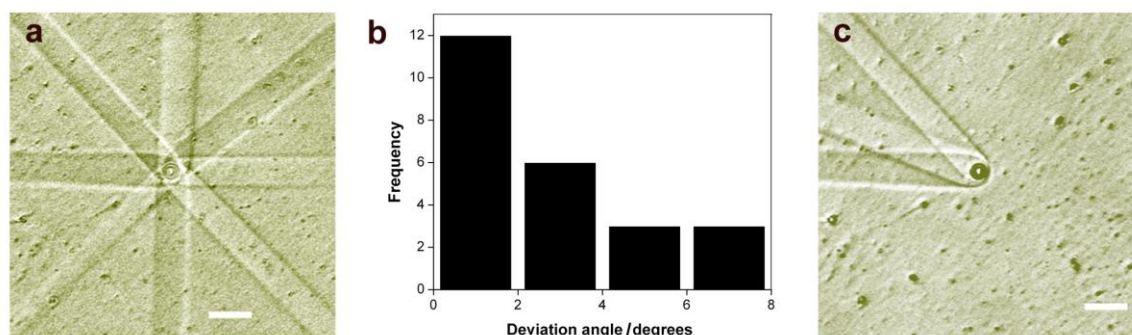


Figure 2.3: Controlling stream directionality in the cell-dosing chamber. (a) An overlay of eight images of 6% BSA streams originating from a central pore, with orientations obtained by opening each valve individually. (b) Accuracy of stream directionality. The histogram shown reports the deviation angle, defined as the angular difference between the expected and obtained flow directions, measured from 24 reagent streams obtained by opening individual valves. The deviation was found to be $2.2 \pm 2.3^\circ$ (mean \pm standard deviation). To minimize errors, the stream angles were measured $\sim 100 \mu\text{m}$ downstream from the pore. (c) An overlay of three images of 6% BSA streams demonstrating the increased angular resolution (less than 45°) achieved by opening two adjacent valves simultaneously. The two outer streams, separated by $\sim 45^\circ$, were obtained by opening single valves (*i.e.*, by activating a single pair of inlet and outlet ports), while the central stream was produced by activating these two valves simultaneously (*i.e.*, two pairs of activated inlet and outlet ports). For both (a) and (c), PBS (phosphate-buffered saline) solution was flowed in the cell-dosing chamber at a volumetric rate of 0.30 mL min^{-1} , and 6% BSA was flowed at 0.15 mL min^{-1} in the reagent chamber. Scale bars in (a) and (c), $20 \mu\text{m}$.

The design of the multi-directional flow chamber relies on pairing of inlet and outlet ports oriented 180° from each other. Although fluid flow near the center of the chamber is expected to be colinear (i.e., parallel) with the vectors that connect each inlet and outlet pair, flow paths at more peripheral regions must deviate from this direction in order to converge at the flow chamber outlet. To investigate the extent of this effect, the stream directionality was characterized as a function of pore location along a diameter perpendicular to the nominal flow direction (i.e., along the center line of the flow chamber). For streams emerging from pores ablated at distances between $\sim 0 - 350\ \mu\text{m}$ from the center of the flow chamber perpendicular to the nominal flow direction, negligible differences were found between stream directions over their initial $100\ \mu\text{m}$ (downstream from the pore)—a distance within which cells typically are dosed. Even for pore distances as great as $500\ \mu\text{m}$ from the center, the deviation in the absolute flow angle for a dosing stream was less than 5° over the initial $100\ \mu\text{m}$ (**Figure 2.4a**). Beyond this initial $100\ \mu\text{m}$, stream deviations could be significantly larger, especially in case of pores located at distances greater than $250\ \mu\text{m}$ from the center, possibly a result of fluid leaks through closed pinch valves and/or misalignment of the multi-directional flow cell between the outlet hole (in the plastic coverslip) and the flow channel (**Figure 2.4b**). The data shown in **Figure 2.4** was acquired using a simplified cross cell-dosing chamber (see Experimental Methods). This design (giving four possible orientations) was used to simplify the cell-dosing chamber setup for the analysis. Further experiments with the asterisk chamber are warranted for investigating the flow patterns inside the dosing chamber.

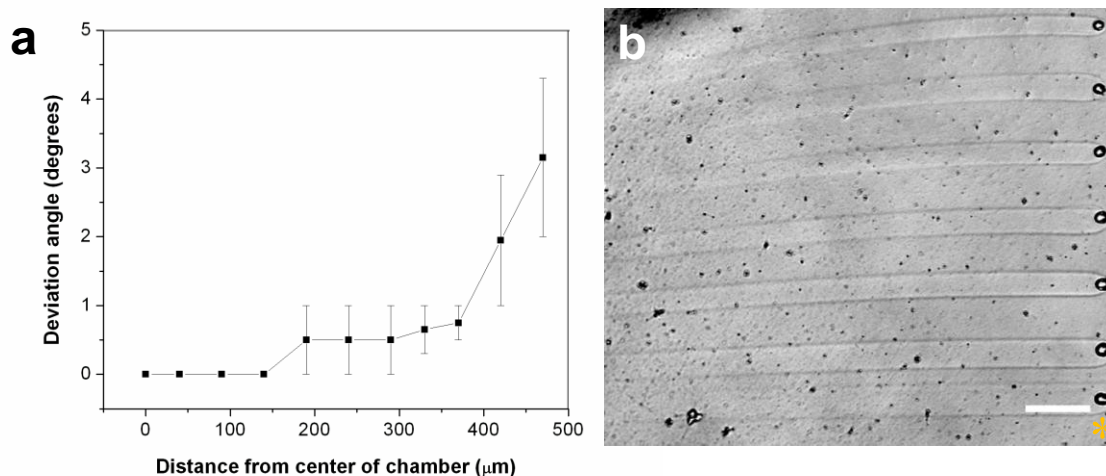


Figure 2.4: Deviation in stream directionality as a function of pore location. (a) The graph shows the deviation in reagent streams originating from photo-ablated pores along the center line of the cell-dosing chamber perpendicular to the activated flow orientation. All angles were measured $\sim 100 \mu\text{m}$ downstream from the pore, and the deviation was calculated with respect to the center stream direction. Data were acquired for two different flow orientations, and the error bars represent the standard error of the mean of the 2 trials. (b) BSA streams originating from pores ablated along the center line of the dosing chamber. The lowermost pore position (asterisk) corresponds to the center of the chamber. As seen, bending of streams occurs at increasing pore distances from the center. For both (a) and (b), PBS solution was flowed in the cell-dosing chamber at 0.5 mL min^{-1} , and 3% BSA was flowed in the reagent chamber at 0.15 mL min^{-1} . Scale bar, $50 \mu\text{m}$.

Another parameter evaluated was the reproducibility of stream directionality as a function of the switching angle needed to reach a target direction (in the absence of cells). In these studies, a given valve (regulating a single source/drain pair) was activated in conjunction with closing each of the seven remaining valves, allowing the final stream direction for each trial to be compared with the mean of the data set. This procedure was performed for four target directions. In 25 of the 28 trials, the final stream direction varied from the mean of the respective data set by less than 1° , with a mean magnitude of

variation equal to $0.4 \pm 0.5^\circ$ (mean \pm standard deviation; **Figure 2.5**). The variation in the directionality of the streams remained similarly low when the measurements were repeated 30 minutes later in the same flow-cell device.

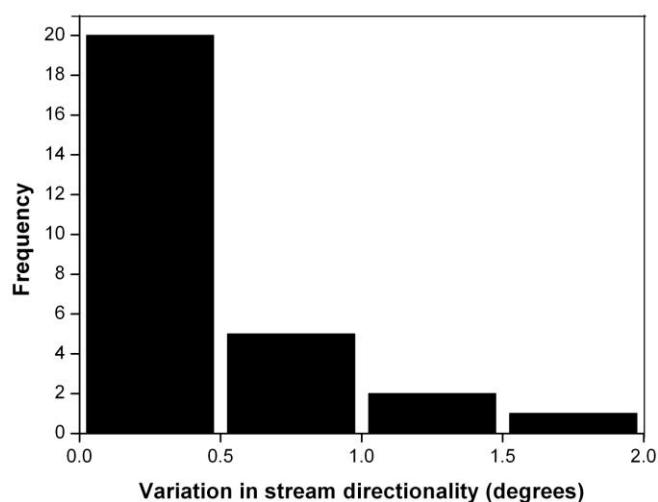


Figure 2.5: Reproducibility of stream directionality. To assess the reproducibility, a given valve was activated in conjunction with closing each of the seven remaining valves. The histogram reports the variation in the final stream direction obtained for each trial from the mean of the data set. This procedure was performed for four target stream directions providing 28 reagent streams for the analysis. For these studies, PBS was flowed in the cell-dosing chamber at 0.10 mL min^{-1} , and 3% BSA was flowed in the reagent chamber at 0.35 mL min^{-1} .

To increase the angular resolution of possible stream orientations, the results of opening two adjacent valves simultaneously (*i.e.*, giving two pairs of activated inlet and outlet ports) were evaluated. Assuming flow resistances in the two channels are equal, the resultant stream orientation ideally should lie in the center of the two activated flow vectors, providing an angular resolution of 22.5° (*i.e.*, 16 possible directions). Although deviations from the expected flow orientations were larger when simultaneously activating two valves instead of one (likely the result of variability in resistances between channels), the improvement in angular resolution obtained by this approach (**Figure 2.3c**) was useful in studies of chemotactic guidance that will be presented in the next chapter.

2.3.2 Speed of switching stream orientation

Polarized cellular processes, such as directional migration and axonal pathfinding, are controlled by dynamic chemical cues. In many instances, important variations in chemical signals take place on timescales of milliseconds to seconds, making it critical to develop techniques that not only have the ability to establish *in vitro* chemical landscapes with micrometer resolution, but can rapidly re-cast these landscapes. The capability to rapidly switch the direction of laminar flow streams would provide a means to expose cells briefly to reagents by simply changing the flow direction. This could also be useful in dosing alternate sites within a culture or on a single cell, and would provide insights into the time taken for intracellular processing and propagation of chemical signals.

To assess how rapidly the orientation of streams can be modified, video-rate imaging (*i.e.*, at 30 fps) was performed using a commercial CCD video camera and a video capture card. Solution flow was initiated in a simplified cross cell-dosing chamber

(see Experimental Methods) by opening a given pinch valve, and was switched to a direction nominally 90° away by closing the valve and opening an alternate valve.

Using this arrangement, streams could be directed through a 90° arc in ~300 ms with high reproducibility. Angular changes in flow streams proceeded in a continuous manner, though not at a constant speed, initially changing rapidly and then slowing as the cycle progressed (likely related to closing of valves; **Figure 2.6**). Because of rapid initial changes in stream orientation and the uncertainty in the start time of the valve switch relative to data acquisition (~1 frame), larger standard error bars were obtained during the initial portion of the 300 ms cycle. Notably, no gross bending of reagent streams downstream from the center of the pore was observed, at least over the 175 µm distance of assessment (even though reagent molecules close to the pore have to travel shorter arc distances compared to those further downstream). Importantly, although streams require ~300 ms to cover an entire 90° arc, much smaller angular changes may be sufficient for a stream to initiate and then terminate dosing as it sweeps across or away from a cell many micrometers away from a pore.

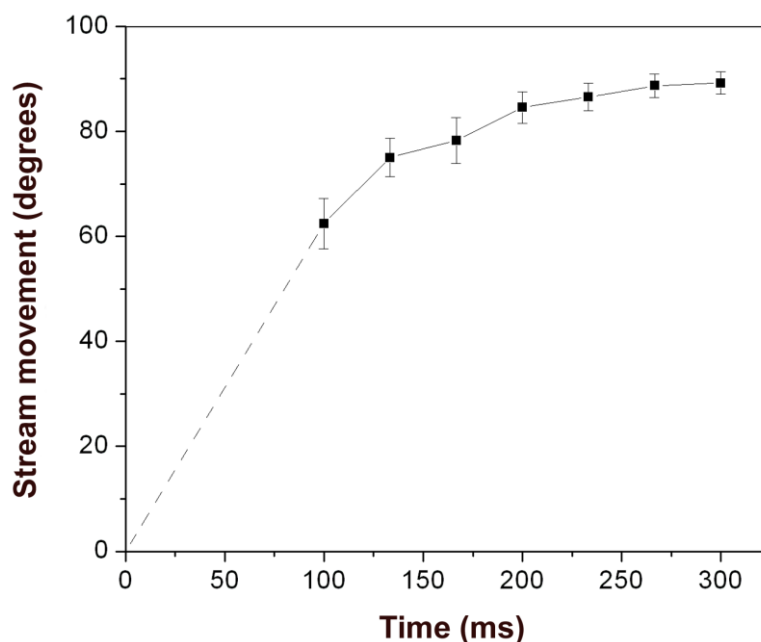


Figure 2.6: Rapid switching of stream directionality. Time plot showing the path traced by 3% BSA streams when switched between flow orientations that were 90° apart. The plot reveals a rapid initial phase followed by a decline in angular velocity as the stream approaches its final position. Data were acquired from 10 switching cycles using a video camera, and the error bars represent the standard error of the mean of the 10 trials. The rapid initial angular velocity made it difficult to image streams immediately after a switch was initiated (*i.e.*, for $t < 100$ ms). As a result, data for 33.3 ms and 66.7 ms could not be included in the plot. The $t = 0$ point was arbitrarily assigned an angle of 0°. For these studies, PBS was flowed in the dosing chamber at 0.30 mL min⁻¹, and 3% BSA was flowed in the reagent chamber at 0.20 mL min⁻¹.

The reagent streams could be switched even faster when the stream orientation was modified by opening a second valve (*i.e.*, two pairs of activated inlets/outlets). Using this arrangement, the switching time was equal to be 129 ± 33 ms (mean \pm standard deviation from 8 separate trials).

Rapid angular control provided by this dosing approach may enable studies focused on temporal dynamics of cell polarization and migration. Gradient switches inside microfluidic chambers reported by other researchers have required, in the best cases, at least one second (using a combination of photolytic cleavage and microfluidics) [53], and usually substantially longer [25, 26]. Here, the temporal resolution for cell dosing was examined by sweeping a stream of 100 nM fMLP, a bacterially derived chemoattractant tri-peptide, through an angular path that intersected an HL-60 cell. **Figure 2.7a** is a processed overlay of two sequential video images showing an HL-60 cell being dosed for the duration of a single frame period, 33.33 ms.

Various factors, including the width of a dosing stream, the distance of a cell from the pore, and the position of a cell along the 90° switching arc, can be changed to tune the time that a cell or a subcellular feature is exposed to a dosing stream. Valving parameters can also be altered to slow down the time taken for the switch. This can be achieved by appropriate selection of the flow rate, pore location, valves and direction of switch, and the valve dwell time. **Figure 2.7b** shows the same cell, which was dosed for 33.33 ms in **Figure 2.7a**, now dosed 10 times longer (333.33 ms) simply by altering the direction of switch.

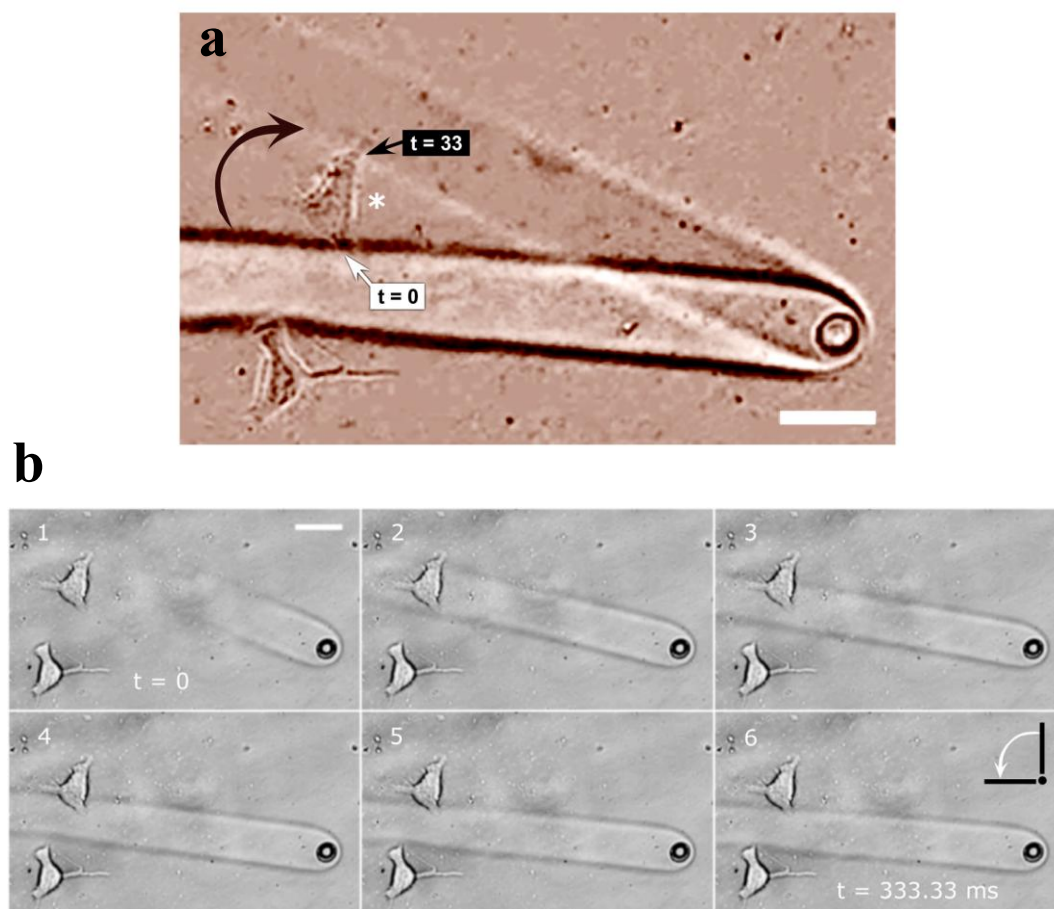


Figure 2.7: Millisecond dosing of HL-60 cells. (a) An overlay of two sequential images, each consisting of one BSA stream (and two cells), showing an individual cell (see white asterisk) dosed for the duration of a frame (*i.e.*, 33.33 ms) as the dosing stream moves in a clockwise fashion. (b) Image series showing the same cell—white asterisk in (a)—dosed 10 times longer (*i.e.*, 333.33 ms) as the dosing stream moves in a counter-clockwise fashion (white arrow in 6), dosing the cell during the slow phase of the switching cycle (**Figure 2.6**). The images are spaced 66.67 ms apart. For the fMLP concentrations and dosing periods used in these studies (four separate trials), no gross effects on cell position or polarity were observed. Gey's medium was flowed in the upper chamber at 0.30 mL min^{-1} , and 6% BSA solution containing 100 nM fMLP was flowed in the reagent (lower) chamber at 0.25 mL min^{-1} . Valving parameters were altered to allow 500 ms for the switch. Scale bars, 20 μm .

2.3.3 Application to neutrophil cultures

The ability to dose specific cells and subcellular regions with a labeling reagent was evaluated using a mitochondrial dye, MitoTracker Green FM, which is fluorescent principally when incorporated into lipid environments (*e.g.*, organelles). dHL-60 cells were attached to fibronectin-coated Mylar membranes mounted inside the flow-cell device. After ablation of a pore in Mylar, 2 μ M MitoTracker Green was flowed in the reagent chamber forming a well-defined fluorescence stream in the cell-dosing chamber, which could be directed at selected cellular targets.

Although low concentrations of MitoTracker Green (≤ 200 nM) have been reported by the reagent's supplier (Invitrogen) to selectively label mitochondria of cells, a higher concentration was used in these experiments to improve the signal-to-noise ratio. The presence of the dye in the lower chamber, Mylar autofluorescence, and adsorption of the dye to the Mylar membrane, all masked the fluorescence signal of interest (from the targeted cells). These problems could be reduced by using higher dye concentrations and extensive dye washouts (by replacing MitoTracker with buffer in the reagent chamber after dosing selected subcellular regions), as illustrated in the plot of **Figure 2.8**. At the dye concentration used in the following experiments (2 μ M), MitoTracker has been reported by the reagent's supplier (Invitrogen) to show low cellular staining specificity, localizing to a variety of cellular structures.

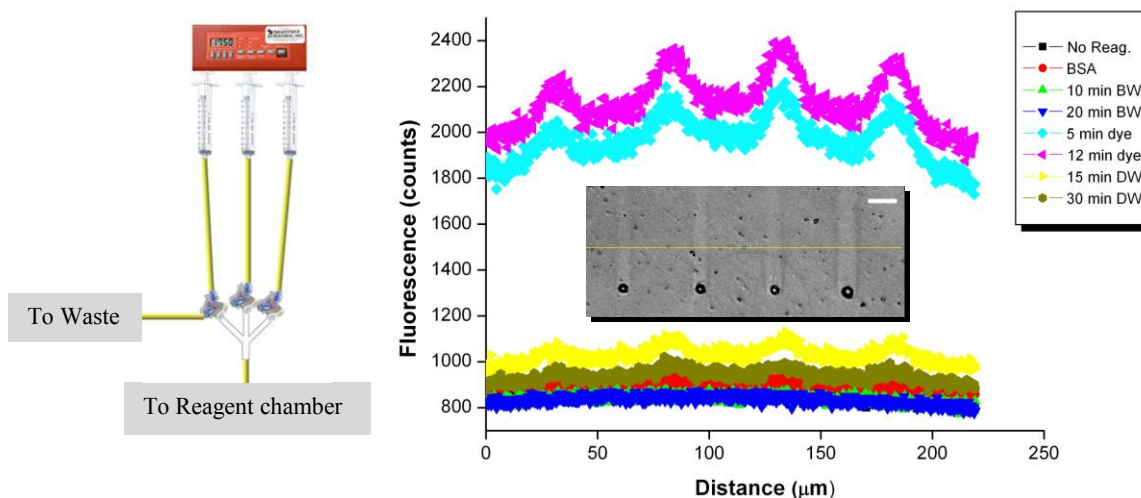


Figure 2.8: Reducing background fluorescence during MitoTracker labeling experiments. To reduce background fluorescence obtained from Mylar membranes, which served as support for adherent HL-60 cells, extensive washouts were carried out. 3-way valves, commonly used in intravenous applications, were used to switch between three solutions flowed in the reagent chamber—4% BSA (for visualization of reagent streams), 2 μ M MitoTracker, and Gey’s medium (left panel). After formation of pores, BSA was flowed in the reagent chamber forming well-defined streams in the dosing chamber (plot inset). This led to a small increase in the fluorescence, which returned to baseline values after 10 – 20 min of washout with Gey’s medium (indicated as BW in legend). Next, the dye was flowed in the chamber followed by another washout (DW). As can be seen, the fluorescence decreases to baseline values with longer dye washouts, but this also reduces the signal (4 peaks in the plot obtained from the 4 streams). All values were measured along the yellow profile line shown in the inset. Gey’s medium was flowed in the dosing chamber. Both the cell medium and reagents were flowed at 0.15 mL min⁻¹. Scale bar, 20 μ m.

As shown in **Figure 2.9**, following dosing with MitoTracker, there was a ~30% increase in emission (compared to baseline values) from a cell that was in the direct path of the reagent stream. The stream direction was controlled by activation of an individual valve (and thus, a particular source/drain pair). The only other significant emission was from the ablated pore. In **Figure 2.10**, two dHL-60 cells were dosed using a MitoTracker stream orientation obtained by opening two valves simultaneously (*i.e.*, two source/drain pairs). Out of the two labeled cells, one showed a ~25% increase in emission (from baseline values), while the second showed a ~40% increase. All other cells in the field of view showed negligible changes in their fluorescence emission values.

Figure 2.11 shows two other examples of subcellular targeting of narrow regions of dHL-60 cells, such as the leading and trailing edges (extending ~10 μm), with BSA by choosing appropriate stream orientations.

These experiments demonstrate the feasibility of using this multi-directional flow device for subcellular targeting of small motile dHL-60 cells (typically, 20 – 30 μm long). By targeting the leading and trailing edges of these cells with chemotactic molecules, such as fMLP, cell migration can be affected to provide information on how motile cells perceive and respond to chemical gradients—a goal that was pursued in experiments presented in Chapter 3.

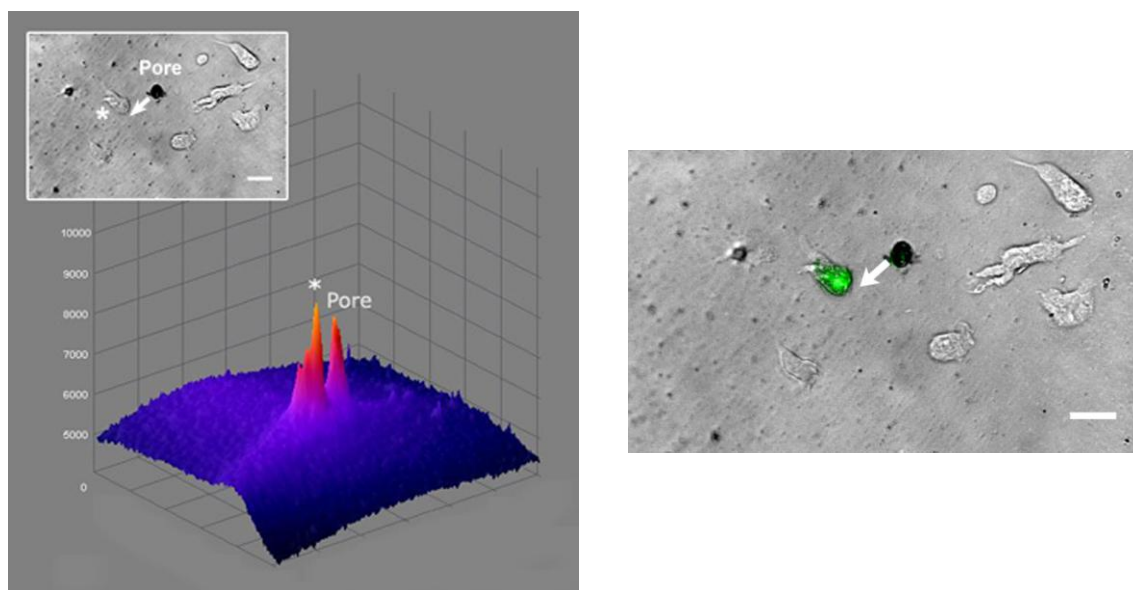


Figure 2.9: Selective labeling of HL-60 cells. The left panel shows a fluorescence intensity surface plot of the cell field (inset) after a 5-min exposure to 2 μM MitoTracker Green. The targeted cell (asterisk) is dosed using a reagent stream orientation obtained by activation of a single valve. The right panel is an overlay of the bright field and fluorescence images (acquired at almost the same time). Arrows indicate direction of flow in the cell-dosing chamber. Gey's medium with 0.5% BSA was flowed in the cell-dosing chamber at 0.20 mL min^{-1} , and the dye was flowed in the reagent chamber at 0.18 mL min^{-1} . Scale bars, $20 \mu\text{m}$.

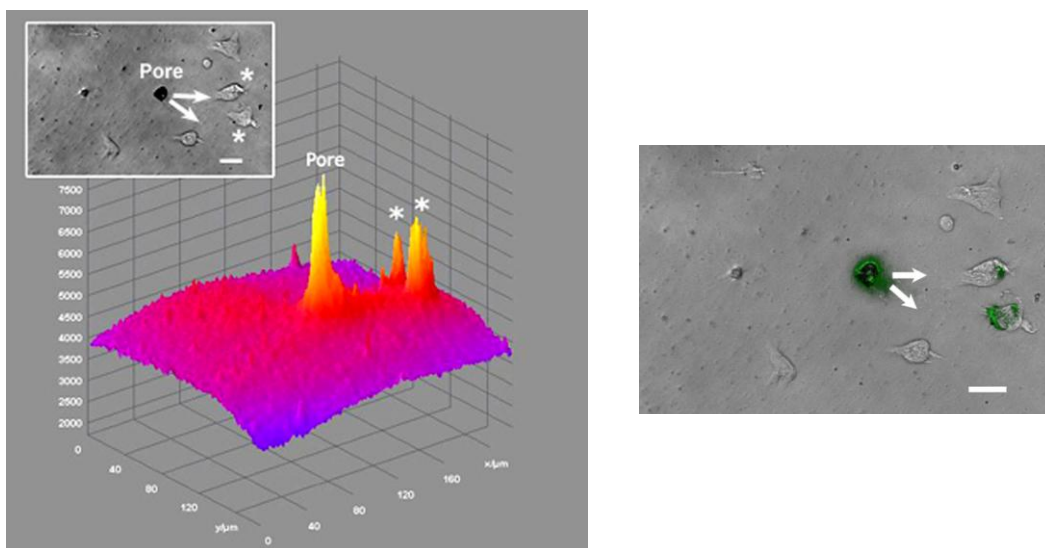


Figure 2.10: Laminar flow dosing of HL-60 cells. The left image is a fluorescence intensity surface plot of the cell field (top inset) after 10 minute exposure to 2 μM MitoTracker Green dye followed by 5 minutes of dye washout. The asterisk denotes the labeled cells. The dye orientation was obtained by opening two valves simultaneously (*i.e.*, two pairs of activated inlets and outlets). The right panel is an overlay of bright field and fluorescence images (acquired at almost the same time). Arrows represent direction of flow in the cell-dosing chamber. Gey's medium with 0.5% BSA was flowed in the cell-dosing chamber at 0.20 mL min^{-1} , and the dye was flowed in the reagent chamber at 0.18 mL min^{-1} . Scale bars, 20 μm .

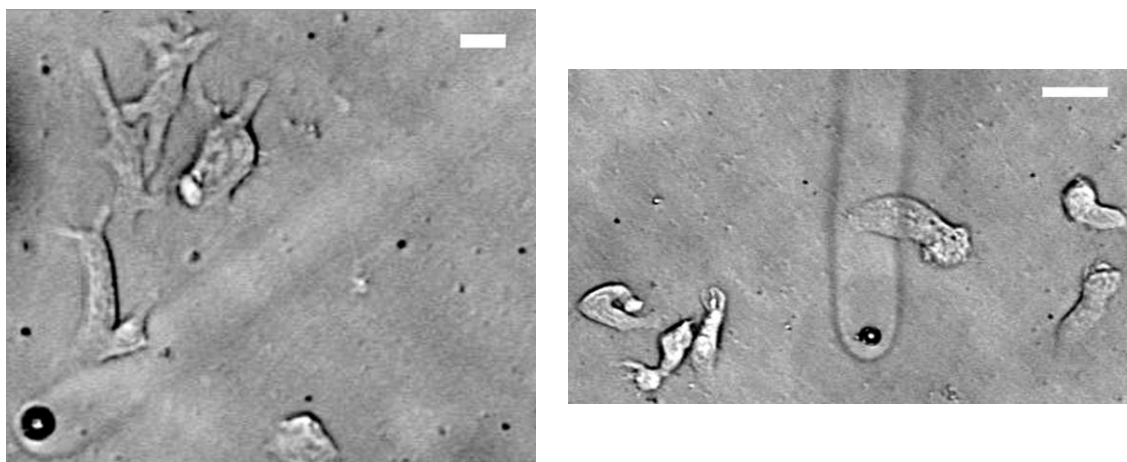


Figure 2.11: Targeting leading and trailing edges of motile cells. By controlling the directionality of BSA dosing streams, the pseudopod (leading edge) of an HL-60 cell is dosed in the left panel, and the uropod (trailing edge) of another cell (from a different experiment) is dosed in the right panel. Reagent stream orientations were obtained by activation of single pinch valves. 6% BSA was flowed in the reagent chamber, and Gey's medium with 0.5% BSA was flowed in the cell-dosing chamber. Scale bar in the left panel, 10 μm , and in the right panel, 20 μm .

2.4 CONCLUSION

These studies demonstrate an approach for creating microscopic chemical streams whose direction of flow, and thus gradient orientation at stream boundaries, can be modified with high precision and accuracy. By incorporating signal-transduction effectors within these streams, chemical signals can be presented to adherent cells with high spatiotemporal control for probing the role of external cues on polarized cellular behaviors. The versatility of this dosing strategy, in which gradients of any water-soluble effector can be repositioned within milliseconds or sustained for hours, should enable investigation of processes that transpire over a wide range of timescales.

Investigations of polarized cellular processes depend on tools for recasting extracellular chemical landscapes on time scales faster than the cellular events under study. In particular, the mechanisms by which chemotactic, motile cells respond to changes in the chemical environment have been reported to depend on the speed at which the changes take place [25]. The capability to dose neutrophils with millisecond resolution opens possibilities for rapidly modulating alternate sites within a culture, such as multiple sites on the surface of a single cell, allowing studies to be carried out on the kinetics of intracellular processing and propagation of chemical signals.

Reagent streams were directed at leading and trailing edges of motile HL-60 cells by choosing appropriate stream orientations, indicating the possibility of cell guidance, a topic that will be examined in Chapter 3.

In the present configuration, discrete flow orientations are obtained by activation of solenoid pinch valves, which are either fully open or completely restrictive to flow. Use of valves that can partially occlude flow will permit reagent-stream orientations to be changed with smaller angular increments, to obtain, in principal, any desired stream orientation (a topic that will be discussed in Chapter 4). It also may be possible to reduce the cell-dosing time further by using faster valves, such as diaphragm-based valves (*e.g.*, Bio-Chem Fluidics, 0.38 or 0.39 series), which generally have a response time of less than 5 ms. Here, valve action is achieved by motion of the diaphragm. This modification could be of particular value in studies on fast excitable cells such as cultured neurons.

Finally, a laser cutter, available at the School of Architecture at UT Austin, was used for fabrication of the flow cells described in this chapter, offering an alternative to conventional microfabrication processes, such as photolithography and PDMS molding.

In the recent years, photolithography has been extensively used for the development of microfluidic chips with potential uses in distributed healthcare industry [54, 55]. Although commonly used for microfabrication, changes in chip designs using lithographic processes require fabrication of new masters, which is often time-consuming and expensive. Also, manufacturing facilities have to be contained within a cleanroom. On the other hand, the laser cutter offers a cheap and easy-to-use alternative for rapid prototyping and development of microfluidic devices. Its usability is further enhanced by its ease of maintenance, finding a common place in academic and commercial (*e.g.*, CAD/CAM services) arenas. Although this chapter described fabrication of simple 1 mm wide channels, relatively intricate designs (helices, T- and Y-shaped channels), with feature sizes of $\sim 400\text{ }\mu\text{m}$ have been cut (Chapter 5), a first step towards realizing a fabrication platform for more complex applications.

2.5 REFERENCES

- [1] Moorjani S, Nielson R, Chang XA, Shear JB. Dynamic remodeling of subcellular chemical gradients using a multi-directional flow device. *Lab on a Chip*. 2010;10:2139-46.
- [2] Ismagilov RF, Stroock AD, Kenis PJA, Whitesides GM, Stone HA. Experimental and theoretical scaling laws for transverse diffusive broadening in two-phase laminar flows in microchannels. *Applied Physics Letters*. 2000;76:2376-8.
- [3] Truskey GA, Yuan F, Katz DF. In: *Transport Phenomena in Biological Systems*. Pearson/Prentice Hall; New Jersey: 2003.
- [4] Phung YT, Bekker JM, Hallmark OG, Black SM. Both neuronal NO synthase and nitric oxide are required for PC12 cell differentiation: a cGMP independent pathway. *Molecular Brain Research*. 1999;64:165-78.
- [5] Contestabile A, Ciani E. Role of nitric oxide in the regulation of neuronal proliferation, survival and differentiation. *Neurochemistry International*. 2004;45:903-14.
- [6] Weiner OD, Servant G, Welch MD, Mitchison TJ, Sedat JW, Bourne HR. Spatial control of actin polymerization during neutrophil chemotaxis. *Nature Cell Biology*. 1999;1:75-81.
- [7] Servant G, Weiner OD, Herzmark P, Balla T, Sedat JW, Bourne HR. Polarization of chemoattractant receptor signaling during neutrophil chemotaxis. *Science*. 2000;287:1037-40.
- [8] Wang F, Herzmark P, Weiner OD, Srinivasan S, Servant G, Bourne HR. Lipid products of PI(3)Ks maintain persistent cell polarity and directed motility in neutrophils. *Nature Cell Biology*. 2002;4:513-8.
- [9] Song H, Poo M. Signal transduction underlying growth cone guidance by diffusible factors. *Current Opinion in Neurobiology*. 1999;9:355-63.
- [10] Wang GX, Poo M. Requirement of TRPC channels in netrin-1-induced chemotropic turning of nerve growth cones. *Nature*. 2005;434:898-904.
- [11] Ji D, Lape R, Dani JA. Timing and location of nicotinic activity enhances or depresses hippocampal synaptic plasticity. *Neuron*. 2001;31:131-41.
- [12] Latour I, Gee CE, Robitaille R, Lacaille JC. Differential mechanisms of Ca^{2+} responses in glial cells evoked by exogenous and endogenous glutamate in rat hippocampus. *Hippocampus*. 2001;11:132-45.

- [13] Brown EB, Shear JB, Adams SR, Tsien RY, Webb WW. Photolysis of caged calcium in femtoliter volumes using two-photon excitation. *Biophysical Journal*. 1999;76:489-99.
- [14] Callaway EM, Yuste R. Stimulating neurons with light. *Current Opinion in Neurobiology*. 2002;12:587-92.
- [15] Boucsein C, Nawrot M, Rotter S, Aertsen A, Heck D. Controlling synaptic input patterns in vitro by dynamic photo stimulation. *Journal of Neurophysiology*. 2005;94:2948-58.
- [16] Takayama S, Ostuni E, LeDuc P, Naruse K, Ingber DE, Whitesides GM. Selective chemical treatment of cellular microdomains using multiple laminar streams. *Chemistry & Biology*. 2003;10:123-30.
- [17] Takayama S, Ostuni E, LeDuc P, Naruse K, Ingber DE, Whitesides GM. Laminar flows: Subcellular positioning of small molecules. *Nature*. 2001;411:1016.
- [18] Jeon NL, Baskaran H, Dertinger SKW, Whitesides GM, Van de Water L, Toner M. Neutrophil chemotaxis in linear and complex gradients of interleukin-8 formed in a microfabricated device. *Nature Biotechnology*. 2002;20:826-30.
- [19] Saadi W, Wang SJ, Lin F, Jeon NL. A parallel-gradient microfluidic chamber for quantitative analysis of breast cancer cell chemotaxis. *Biomedical Microdevices*. 2006;8:109-18.
- [20] Nielson R, Shear JB. Parallel chemical dosing of subcellular targets. *Analytical Chemistry*. 2006;78:5987-93.
- [21] Dertinger SKW, Chiu DT, Jeon NL, Whitesides GM. Generation of gradients having complex shapes using microfluidic networks. *Analytical Chemistry*. 2001;73:1240-6.
- [22] Jeon NL, Dertinger SKW, Chiu DT, Choi IS, Stroock AD, Whitesides GM. Generation of solution and surface gradients using microfluidic systems. *Langmuir*. 2000;16:8311-6.
- [23] Lin F, Nguyen CMC, Wang SJ, Saadi W, Gross SP, Jeon NL. Neutrophil migration in opposing chemoattractant gradients using microfluidic chemotaxis devices. *Annals of Biomedical Engineering*. 2005;33:475-82.
- [24] Irimia D, Geba DA, Toner M. Universal microfluidic gradient generator. *Analytical Chemistry*. 2006;78:3472-7.

- [25] Irimia D, Liu SY, Tharp WG, Samadani A, Toner M, Poznansky MC. Microfluidic system for measuring neutrophil migratory responses to fast switches of chemical gradients. *Lab on a Chip*. 2006;6:191-8.
- [26] Goulpeau J, Lonetti B, Trouchet D, Ajdari A, Tabeling P. Building up longitudinal concentration gradients in shallow microchannels. *Lab on a Chip*. 2007;7:1154-61.
- [27] Hauert AB, Martinelli S, Marone C, Niggli V. Differentiated HL-60 cells are a valid model system for the analysis of human neutrophil migration and chemotaxis. *International Journal of Biochemistry & Cell Biology*. 2002;34:838-54.
- [28] Collins SJ, Ruscetti FW, Gallagher RE, Gallo RC. Normal functional characteristics of cultured human promyelocytic leukemia cells (HL-60) after induction of differentiation by dimethylsulfoxide. *Journal of Experimental Medicine*. 1979;149:969-74.
- [29] Millius A, Weiner OD. Chemotaxis in neutrophil-like HL-60 cells. In: *Methods in Molecular Biology*. New Jersey: 2009;571. p. 167-77.
- [30] Truskey GA, Yuan F, Katz DF. In: *Transport Phenomena in Biological Systems*. Pearson/Prentice Hall; New Jersey: 2003.
- [31] Wetzel R, Becker M, Behlke J, Billwitz H, Böhm S, Ebert B, Hamann H, Krumbiegel J, Lassmann G. Temperature behaviour of human serum albumin. *European Journal of Biochemistry*. 1980;104:469-78.
- [32] Nathan C, Xie QW, Halbwachs-Mecarelli L, Jin WW. Albumin inhibits neutrophil spreading and hydrogen peroxide release by blocking the shedding of CD43 (sialophorin, leukosialin). *Journal of Cell Biology*. 1993;122:243-56.
- [33] Leclerc E, Sakai Y, Fujii T. Cell culture in 3-dimensional microfluidic structure of PDMS (polydimethylsiloxane). *Biomedical Microdevices*. 2003;5:109-14.
- [34] Leclerc E, Sakai Y, Fujii T. Microfluidic PDMS (polydimethylsiloxane) bioreactor for large-scale culture of hepatocytes. *Biotechnology Progress*. 2004;20:750-5.
- [35] Wood JG, Johnson JS, Mattioli LF, Gonzalez NC. Systemic hypoxia increases leukocyte emigration and vascular permeability in conscious rats. *Journal of Applied Physiology*. 2000;89:1561-8.

- [36] Hannah S, Mecklenburgh K, Rahman I, Bellingan GJ, Greening A, Haslett C, Chilvers ER. Hypoxia prolongs neutrophil survival in vitro. *Federation of European Biochemical Societies Letters*. 1995;372:233-7.
- [37] Friedman GB, Taylor CT, Parkos CA, Colgan SP. Epithelial permeability induced by neutrophil transmigration is potentiated by hypoxia: Role of intracellular cAMP. *Journal of Cell Physiology*. 1998;176:76-84.
- [38] Shirk MD, Molian PA. A review of ultrashort pulsed laser ablation of materials. *Journal of Laser Applications*. 1998;10:18-28.
- [39] Schaffer CB, Jamison AO, Garcia JF, Mazur E. Structural changes induced in transparent materials with ultrashort laser pulses. In: Sucha G, editor. *Ultrafast Lasers*. Marcel Dekker, Inc.; New York: 2003. p. 395-418.
- [40] Nahen K, Vogel A. Plasma formation in water by picosecond and nanosecond Nd:YAG laser pulses. II. Transmission, scattering, and reflection. *IEEE Journal of Selected Topics in Quantum Electronics*. 1996;2:861-71.
- [41] Stuart BC, Feit MD, Rubenchik AM, Shore BW, Perry MD. Laser-induced damage in dielectrics with nanosecond to subpicosecond pulses. *Physical Review Letters*. 1995;74:2248-51.
- [42] Joglekar AP, Liu H, Meyhöfer E, Mourou G, Hunt AJ. Optics at critical intensity: Applications to nanomorphing. *Proceedings of the National Academy of Sciences of the United States of America*. 2004;101:5856-61.
- [43] Chen SY, Yang B, Jacobson K, Sulik KK. The membrane disordering effect of ethanol on neural crest cells in vitro and the protective role of GM1 ganglioside. *Alcohol*. 1996;13:589-95.
- [44] Ewald SJ, Shao H. Ethanol increases apoptotic cell death of thymocytes in vitro. *Alcoholism: Clinical and Experimental Research*. 1993;17:359-65.
- [45] Li GC, Shiu EC, Hahn GM. Similarities in cellular inactivation by hyperthermia or by ethanol. *Radiation Research*. 1980;82:257-68.
- [46] Chen S, Sulik KK. Free radicals and ethanol-induced cytotoxicity in neural crest cells. *Alcoholism: Clinical and Experimental Research*. 1996;20:1071-6.
- [47] Abramoff MD, Magelhaes PJ, Ram SJ. Image processing with ImageJ. *Biophotonics International*. 2004;11:36-42.
- [48] Brody JP, Yager P, Goldstein RE, Austin RH. Biotechnology at low Reynolds numbers. *Biophysical Journal*. 1996;71:3430-41.

- [49] Roca-Cusachs P, Almendros I, Sunyer R, Gavara N, Farré R, Navajas D. Rheology of passive and adhesion-activated neutrophils probed by atomic force microscopy. *Biophysical Journal*. 2006;91:3508-18.
- [50] Chen S, Springer TA. An automatic braking system that stabilizes leukocyte rolling by an increase in selectin bond number with shear. *Journal of Cell Biology*. 1999;144:185-200.
- [51] Jones DA, Smith CW, McIntire LV. Effects of fluid shear stress on leukocyte adhesion to endothelial cells. In: Granger DN, Schmid-Schonbein GW, editors. *Physiology and Pathophysiology of Leukocyte Adhesion*. Oxford University Press; New York: 1995. p. 148–68.
- [52] Rainger GE, Buckley CD, Simmons DL, Nash GB. Neutrophils sense flow-generated stress and direct their migration through $\alpha V\beta 3$ -integrin. *American Journal of Physiology*. 1999;276:H858-64.
- [53] Beta C, Wyatt D, Rappel WJ, Bodenschatz E. Flow photolysis for spatiotemporal stimulation of single cells. *Analytical Chemistry*. 2007;79:3940-4.
- [54] Martinez AW, Phillips ST, Whitesides GM. Three-dimensional microfluidic devices fabricated in layered paper and tape. *Proceedings of the National Academy of Sciences of the United States of America*. 2008;105:19606-11.
- [55] Martinez AW, Phillips ST, Whitesides GM, Carrilho E. Diagnostics for the developing world: Microfluidic paper-based analytical devices. *Analytical Chemistry*. 2010;82:3-10.

Chapter 3: Directing Cell Migration by Dynamic Repositioning of Chemotactic Laminar Streams

3.1 INTRODUCTION

In 1981, Sally Zigmond and coworkers published a paper in the *Journal of Cell Biology* that examined the pattern of neutrophil locomotion in a homogeneous concentration of chemotactic factors, the response of these cells to increases in the homogeneous concentration, and most importantly, to changes in the direction of chemotactic gradients [1]. Although neutrophil chemotaxis had been previously studied, at least to a small extent, under homogeneous chemoattractant conditions by Zigmond and others [2-7], the investigation on cellular responses to chemoattractant gradient changes became one of the seminal works in the field to be often re-visited and re-debated in the years to come. The 1981 paper presented a model on how neutrophils change their direction of migration in response to chemoattractant gradient reversals. The authors found that the front of a moving neutrophil was more responsive to stimulation by chemotactic factors than its tail, and in the event of gradient reversals, cells reoriented by responding at their front and “walking around” in a circle. They proposed that the unresponsiveness of the tail could be due to the absence or inactivation of cellular machinery involved in transduction of chemotactic signals [1].

Though much progress has been made in the study of neutrophil polarization and migration, especially with respect to the types of chemotactic molecules that cells can sense [8-11] and concomitant second messenger signaling [12-20], questions regarding how neutrophils reorient themselves when the direction of chemotactic gradients are

switched still remain unanswered, largely due to the lack of tools needed to carry out such investigations. These questions are of interest, not only to the study of the inflammatory process [21, 22], but also for understanding oriented cell movements that occur during morphogenesis [23, 24]. Misregulation of neutrophil chemotaxis can play critical roles in a variety of diseases. One example is atherosclerosis in which phagocytic cells migrate toward plaques inside blood vessels, effectively increasing the size of obstruction and the likelihood of myocardial infarction [25, 26]. A second area is cancer metastasis, where neutrophils aid migration of tumor cells that eventually leads to the spread of cancer to other tissues and organs [27-31]. Lastly, neutrophils also have been implicated in the rejection of scaffolds and implants [32], underscoring the importance of understanding the mechanisms by which these motile cells respond to their local chemical microenvironments. Such studies will ultimately help in developing therapeutic strategies that optimize microbial killing and minimize host tissue damage.

Transwell assay systems, such as the Boyden chamber [33-36], are commonly used for studying chemotaxis. In these two-chamber assays, cells are placed in one of the chambers and the cellular effector in the other, with a porous filter serving as a barrier between the two compartments. Motility is measured by counting the number of cells that migrate through the filter into the compartment containing the cellular effector. In spite of the popularity of transwell assays, a result of its simplicity of use, these techniques do not allow visualization of cellular migration paths or polarization changes that occur during directed motility, thus providing only an endpoint measurement—the number of migrating cells.

A second approach for studying chemotaxis relies on the use of micropipettes for delivery of chemical agents, details of which were presented in Chapter 1. This approach has been commonly employed by Bourne and coworkers for studying neutrophil polarization and chemotaxis [14, 16, 37], and allows visualization of the motility process in single cells. An important limitation of this method is the inability to maintain concentration gradients over extended periods. Quantitative descriptions of gradient changes over time require complicated and time-consuming mathematical modeling. Lastly, the gradients created using this method are typically shallow.

To address inquiries of polarized cellular events, such as chemotaxis, tools are required that can rapidly reshape the chemical environment in which cells migrate. Although confluent laminar streams inside pre-fabricated devices have been used for the study of chemotaxis (Chapter 1) [38-40], they rely on compatibility between position of cells and dosing streams, making it difficult to dynamically target motile cells over extended periods. In Chapter 2, a multi-directional flow device was used for creating and reorienting microscopic chemical gradients *in vitro* on millisecond timescales, providing new abilities to chemically interface with cells on spatiotemporal scales relevant to biological function. In this approach, dosing streams containing any water-soluble effector are created at desired sites in culture by using a focused laser to ablate pores in an ultra-thin polymer membrane that serves as a support for adherent cells and as a barrier to an underlying reservoir containing the dosing reagent. The reagents emerging through these pores are incorporated into sharp well-defined streams by the laminar flow conditions present within the cell culture environment and are directed toward desired targets by specifying the direction of flow using a series of computer-activated sources

and drains positioned along the perimeter of the culture chamber. The power of this approach to influence and probe cell activity is demonstrated in this chapter by guidance of human neutrophil precursor cells through migration paths specified by gradients of a chemoattractant peptide. Rapid repositioning of the peptide gradients is found to guide chemotaxis via intracellular remodeling that ranges from gradual pseudopod turning to complete polarity reversal, depending on the subcellular localization of the gradients.

3.2 EXPERIMENTAL METHODS

This chapter describes the use of the multi-directional flow device presented in Chapter 2 for guidance of HL-60 cells along assigned migration paths. All device fabrication and cell culture procedures used here have already been described in the previous chapter. Although two cell-dosing chamber designs—asterisk and cross—were used in previous studies, only the asterisk cell-dosing chamber was used in the studies presented here.

3.3 RESULTS AND DISCUSSION

The utility of controlling the orientation of steep, microscopic chemical gradients, using the strategy described in Chapter 2, was assessed by investigating dynamic repolarization and motility of dHL-60 cells, a model system for neutrophil migration and chemotaxis [41, 42]. Here, dHL-60 cells were attached to fibronectin-coated Mylar membranes mounted inside the flow-cell device. After pore formation, 100 nM of fMLP, a bacterially-derived chemoattractant, was flowed in the reagent chamber, producing a chemotactic laminar flow stream in the cell-dosing chamber that could be directed at selected cellular targets. As shown in **Figure 3.1**, targeted dHL-60 cells changed their direction of movement when an fMLP gradient was established in a direction opposed to cell migration. For the data shown in **Figure 3.1**, an fMLP stream was switched multiple times between two angular orientations achieved by leaving a single valve open at all times (and thus, a particular source/drain pair) and sequentially opening and closing an adjacent source/drain pair (thus yielding a switching angle less than 45°). Although some morphological changes were apparent within a single frame of the 0.5 Hz time-lapse acquisition (*i.e.*, within 2 s) after stream reorientation, cells generally required several minutes to undergo complete repolarization.

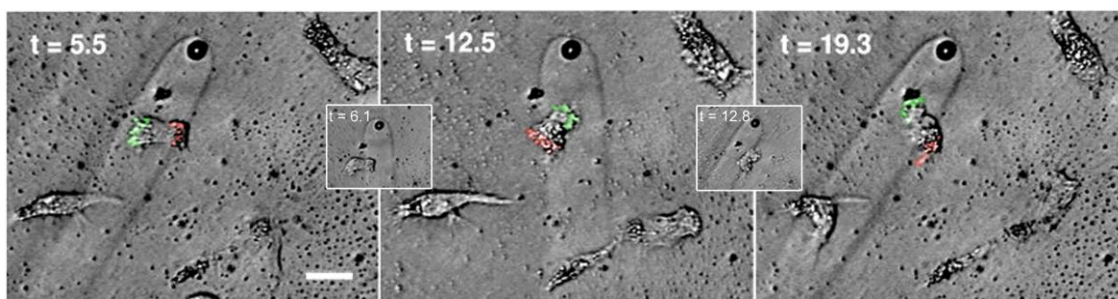


Figure 3.1: Controlling polarization and motility of HL-60 cells using streams of a chemotactic peptide. Time sequence showing an HL-60 cell changing its direction in response to reorientation of a 100 nM fMLP stream. Two instances of cell repolarization are shown. Insets show placement of the cell inside the new stream immediately after the stream orientation was switched. The gradient switch generally occurred within a single 2 s long frame of the time-lapse video. To aid in visualizing polarization, the leading and trailing edges of the cell are indicated by green and red, respectively. Time in minutes (from the time-lapse video) is denoted as t . Complete repolarization of cells occurred within 6 min after the peptide gradient flip. Throughout cell dosing, both Gey's medium and fMLP were flowed at a volumetric rate of 0.25 mL min^{-1} . 3% BSA was added for visualization of the fMLP streams. Scale bar, 20 μm .

Cells were observed to repeatedly track chemoattractant streams by changing their polarity, a process mediated by internal movement and reorganization of structural and adhesion molecules (*e.g.*, F-actin, CD44) [16, 43-45]. Following a change in stream orientation, in most cases, a cell underwent an initial collapse of its pseudopod (or leading edge) and a rearward movement of cytoplasm toward its uropod (also known as the tail or the trailing edge). This collapse led to complete or partial cell depolarization. In case of the former, the cell became rounded, whereas in the latter occurrence, the cell retained some of its morphology before repolarization. Subsequently, a new pseudopod either emerged from an entirely new position on the cell (**Figure 3.2**), or in the case of

complete polarity reversal, at the site of the former uropod (**Figure 3.3**). On occasion, a cell was able to reorient to a new fMLP gradient most efficiently by turning (rather than fully collapsing) its pseudopod (**Figure 3.4**).

Polarity reversals were characterized by a sequence of partially overlapping stages: an initial collapse of the existing protrusions at the front end of the cell, rearward movement of the cytoplasm toward the uropod, enlargement and formation of new protrusions at the (former) uropod, and contraction of the former front to form a new uropod (**Figure 3.3**) [46]. This reversal requires an internal movement and reorganization of structural molecules, including F-actin and α -actinin, at the newly formed leading portion of the cell [16, 43], and concentration of adhesion molecules, such as CD43 and CD44, at the new uropod [44, 45].

A similar sequence of events occurred when the pseudopod emerged from an entirely new position on the cell (*i.e.*, from the side). In this case, after the initial collapse of the pseudopod and rearward cytoplasmic movement, protrusions formed at a new site, which subsequently became the leading edge, often with some conservation of the uropod (**Figure 3.2**). In such cases, it has been reported that α -actinin and F-actin redistribute from the collapsed lamellipodia at the leading edge of the cell to the newly formed lamellipodia at the side, but not to the uropod [46].

In contrast, cells that changed their direction by turning (rather than fully collapsing their pseudopod; **Figure 3.4**) maintained their polarity while gradually altering their migration direction to reorient themselves with the new fMLP gradient. This mechanism of reorientation probably requires minimal redistribution of structural

molecules, such as α -actinin and F-actin, with no internal movement of adhesion molecules since the uropod is conserved.

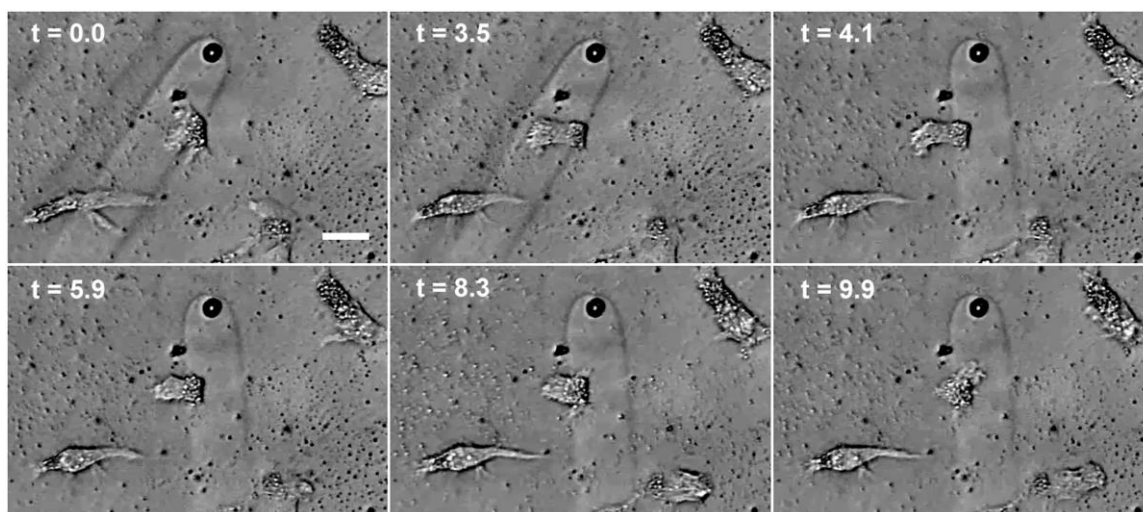


Figure 3.2: HL-60 cell reorientation by formation of pseudopod at a new site. Time sequence showing an HL-60 cell changing its direction in response to reorientation of a 100 nM fMLP stream. HL-60 cell reorientation inside the newly established fMLP gradient occurred by formation of a new pseudopod from the side of the uropod, with a partial conservation of the uropod. Time in minutes (from the time-lapse video) is denoted as t . The two angular orientations were achieved by activating two adjacent valves (and thus, two source/drain pairs) followed by closing one of the valves, respectively (thus yielding a switching angle less than 45°). Throughout dosing, both Gey's medium and fMLP were flowed at 0.25 mL min^{-1} . 3% BSA was added for visualization of the fMLP streams. Scale bar, 20 μm .

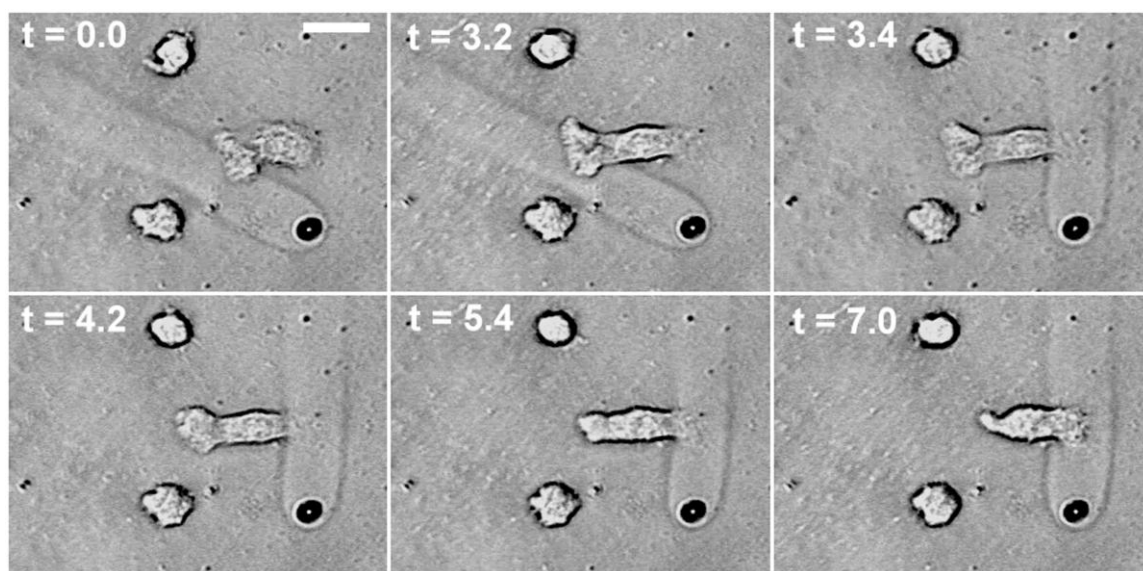


Figure 3.3: HL-60 cell reorientation via polarity reversal. Time sequence showing an HL-60 cell changing its direction in response to reorientation of a 100 nM fMLP stream. Cell reorientation inside the newly established fMLP gradient occurred by formation of a new pseudopod at the site of the former uropod preceded by the contraction of the former pseudopod to form a new uropod. Time in minutes (from the 0.5 Hz time-lapse video acquisition) is denoted as t . The two angular orientations were achieved by opening a given valve (and thus, a particular source/drain pair) followed by closing that valve and opening an adjacent valve. Throughout dosing, Gey's medium was flowed in the cell-dosing chamber at a volumetric rate of 0.20 mL min^{-1} , and fMLP was flowed in the reagent chamber at 0.15 mL min^{-1} . 3% BSA was added for visualization of the fMLP streams. Scale bar, $20 \text{ }\mu\text{m}$.

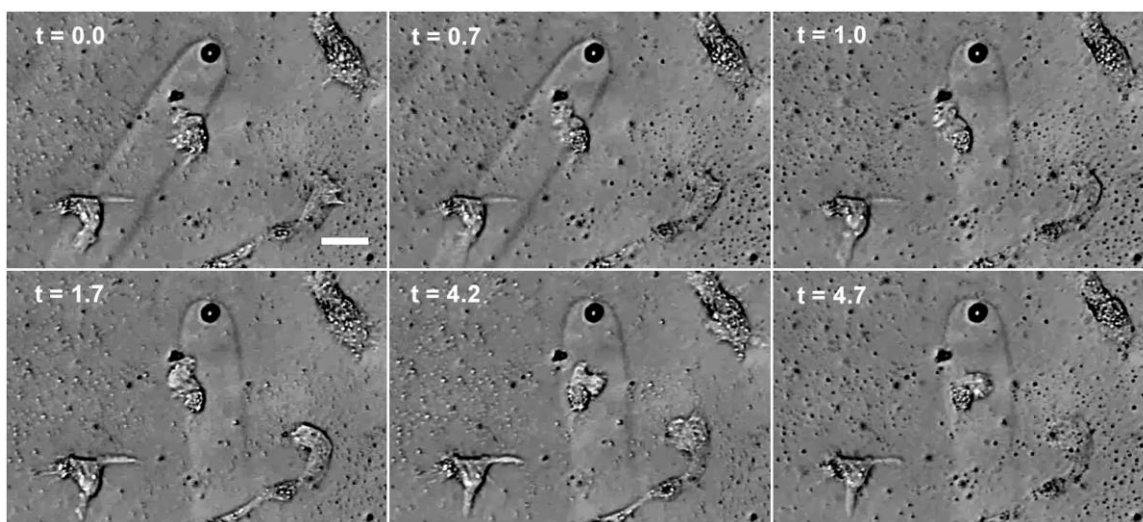


Figure 3.4: HL-60 cell reorientation via gradual turning. Time sequence showing an HL-60 cell changing its direction in response to reorientation of a 100 nM fMLP stream. Cell reorientation inside the newly established chemoattractant gradient occurred by gradual turning of the pseudopod in the direction of the new gradient while maintaining cell polarity. Time in minutes (from the time-lapse video acquisition) is denoted as t . The two angular orientations were achieved by activating two adjacent valves (*i.e.*, two source/drain pairs) followed by closing one of the valves, respectively (thus yielding a switching angle less than 45°). Throughout dosing, both Gey's medium and fMLP were flowed at 0.25 mL min^{-1} . 3% BSA was added for visualization of the fMLP streams. Scale bar, 20 μm .

Out of a total of 16 gradient switches, it was found that in half of the cases, cells changed their direction by polarity reversals, in approximately one third of the cases (5 out of 16), cells extended pseudopods from new sites, and in the remaining cases (3 out of 16), cells executed a turn to reorient themselves inside the new chemoattractant gradient (**Table 3.1**). This data was obtained from 6 different cells, some of which were exposed to multiple gradient switches.

<i>ID</i>	<i>Mechanism of reorientation</i>	<i>Number of instances</i>	<i>Example</i>
1	Formation of pseudopod at a new site	5	Figure 3.2
2	Polarity reversal	8	Figure 3.3
3	Turn	3	Figure 3.4

Table 3.1: Cellular responses to fMLP gradient switches. HL-60 cells responded to gradient switches via three different reorientation mechanisms. The *Number of instances* column indicates the number of times a particular reorientation mechanism was adopted by cells out of a total of sixteen gradient switches.

The mechanisms used by motile cells to reorient themselves following gradient switches have been debated for many years. In the 1981 paper published by Zigmond and coworkers that was discussed in the Introduction to this chapter, the researchers found that in the event of gradient reversals, achieved by placing a micropipette containing chemotactic peptide directly behind a moving cell (with reported gradient switching time of ~ 3 min), 5 out of the 8 observed cells responded by “walking around” in a circle making a series of small turns initiated near the front of the cells. The remaining 3 cells rounded to such an extent that it was impossible to determine the location on the cell that gave rise to the new pseudopod (relative to the cell morphology before depolarization). Remarkably, the researchers found that cells never projected pseudopods from their tail. Furthermore, they reported that cells rarely projected new pseudopods from the posterior half of their body [1]. These findings were corroborated by experiments conducted by Bourne and coworkers. In their 2003 paper published in *Cell*, they proposed a model that attempted to explain why a neutrophil’s pseudopod showed much greater responsiveness to the attractant than its sides or trailing edge, consequently resulting in cells following

their pseudopods and performing turns, instead of simply reversing their polarity during gradient flips [47].

The observations made by Zigmond and Bourne [1, 47] are very different from the findings of the work reported in this chapter. In 50% of the gradient switches (8 out of 16) reported here, it was found that cells changed their migration direction by reversing their polarity (**Table 3.1**). Even in the case of cells that developed pseudopods from entirely new positions (5 switches out of 16; **Table 3.1**), the new site, at least in two cases, was the side of the tail, and in another two, it involved both anterior and posterior regions of cells (**Table 3.2**). Although more studies need to be conducted to trace cellular reorientation pathways, the data in the two tables provides evidence for formation of new pseudopods from the tail and posterior region of cells in the event of gradient switches.

<i>ID</i>	<i>Site of new pseudopod</i>	<i>Number of instances</i>
1	Side of the front	1
2	Side of the tail (<i>e.g.</i> , Figure 3.2)	2
3	Side of the cell involving both anterior and posterior regions	2

Table 3.2: Sites of new pseudopods developed during fMLP gradient switches. HL-60 cells responded to fMLP gradient switches via three different reorientation mechanisms, one of which was development of a pseudopod from a new site (relative to the cell morphology before the switch). The new site involved the side of the cells. Shown is the specific location of the new site on the cells in five instances of reorientation using this mechanism.

The results obtained by Zigmond and coworkers [1] contradicted a study published by W. S. Ramsey in 1972, who investigated cellular responses to a moving micropipette (positioned using micromanipulators) containing *Staphylococcus albus* cells suspended in agar. Ramsey found that when the pipette containing the bacterial chemotactic stimulant was switched from one side of the cell to the other, the cell responded to the movement of the attractant by production of a new pseudopod on the side closer to the new location of the attractant, while the tail remained intact. If, however, the cell was moving directly toward the attractant before the gradient reversal, Ramsey found that the cell produced the new pseudopod at the region of the old tail and made a new tail in the region of the old pseudopod (*i.e.* a polarity reversal occurred) [48]. The findings of this chapter are qualitatively similar to those reported by Ramsey. Combined together they suggest that the neutrophil tail is not a permanent structure, and a cell is not always required to “turn” around to change its direction (while maintaining its polarity). Rather the cell is capable of reversing its migration direction using other mechanisms, such as forming pseudopods from entirely new subcellular sites, involving (anterior and/or posterior) side of cells, or by reversing its polarity.

Irimia *et al.* recently reported observing only polarity reversals during fast gradient switches (with switching time of ~5 s) that were always preceded by cell depolarization. No cell turning events were observed in their study [49]. This provides more evidence for the dynamic nature of cell reorientation processes during chemotactic gradient switches.

Although more polarity reversals were seen in the study reported in this chapter in comparison to the other two mechanisms of reorientation, the response to gradient

switches is probably a dynamic process in which the decision to change direction by forming pseudopods at new locations, making a turn, or a reversal depend on the initial positioning of cells within the newly established chemoattractant gradient. The steepness of the gradient and the gradient switching times are other factors that may affect the path chosen by a cell reversing its direction, which may explain the variability in cellular reorientation mechanisms observed by neutrophil biologists. Qualitatively similar to previous results published by Ramsey [48], the present study found that polarity reversals were more common when the stream was switched between the leading and trailing edges of the cell, whereas cells changed their direction via formation of a pseudopod at a new position, or by turning their existing pseudopod, when the new stream orientation intersected the side of the cells.

Lastly, the feasibility for directing dHL-60 cells over extended migration paths also was examined. **Figure 3.5** shows guidance of a dHL-60 cell through $\sim 90^\circ$ in a clockwise arc by changing the orientation of a stream of 100 nM fMLP through a series of six steps. In this experiment, stream orientations were changed in increments smaller than 45° . For each of the six dHL-60 cells steered in this manner, cells continuously reinforced their polarity (and thus, movement) toward the gradient established by the chemoattractant streams.

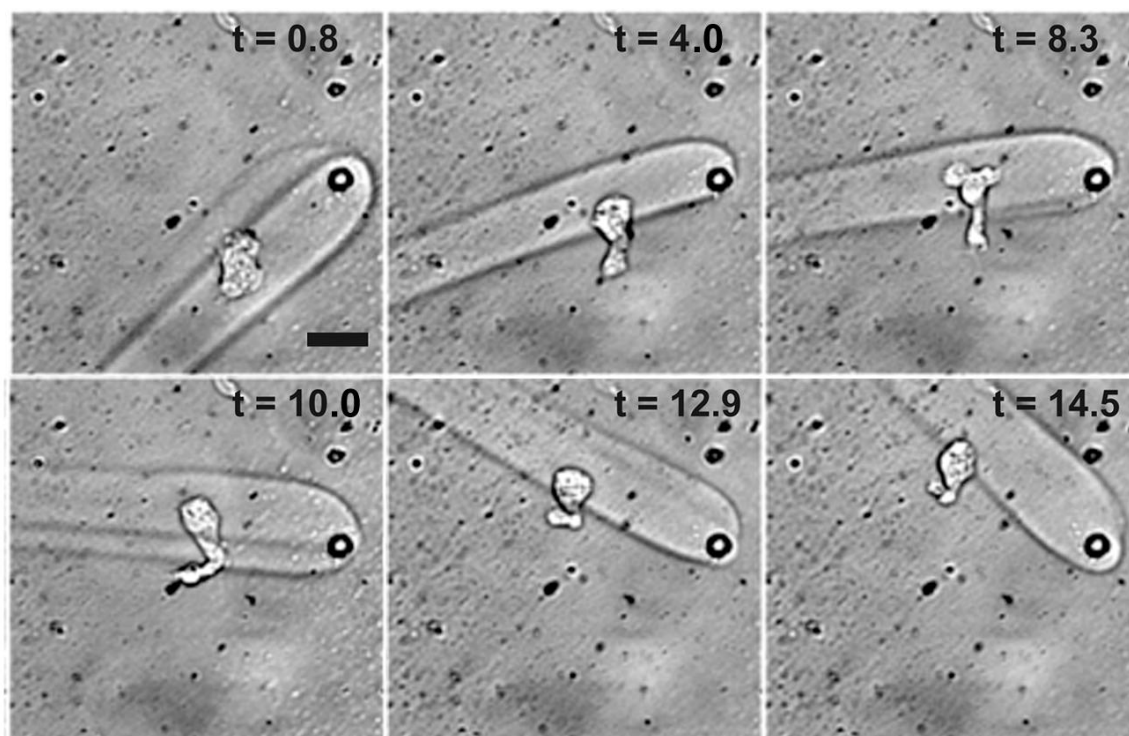


Figure 3.5: Steering an HL-60 cell through a 90° arc. An HL-60 cell is directed in a clockwise path by changing the directionality of a 100 nM fMLP stream. No backward (counter-clockwise) cell movement was observed during the entire 15 minute long time-lapse acquisition. There is a split seen in some of the stream orientations, probably caused by remnants of membrane near the pore. Time, t is given in minutes (from the time-lapse video). Gey's medium with 1% BSA (to promote cell migration) [33] was flowed in the cell-dosing chamber at 0.25 mL min^{-1} , and fMLP was flowed in the reagent chamber at 0.20 mL min^{-1} . 3% BSA was added for visualization of the fMLP streams. Scale bar, 20 μm .

3.4 CONCLUSION

In these studies, streams of the bacterially derived peptide, fMLP were directed at HL-60 cells, allowing chemotaxis to be examined with true subcellular resolution. By rapidly and precisely modifying the orientation of resultant fMLP gradients relative to the migration direction of individual cells, a range of mechanisms for altering cellular migration paths were identified. In combination with molecular imaging of cytoskeletal reorganization [12, 15], these advances in chemical dosing will enable detailed studies into how neutrophils interpret gradients of soluble chemical factors secreted by invading bacteria and effectively navigate toward sites of infection. More generally, misregulation of neutrophil chemotaxis can play critical roles in a variety of diseases, including atherosclerosis and cancer metastasis [25, 27, 28], underscoring the importance of understanding the mechanisms by which motile cells respond to their local environments.

The studies described in this chapter also demonstrated capabilities for guiding motile cells through arbitrary migration paths with micrometer resolution ($< 5 \mu\text{m}$). Such abilities to dynamically assign the positions of individual cells within culture should be useful in creating and studying the properties of small, well-defined populations of numerous cell types, including neurons, glia, and stem cells.

Notably, motile cells can sense flow-generated stress, and respond by preferential orientation and migration along the flow axis [50], making it harder to target subcellular features (like leading and trailing edges of cells) using traditional dosing approaches that have a fixed direction of solution flow. By dynamic repositioning of laminar flow streams containing chemoattractant peptides, cell guidance was achieved along defined migration

paths to obtain information on how neutrophils reorient themselves during gradient switches.

The next chapter describes methods for changing the reagent stream orientation along arbitrarily desired angles. In the configuration described in Chapter 2, discrete flow orientations are obtained by activation of solenoid pinch valves, which are either fully open or completely restrictive to flow. Use of valves that can partially occlude flow will permit reagent stream orientations to be changed with smaller angular increments, to obtain, in principal, any desired stream orientation, further enhancing the spatial control obtained using this cell dosing approach. This will allow for cell guidance and precise control of motility along extended migration paths.

3.5 REFERENCES

- [1] Zigmond SH, Levitsky HI, Kreel BJ. Cell polarity: an examination of its behavioral expression and its consequences for polymorphonuclear leukocyte chemotaxis. *Journal of Cell Biology*. 1981;89:585-92.
- [2] Allan RB, Wilkinson PC. A visual analysis of chemotactic and chemokinetic locomotion of human neutrophil leucocytes. Use of a new chemotaxis assay with *Candida albicans* as gradient source. *Experimental Cell Research*. 1978;111:191-203.
- [3] Nossal R, Zigmond SH. Chemotropism indices for polymorphonuclear leukocytes. *Biophysical Journal*. 1976;16:1171-82.
- [4] Zigmond SH. Ability of polymorphonuclear leukocytes to orient in gradients of chemotactic factors. *Journal of Cell Biology*. 1977;75:606-16.
- [5] Zigmond SH. Mechanisms of sensing chemical gradients by polymorphonuclear leukocytes. *Nature*. 1974;249:450-2.
- [6] Rosen G. Chemotactic transport theory for neutrophil leukocytes. *Journal of Theoretical Biology*. 1976;59:371-80.
- [7] Smith CW, Hollers JC, Patrick RA, Hassett C. Motility and adhesiveness in human neutrophils: Effects of chemotactic factors. *Journal of Clinical Investigation*. 1979;63:221-9.
- [8] Matsushima K, Morishita K, Yoshimura T, Lavu S, Kobayashi Y, Lew W, Appella E, Kung HF, Leonard EJ, Oppenheim JJ. Molecular cloning of a human monocyte-derived neutrophil chemotactic factor (MDNCF) and the induction of MDNCF mRNA by interleukin 1 and tumor necrosis factor. *Journal of Experimental Medicine*. 1988;167:1883-93.
- [9] Van Damme J, Van Beeumen J, Opdenakker G, Billiau A. A novel, NH₂-terminal sequence-characterized human monokine possessing neutrophil chemotactic, skin-reactive, and granulocytosis-promoting activity. *Journal of Experimental Medicine*. 1988;167:1364-76.
- [10] Yoshimura T, Matsushima K, Tanaka S, Robinson EA, Appella E, Oppenheim JJ, Leonard EJ. Purification of a human monocyte-derived neutrophil chemotactic factor that has peptide sequence similarity to other host defense cytokines. *Proceedings of the National Academy of Sciences of the United States of America*. 1987;84:9233-7.

- [11] Nakamura H, Herzenberg LA, Bai J, Araya S, Kondo N, Nishinaka Y, Yodoi J. Circulating thioredoxin suppresses lipopolysaccharide-induced neutrophil chemotaxis. *Proceedings of the National Academy of Sciences of the United States of America*. 2001;98(26):15143-8.
- [12] Millius A, Dandekar SN, Houk AR, Weiner OD. Neutrophils establish rapid and robust WAVE complex polarity in an actin-dependent fashion. *Current Biology*. 2009;19:253-9.
- [13] Servant G, Weiner OD, Herzmark P, Balla T, Sedat JW, Bourne HR. Polarization of chemoattractant receptor signaling during neutrophil chemotaxis. *Science*. 2000;287:1037-40.
- [14] Wang F, Herzmark P, Weiner OD, Srinivasan S, Servant G, Bourne HR. Lipid products of PI(3)Ks maintain persistent cell polarity and directed motility in neutrophils. *Nature Cell Biology*. 2002;4:513-8.
- [15] Weiner OD, Marganski WA, Wu LF, Altschuler SJ, Kirschner MW. An actin-based wave generator organizes cell motility. *Public Library of Science Biology*. 2007;5:2053-63.
- [16] Weiner OD, Servant G, Welch MD, Mitchison TJ, Sedat JW, Bourne HR. Spatial control of actin polymerization during neutrophil chemotaxis. *Nature Cell Biology*. 1999;1:75-81.
- [17] Kritikou E. Chemical detectors or polarity cues? *Nature Reviews Molecular Cell Biology*. 2007;8:93.
- [18] Nishio M, Watanabe K, Sasaki J, Taya C, Takasuga S, Iizuka R, Balla T, Yamazaki M, Watanabe H, Itoh R. Control of cell polarity and motility by the PtdIns (3, 4, 5) P3 phosphatase SHIP1. *Nature Cell Biology*. 2006;9:36-44.
- [19] Ferguson GJ, Milne L, Kulkarni S, Sasaki T, Walker S, Andrews S, Crabbe T, Finan P, Jones G, Jackson S. PI(3)K γ has an important context-dependent role in neutrophil chemokinesis. *Nature Cell Biology*. 2006;9:86-91.
- [20] Suire S, Condliffe AM, Ferguson GJ, Ellson CD, Guillou H, Davidson K, Welch H, Coadwell J, Turner M, Chilvers ER. G $\beta\gamma$ s and the Ras binding domain of p110 are both important regulators of PI3K γ signalling in neutrophils. *Nature Cell Biology*. 2006;8:1303-9.
- [21] Lloyd AR, Oppenheim JJ. Poly's lament: the neglected role of the polymorphonuclear neutrophil in the afferent limb of the immune response. *Immunology Today*. 1992;13:169-72.

- [22] Ratcliffe DR, Nolin SL, Cramer EB. Neutrophil interaction with influenza-infected epithelial cells. *Blood*. 1988;72:142-9.
- [23] Martin P, Parkhurst SM. Parallels between tissue repair and embryo morphogenesis. *Development*. 2004;131:3021-34.
- [24] Gwira JA, Wei F, Ishibe S, Ueland JM, Barasch J, Cantley LG. Expression of neutrophil gelatinase-associated lipocalin regulates epithelial morphogenesis in vitro. *Journal of Biological Chemistry*. 2005;280:7875-82.
- [25] Zerneck A, Bot I, Talab YD, Shagdarsuren E, Bidzhekov K, Meiler S, Krohn R, Schober A, Sperandio M, Soehnlein O. Protective role of CXC receptor 4/CXC ligand 12 unveils the importance of neutrophils in atherosclerosis. *Circulation Research*. 2008;102:209-17.
- [26] Scaccini C, Jialal I. LDL modification by activated polymorphonuclear leukocytes: a cellular model of mild oxidative stress. *Free Radical Biology and Medicine*. 1994;16:49-55.
- [27] Kim YJ, Borsig L, Varki NM, Varki A. P-selectin deficiency attenuates tumor growth and metastasis. *Proceedings of the National Academy of Sciences of the United States of America*. 1998;95:9325-30.
- [28] Honn KV, Tang DG, Crissman JD. Platelets and cancer metastasis: a causal relationship? *Cancer Metastasis Review*. 1992;11:325-51.
- [29] Coussens LM, Werb Z. Inflammation and cancer. *Nature*. 2002;420:860-7.
- [30] Opdenakker G, Van Damme J. Cytokines and proteases in invasive processes: molecular similarities between inflammation and cancer. *Cytokine*. 1992;4:251-8.
- [31] Weitzman SA, Gordon LI. Inflammation and cancer: role of phagocyte-generated oxidants in carcinogenesis. *Blood*. 1990;76:655-63.
- [32] Eriksson C, Nygren H. Polymorphonuclear leukocytes in coagulating whole blood recognize hydrophilic and hydrophobic titanium surfaces by different adhesion receptors and show different patterns of receptor expression. *Journal of Laboratory and Clinical Medicine*. 2001;137:296-302.
- [33] Boyden S. The chemotactic effect of mixtures of antibody and antigen on polymorphonuclear leucocytes. *Journal of Experimental Medicine*. 1962;115:453-66.

- [34] Grotendorst GR, Seppä HE, Kleinman HK, Martin GR. Attachment of smooth muscle cells to collagen and their migration toward platelet-derived growth factor. *Proceedings of the National Academy of Sciences of the United States of America*. 1981;78:3669-72.
- [35] Albini A, Iwamoto Y, Kleinman HK, Martin GR, Aaronson SA, Kozlowski JM, McEwan RN. A rapid in vitro assay for quantitating the invasive potential of tumor cells. *Cancer Research*. 1987;47:3239-45.
- [36] Wilkinson PC. Assays of leukocyte locomotion and chemotaxis. *Journal of Immunological Methods*. 1998;216:139-53.
- [37] Xu J, Wang F, Van Keymeulen A, Herzmark P, Straight A, Kelly K, Takuwa Y, Sugimoto N, Mitchison T, Bourne HR. Divergent signals and cytoskeletal assemblies regulate self-organizing polarity in neutrophils. *Cell*. 2003;114:201-14.
- [38] Takayama S, Ostuni E, LeDuc P, Naruse K, Ingber DE, Whitesides GM. Laminar flows: Subcellular positioning of small molecules. *Nature*. 2001;411:1016.
- [39] Jeon NL, Baskaran H, Dertinger SKW, Whitesides GM, Van de Water L, Toner M. Neutrophil chemotaxis in linear and complex gradients of interleukin-8 formed in a microfabricated device. *Nature Biotechnology*. 2002;20:826-30.
- [40] Saadi W, Wang SJ, Lin F, Jeon NL. A parallel-gradient microfluidic chamber for quantitative analysis of breast cancer cell chemotaxis. *Biomedical Microdevices*. 2006;8:109-18.
- [41] Hauert AB, Martinelli S, Marone C, Niggli V. Differentiated HL-60 cells are a valid model system for the analysis of human neutrophil migration and chemotaxis. *International Journal of Biochemistry & Cell Biology*. 2002;34:838-54.
- [42] Collins SJ, Ruscetti FW, Gallagher RE, Gallo RC. Normal functional characteristics of cultured human promyelocytic leukemia cells (HL-60) after induction of differentiation by dimethylsulfoxide. *Journal of Experimental Medicine*. 1979;149:969-74.
- [43] Keller HU, Niggli V. Colchicine-induced stimulation of PMN motility related to cytoskeletal changes in actin, alpha-actinin, and myosin. *Cell Motility and the Cytoskeleton*. 1993;25:10-8.
- [44] Seveau S, Eddy RJ, Maxfield FR, Pierini LM. Cytoskeleton-dependent membrane domain segregation during neutrophil polarization. *Molecular Biology of the Cell*. 2001;12:3550-62.

- [45] Vicente-Manzanares M, Sancho D, Yanez-Mo M, Sanchez-Madrid F. The leukocyte cytoskeleton in cell migration and immune interactions. *International Review of Cytology*. 2002;216:233-89.
- [46] Zadeh AD, Keller H. Chemotactically directed redistribution of α -actinin precedes morphological polarization and reversal of polarity in human polymorphonuclear leucocytes (PMNs). *European Journal of Cell Biology*. 2003;82:93-6.
- [47] Xu J, Wang F, Van Keymeulen A, Herzmark P, Straight A, Kelly K, Takuwa Y, Sugimoto N, Mitchison T, Bourne HR. Divergent signals and cytoskeletal assemblies regulate self-organizing polarity in neutrophils. *Cell*. 2003;114:201-14.
- [48] Ramsey WS. Analysis of individual leucocyte behavior during chemotaxis. *Experimental Cell Research*. 1972;70:129-39.
- [49] Irimia D, Liu SY, Tharp WG, Samadani A, Toner M, Poznansky MC. Microfluidic system for measuring neutrophil migratory responses to fast switches of chemical gradients. *Lab on a Chip*. 2006;6:191-8.
- [50] Rainger GE, Buckley CD, Simmons DL, Nash GB. Neutrophils sense flow-generated stress and direct their migration through $\alpha_v\beta_3$ -integrin. *American Journal of Physiology*. 1999;276:H858-64.

Chapter 4: Changing Reagent Stream Directionality in a Continuous Manner

4.1 INTRODUCTION

Cells have the capacity to sense extracellular chemical gradients that vary over microscopic scales. Numerous polarized behaviors, including chemotaxis [1-4], differentiation [5-8], and axonal pathfinding [9-12], are regulated by subcellular chemical cues, although the exact nature of how chemical microenvironments influence cellular behavior often is poorly understood. To address such questions, Chapter 2 described a technique for creating [13] and rapidly reorienting laminar dosing streams [14, 15], containing signal transduction effectors, inside cell-culture environment. The applicability of this approach to influence cellular behavior was demonstrated in Chapter 3 by guidance of human neutrophil precursor cells through migration paths specified by gradients of a chemoattractant peptide. The subcellular localization of gradients was shown to influence the morphological evolution of cells as they repolarized in response to changes in reagent stream orientation [16].

The chemical dosing strategy presented in Chapter 2 allows change of reagent stream orientation along defined angles using an asterisk-shaped cell-dosing chamber. In Chapter 3, dHL-60 cells, a neutrophil-like cell line [6, 17, 18], were steered along an arc by incremental changes in the orientation of a chemotactic laminar stream (**Figure 4.1**). Although feasibility for tracking and dosing motile cells was demonstrated, it was often difficult to target the small HL-60 cells (with lengths of attached cells ranging between 10 – 30 μm) with this device over extended migration paths due to the low angular

resolution of stream orientation, nominally 45° with a single pair of activated source and drain. This resolution was increased by simultaneously opening two valves (*i.e.*, two pairs of activated sources and drains), but the deviations from expected flow directions were larger with two valves (compared to activation of individual solenoid pinch valves; **Figure 4.2**), making it difficult to predict, *a priori*, if the new stream orientation would intersect the cell. In cases in which a cell fell between two reagent stream orientations, waiting for the cell to move into the next stream was not a practical option as the “undosed” cell was often found, as expected, to move in random directions, with the possibility that the cell would enter the next stream being only a matter of chance. Even though the chemical dosing approach presented in the previous chapters offers greater spatio-temporal control compared to the Whitesides’ parallel laminar-stream dosing method that has a single pre-defined flow orientation [19-23], it still suffers from limitations with respect to dynamic assignment of extended migration paths, a capability crucial to the understanding of oriented neutrophil movements that occur during chemotaxis. Neutrophils play important roles in host defense against several classes of infectious agents [24-26] and during morphogenesis [27, 28] but, paradoxically, these cells are also involved in the pathology of various inflammatory conditions [29-38]. Ultimately, unraveling chemotactic signaling pathways will help in developing therapeutic strategies that optimize microbial killing and minimize auto-immune damage.

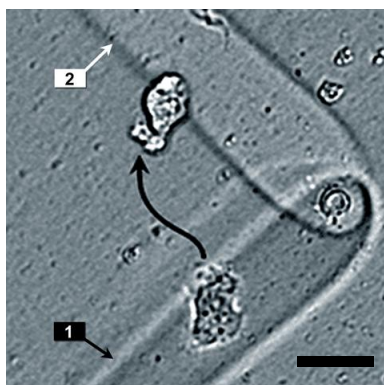


Figure 4.1: Steering chemotactic laminar flow streams in an asterisk-shaped microfluidic chamber directs chemotaxis of motile cells. The chemotactic stream orientation was changed incrementally between positions *1* and *2* over a 15-min dosing period to guide a single HL-60 cell through $\sim 90^\circ$. Scale bar, 20 μm .

Lastly, the asterisk-shaped cell-dosing chamber, used to generate the chemotactic gradient signals, is a cumbersome and time-consuming device to work with, consisting of 8 solenoid pinch valves and 16 tubes running between two syringe pumps and the dosing chamber.

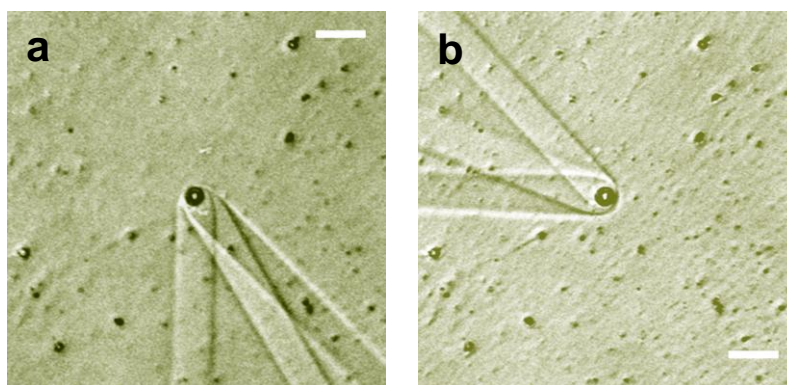


Figure 4.2: Reagent stream orientations obtained by opening two adjacent valves simultaneously. Both (a) and (b) are processed overlays of three images of 6% BSA streams demonstrating the increased angular resolution (less than 45°) achieved by opening two adjacent valves simultaneously. The two outer BSA streams, separated by $\sim 45^\circ$, were obtained by opening single valves (*i.e.*, by activating a single pair of inlet and outlet ports), while the central stream was produced by activating these two valves simultaneously (*i.e.*, two pairs of activated inlet and outlet ports). Note that in both cases the resultant stream orientation (*i.e.*, the central stream) lies closer to one of the outer streams, likely the result of variability in resistances between channels and/or fluid lines. Scale bars, 20 μm .

In the flow device configuration presented in Chapter 2, discrete flow orientations are obtained by activation of solenoid pinch valves, which are either fully open or completely restrictive to flow. To increase the angular resolution of reagent stream orientation without further increasing the complexity of the cell-dosing chamber, this chapter explores the use of valves that can partially occlude flow, permitting reagent-stream orientations to be changed with smaller angular increments, to obtain, in principal, any desired stream orientation. Preliminary results of this endeavor will be presented here.

4.2 EXPERIMENTAL METHODS

The basic design of the cell-dosing device—consisting of two stacked laminar flow chambers separated by a 2.5 μm thick Mylar membrane—remained the same as described previously (Chapter 2), except a simplified cell-dosing chamber was used in these studies. Details of the design and construction of the cell-dosing chamber are presented below. Also, all ablation and microscopy procedures used in these studies were described in Chapter 2.

4.2.1 Design and fabrication of the cell-dosing chamber

The cell-dosing chamber formed the upper chamber of the flow device and was composed of a flow cell and a PDMS gasket. The flow cell consisted of two intersecting channels arranged in a cross-shaped geometry (**Figure 4.3**), cut in 0.12-mm thick adhesive sheets using a laser cutter. Each channel was 31 mm long x 1 mm wide (*i.e.*, same dimensions as the reagent channel). The cut adhesives were aligned with plastic coverslips with holes in them to serve as entry and exit ports for fluid flow. PDMS gaskets, containing access ports for inserting the feed and drain tubes, were used in conjunction with the flow cells to establish flow inside the channels.

Masters for the cell-dosing gasket were created by bending four pieces of solder wires (1.27-mm diameter) in a V-shaped geometry and gluing the pieces to the bottom of a Petri dish using cyanoacrylate. PDMS, mixed at a 10:1 ratio of monomer to curing agent, was poured into the Petri dish mold and cured overnight at 60 °C. The hardened polymer was separated from its master by cutting the wires at the base of the V, then pulling them out. The mold was cut to its final form using a razor.

The feed line supplying cell medium was split into four lines using a PDMS manifold, and computer-controlled solenoid pinch valves were used to deliver the solution to the four inlet ports of the dosing chamber (described below). It was not found necessary to use suction in the cell-dosing chamber due to the absence of leaks, eliminating the use of an extra syringe pump—another simplification of the asterisk flow device used in previous chapters.

Four electrically-controlled solenoid pinch valves were used to switch the flow direction in the cell-dosing chamber (**Figure 4.3**). The pinch valves were interfaced with the computer using a Desktop Connector Block to control the activation of valves using LabView software. Each channel of the cell-dosing chamber was connected to two pinch valves to obtain two flow directions, yielding a total of four flow directions from the two channels of the cross chamber. Additionally, a motorized pinch clamp was used for proportioning the flow rate to obtain intermediate flow directions.

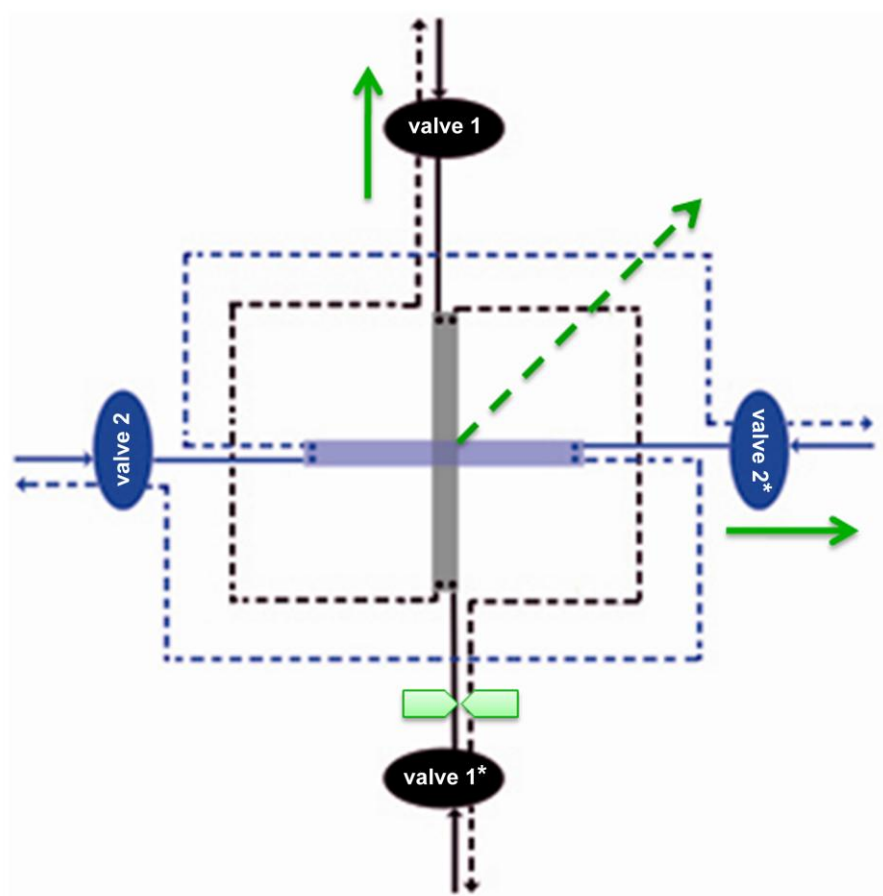


Figure 4.3: Strategy for controlling stream orientation in a continuous manner. Four solenoid pinch valves are used to change flow direction in the cross-shaped cell-dosing chamber. Solid blue and black lines denote the feed tubes and dashed (blue and black) lines denote drains. Each valve controlled one flow direction, yielding a total of four directions, which can be further increased by proportioning flow using a pinch clamp (green pentagons). The solid green arrows indicate the flow orientations obtained by opening valves 1* and 2 individually, while the dashed green arrow indicates the flow direction obtained when the two valves are activated simultaneously. Pinching and un-pinching with the clamp is used to obtain intermediate directions between the dashed and horizontal green arrows. The position of the pinch clamp can be changed during an experiment (since it is not connected “in-line”), and in conjunction with appropriate valves, can be used to obtain other intermediate directions.

For proportioning flow, a 12 V DC stepper motor (Minebea, Astrosyn 17BB-H132-11; Chatsworth, CA) was used to move a screw threaded to the lower jaw of a Delrin pinch clamp, fabricated in the Chemistry machine shop at UT Austin (**Figures 4.3 and 4.4**). Movement of the screw served to open or close the lower jaw, thus pinching or un-pinching the tube inserted between the jaws, which in turn controlled the amount of flow through the tube. A driver circuit was used for powering the motor and for interfacing the motorized pinch clamp with a National Instruments data acquisition (DAQ) card (USB-6008), so that LabView software could be used for controlling the opening and closing of the clamp.

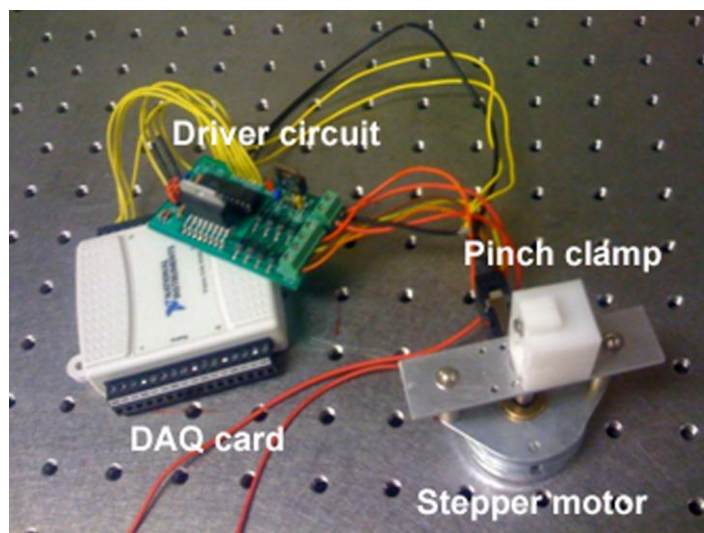


Figure 4.4: Motorized pinch clamp. A 12 V DC stepper motor was used to control movement of the pinch clamp (white). The driver circuit (green chip) powered the motor and interfaced it with a data acquisition (DAQ) card, which allowed control of the clamp using a computer.

In some cases, opening and closing of the pinch clamp was also mediated using a proportional-integral-derivative (PID) controller [39-42], designed in LabView. Real-time values from the pressure sensors, incorporated in feed lines, were input to the PID controller, which also allowed the user to set desired pressure values. The controller then used the input values as feedback for changing the pressure by iterative movement of the clamp until the current pressure was equal to the set value. The LabView interface program, thus, served as a pressure monitor, a pressure controller, and a flow controller.

4.2.2 Chemicals and reagents

Dulbecco's phosphate-buffered saline (DPBS) was obtained from Invitrogen (14190; Carlsbad, CA) and BSA was purchased from Equitech-Bio (BAH64; Kerrville, TX). Gey's medium (6 mM KCl, 138 mM NaCl, 5 mM glucose, 1 mM Na_2HPO_4 , 20 mM HEPES, 1 mM MgCl_2 and 1 mM CaCl_2 , pH 7.4; purchasing information for these chemicals was provided in Chapter 2) was also used in some studies. All chemicals and reagents were used without additional purification.

4.3 RESULTS AND DISCUSSION

To change reagent stream orientation, a cell-dosing chamber composed of a four-ported cross flow cell and a corresponding PDMS gasket, containing four inlet and four outlet ports, was designed. A feed line supplying cell media to the flow chamber was split using a PDMS manifold, and computer-controlled solenoid pinch valves were used to direct solution to any one of the four inlet ports. To designate flow direction, each valve also controlled flow through a drain line from a corresponding outlet port positioned 180° from the inlet (**Figure 4.3**). Thus, release of an individual pinch valve initiated flow in one of the four possible directions. Furthermore, two adjacent valves could be activated simultaneously to obtain additional orientations, yielding a total of eight discrete flow orientations (**Figure 4.5**). The cross cell-dosing chamber described here is a simplified modification of the asterisk chamber design discussed in Chapter 2 (**Figure 2.1**).

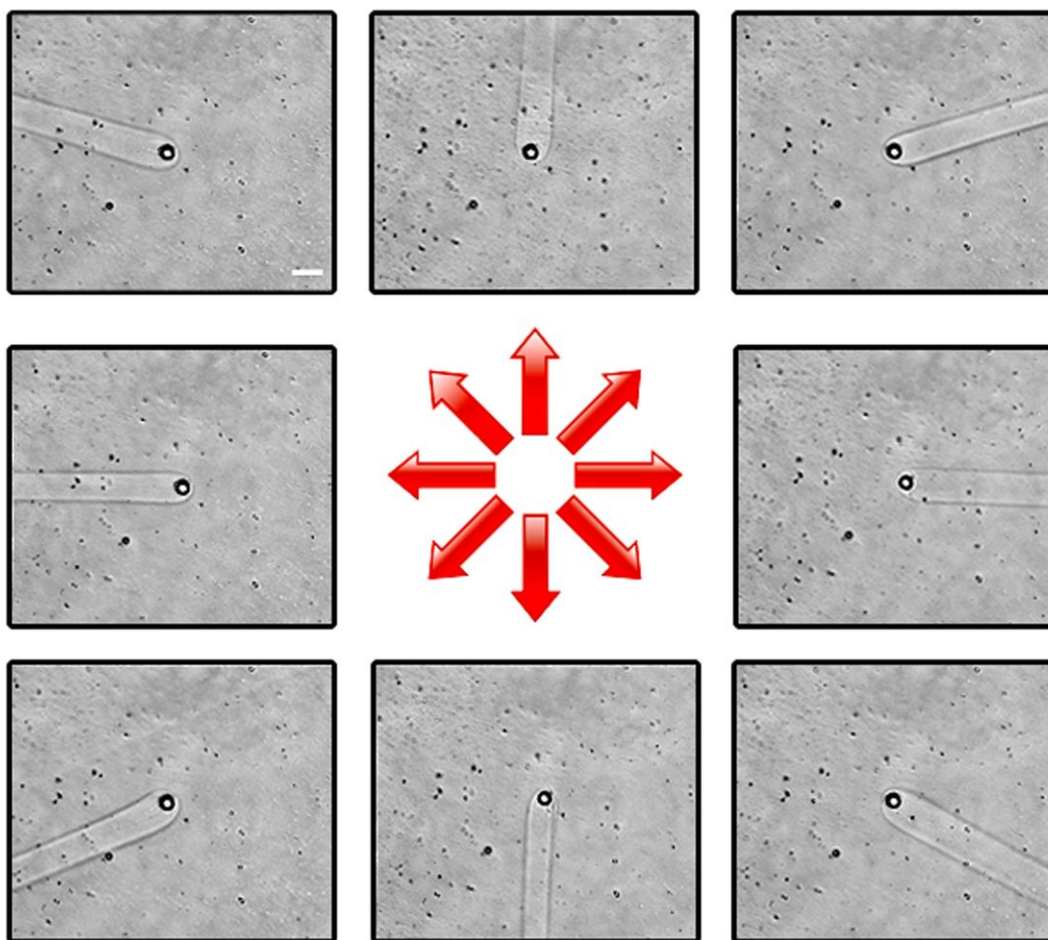


Figure 4.5: Controlling stream directionality in the cross cell-dosing chamber using solenoid pinch valves. Red arrows indicate the expected orientations of 3% BSA streams. Vertical and horizontal orientations were obtained by activation of individual pinch valves and the diagonal orientations were obtained by opening two adjacent valves simultaneously. BSA solution was flowed in the reagent chamber at a volumetric rate of 0.25 mL min^{-1} and DPBS (Dulbecco's phosphate-buffered saline) was flowed in the cell-dosing chamber at 0.50 mL min^{-1} . Scale bar, $20 \text{ }\mu\text{m}$.

Eight discrete flow orientations were obtained using solenoid pinch valves that are either fully open or completely restrictive to flow. The reagent stream orientation can be changed in a continuous manner using valves that can partially occlude or proportion flow through a pinched line. This was achieved by incorporating a motorized pinch clamp in the flow device (**Figures 4.3 and 4.4**). By opening two adjacent solenoid valves, and pinching one of the activated fluidic lines using the “analog” pinch clamp, flow through the pinched line could be proportioned to obtain intermediate stream orientations (between the orientations obtained using the solenoid pinch valves alone). Similarly, gradual opening of the line by “un-pinching” the tube could be used to proportion flow in the reverse direction.

Figure 4.6 illustrates flow proportioning using the motorized pinch clamp to incrementally change the reagent-stream orientation between 0 – 23°. Here, two solenoid valves were activated simultaneously, then the motorized pinch clamp was engaged to gradually pinch one of the activated feed lines, which permitted intermediate stream orientations between fully open and completely flow restrictive positions of the pinch clamp. The two outermost angles of the plot (0 and 23°) represent the stream orientations corresponding to the fully open and completely restrictive clamp positions, orientations that can also be obtained using the solenoids alone, while the intermediate angles were obtained by the gradual pinching action of the motorized clamp. Each angular change using the pinch clamp occurred within a single 3 s long frame of the acquired time-lapse data. The angle covered during a single step only exceeded 5° in 3 instances out of 49 angular changes that occurred during four closing trials from three independent experiments (*i.e.*, two of the trials were from the same experiment), with each experiment

conducted on a different day using new flow cells outfitted with fresh sections of membrane. Notably, a single motorized clamp can be used to proportion multiple fluidic lines without disrupting the experiment since it is not an “in-line” restriction device. Proportioning of flow to increase the angular resolution of stream orientation can be used to dynamically guide motile cells along extended migration paths.

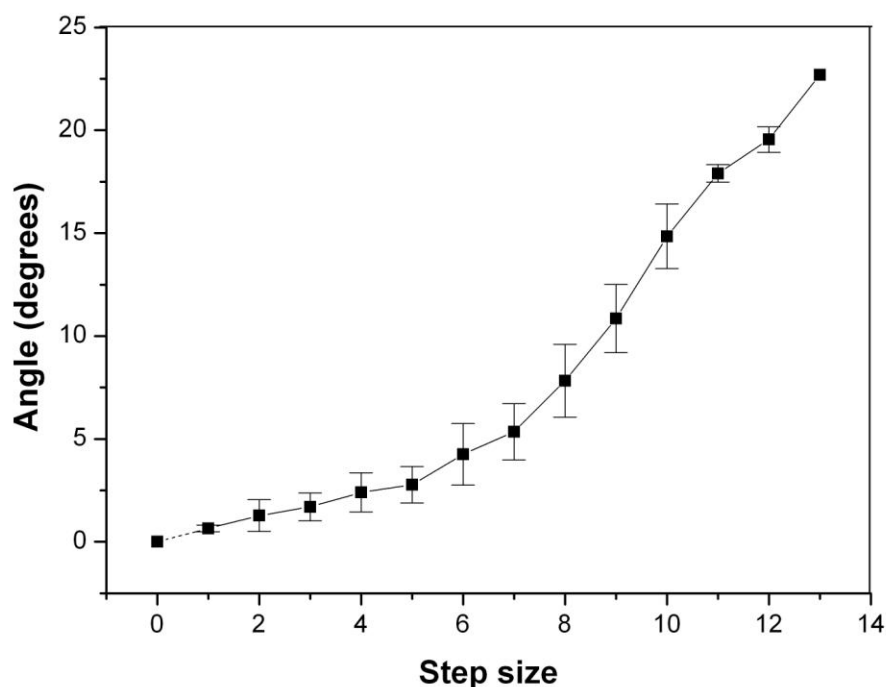


Figure 4.6: Changing stream directionality in a continuous manner. Path traced by 3% BSA streams between 0 – 23°. Data were acquired by activating two solenoid pinch valves simultaneously, followed by gradual closing of one of the activated feed lines using a motorized pinch clamp to obtain intermediate angles between the fully open and completely restrictive positions of the clamp (0 and 23°, respectively). The error bars represent the standard error of the mean of 4 trials (from 3 independent experiments). Note that the total angle covered during this process (nominally 45°) was ~23°, possibly a result of the variability in resistances between the two activated channels and fluidic lines, which affects the angle corresponding to the fully open clamp position, combined with incomplete restriction of flow obtained by pinching the feed lines alone (due to fluid leaks through the un-pinched drain line), which affects the stream angle corresponding to the fully restrictive clamp position. To minimize errors, stream angles were measured ~100 μm downstream from the center of the pore (in ImageJ). The starting point (fully open clamp position) was arbitrarily assigned an angle of 0°. For these studies, Gey's medium was flowed in the cell-dosing chamber, and BSA was flowed in the reagent chamber.

Overall, the system response was unpredictable. In **Figure 4.6**, data from four closing trials with similar angles covered between fully open and completely restrictive pinch clamp positions ($20.7 \pm 1.7^\circ$; mean \pm standard deviation) were pooled together to generate the plot. It was found that similar angles were covered during individual motor steps when the total angle (*i.e.*, the angular difference between fully open and completely closed clamp positions) was similar. This may be due to the fixed number of motor steps for a given diameter tubing, implying that when the angular difference between the two outermost clamp positions was larger, the motor would have to cover relatively larger angles during individual steps to make up for the angular difference. Even so, the motor response for larger total angles (data not shown) couldn't be predicted from the data at smaller total angles, indicating that pinching of tubes using the motorized pinch clamp was inherently a non-linear process. Also, the clamp operation was not reversible, *i.e.*, different individual angles were covered when the cycle was reversed to allow gradual un-pinching of tubes. Lastly, as seen from the plot, steps were not equiangular. These response characteristics are probably symptomatic of the non-linear nature of pinching tubes for restriction of flow. Generating look-up tables (LUTs) for a range of total angles can be cumbersome and time-consuming, and as seen from the plot (**Figure 4.6**), large error bars exist at every step, making the LUTs of little value to the user in predicting, *a priori*, the output angle.

To address some of these limitations, a feedback controller was developed. Pressure values from piezoresistive sensors were input into LabView software, which also allowed the user to set a desired pressure value. Using PID control programming

[43], the pressure was changed by pinching or un-pinching tubes inserted between the jaws of the motorized pinch clamp until the current pressure was equal to the set value.

A PID controller is a closed-loop control system, where the controller determines the input signal to a given process based on the reference signal (*e.g.*, set values of a given variable) and the measurement of the output (which serves as the feedback signal). The function of feedback control is to keep the process variable close to the desired value in spite of disturbances and variations in process dynamics. Applying the PID control law consists of properly applying the sum of three types of control actions: a proportional action, an integral action, and a derivative action [43] (**Figure 4.7**). Implementation of PID controllers requires selection of three PID parameters, the proportional, integral, and derivative gains (K_p , K_i , and K_d , respectively), a process referred to as tuning of PID controllers, and is a crucial issue in the overall controller design [39-45]. Proper selection of PID gains is critical for controlling the accuracy, response time, and stability of the output.

As shown in **Figure 4.7**, the proportional control action is proportional to the current control error, which is the difference between the output and the set values. The integral action is proportional to the integral of the control error, thus accounting for past values of the error. Finally, the derivative control is proportional to the derivative of the error. Increasing the proportional gain leads to a faster but more oscillatory output. Conversely, increasing the integral gain leads to a slower but more stable response, and lastly, increasing the derivative gain provides a damping effect on the system response. More details on the workings of PID controllers can be found in [43].

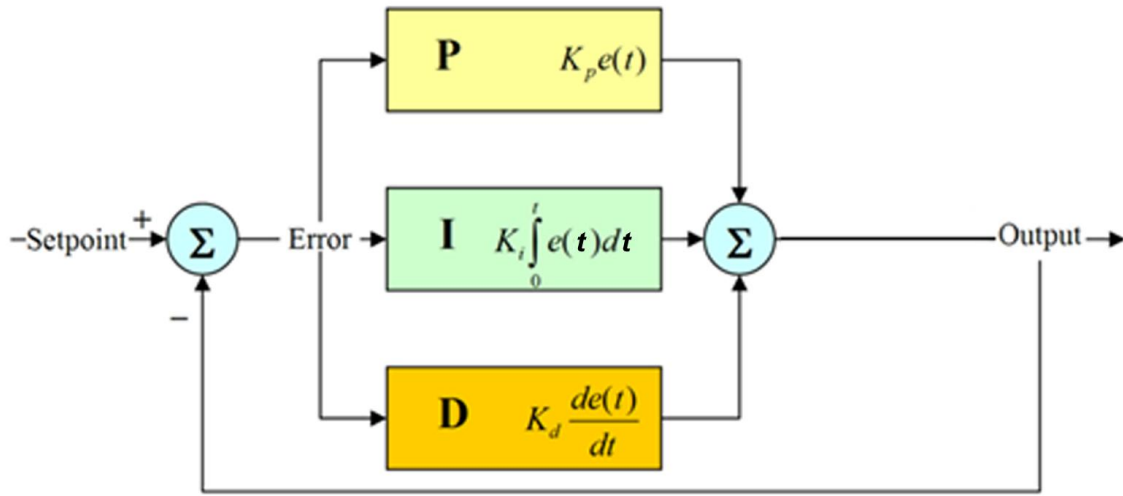


Figure 4.7: Structure of a proportional-integral-derivative (PID) Controller. The output of a PID controller is a summation (Σ) of the proportional (P), integral (I), and derivative (D) actions. The control error—which is the difference between the output and the set values—is input to the P , I , and D modules, and the modular outputs are summed to determine the PID output, which serves as a feedback signal for calculation of the error. The iterative action of PID controllers is used for achieving desired system responses.

Using the PID controller, the stream orientation could be changed in an incremental manner by activating two adjacent pinch valves, then varying the pressure in one of the activated lines by controlled movement of the lower jaw of the motorized pinch clamp, thus pinching or un-pinching the tube inserted between the jaws. When a single feed line supplying media to the cross cell-dosing chamber was split into four lines (to feed the four inlets), activation of two adjacent valves—one connected to the horizontal channel, and the other, to the vertical—followed by restriction of flow through one of the lines simply diverted the flow to the un-restricted line without a significant change in the pressure. A pressure difference was required to enable the PID controller,

which was achieved by feeding media to the cell-dosing chamber using two syringe pumps—one for feeding the two inlets of the horizontal channel, and the other for the vertical channel. Using this setup, a buildup of pressure obtained from restriction of flow was used to change the reagent stream orientation (**Figure 4.8**). The angular changes typically occurred within 5 s.

The stability of reagent stream orientation was often affected by oscillations in the PID output. These oscillations resulted when the set pressure fell between two discrete motor steps, in which case, the controller was found to toggle between the two steps to reach the set value, leading to output oscillations. Using a higher resolution stepper motor may help to reduce this problem.

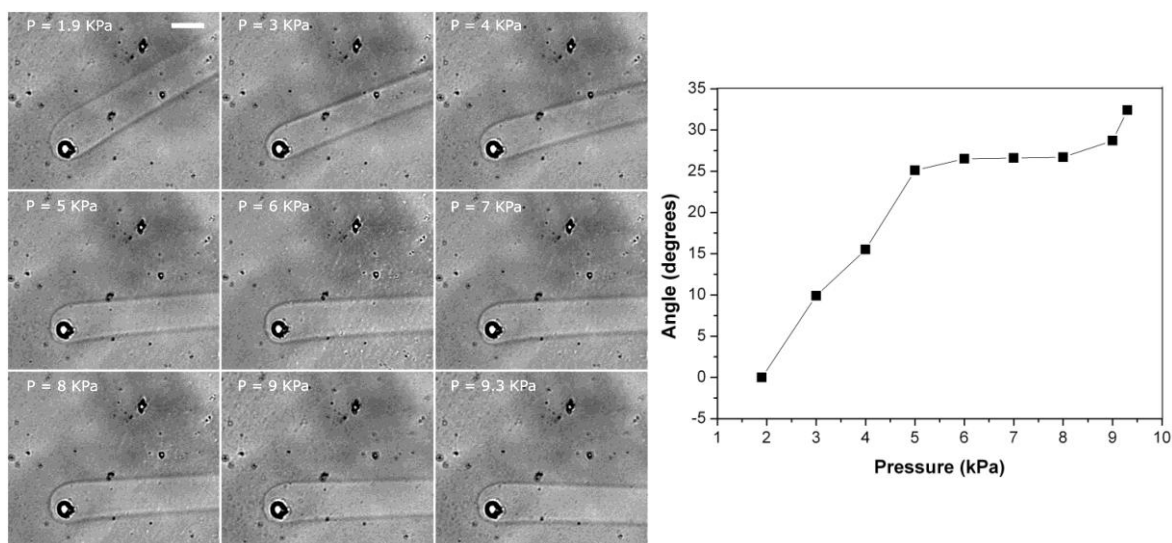


Figure 4.8: Changing orientation of a 3% BSA stream by incremental closing using PID. After activation of two adjacent solenoid pinch valves, the pressure in one of the activated lines was gradually increased, allowing small changes in the reagent stream orientation (left panel). The right panel is a plot of the stream movement data shown in the left panel. For these studies, PID gain values of $K_p = 7$, $K_i = 0.18$, and $K_d = 22$ were used, and both feed and drain tubes were pinched to obtain complete restriction of flow. Pressure changes were not equiangular (*i.e.*, for the same pressure change, different angular outputs were obtained), a result of the non-linear nature of the pinching process. To minimize errors, stream angles were measured $\sim 100 \mu\text{m}$ downstream from the center of the pore. Notably, although the total dosing flow rate is reduced to half at 9.3 kPa (compared to the flow rate at 1.9 kPa), no significant widening of the BSA stream is observed within $100 \mu\text{m}$ from the pore. It is possible that widening of the stream occurs further downstream (*i.e.*, at distances greater than $100 \mu\text{m}$). DPBS was flowed in the dosing chamber using two syringe pumps, each set at 0.25 mL min^{-1} , and BSA was flowed in the reagent chamber at 0.30 mL min^{-1} . Scale bar, $20 \mu\text{m}$.

4.4 CONCLUSION

In these studies, a motorized pinch clamp was used to proportion flow in the cell-dosing chamber for changing the orientation of reagent streams in a continuous manner. The increased resolution obtained using this approach, coupled with the capabilities demonstrated in Chapters 2 and 3, offers on-the-fly control for assignment of cellular migration paths. Such advances will enable studies into how motile cells perceive and respond to their chemical microenvironments.

The studies described in this chapter used a cross-shaped cell-dosing chamber, consisting of two perpendicular channels connected to four solenoid pinch valves. This is a simpler modification of the asterisk flow device discussed in Chapters 2 and 3. The asterisk device is a cumbersome and time-consuming experimental setup to work with, making this modification an important advantage from a practical standpoint. The reduction in complexity should also allow for easier dissemination of the chemical dosing technology.

Although increased angular resolution of stream orientation was demonstrated using a simplified flow device (relative to the asterisk design), much work needs to be done to change the stream orientation with higher accuracy and precision, which would allow the user to predict, *a priori*, the pressure or step input needed to achieve a desired output angle. Modifications such as the use of higher resolution stepper motors or a servo motor may help, especially in reducing some of the stream oscillations found using the PID controller. Other options, such as the incorporation of restriction devices that do not rely on pinching of tubes, *e.g.*, proportional valves, which restrict flow by decreasing the diameter of an internal orifice, may also be explored for increasing device accuracy.

Finally, in place of using pressure as the feedback variable, angular input to the PID controller will allow for change of reagent-stream orientation along user-defined trajectories. Control loops consisting of detection of stream position, computation, and actuation will have to be designed. To achieve angular control, stream positions will be identified by an optical system and the data will be transferred to an image processing algorithm for measuring the (current) stream angle. PID can then be used for iterative movement of the motorized pinch clamp to move the streams to their desired positions. Such control systems have been used before for electro-osmotic actuation in microfluidic channels [46]. Their incorporation in the multi-directional flow device discussed in this dissertation will provide an invaluable tool for truly dynamic changes of reagent-stream orientations.

This chapter concludes development of functionality for the cell-dosing chamber. In Chapters 2 – 4, all studies were conducted with a single reagent in the lower flow chamber. The capability to change the cellular effectors within reagent streams would increase the versatility of this dosing approach. Combined with the ability to change the orientation of reagent streams, a number of cell-dosing studies, such as sequential or simultaneous dosing of neutrophils with a chemoattractant and an inhibitor, can be envisioned. Incorporation of multiple reagents is the topic of Chapter 5.

4.5 REFERENCES

- [1] Bourne HR, Weiner OD. A chemical compass. *Nature*. 2002;419:21.
- [2] Servant G, Weiner OD, Herzmark P, Balla T, Sedat JW, Bourne HR. Polarization of chemoattractant receptor signaling during neutrophil chemotaxis. *Science*. 2000;287:1037-40.
- [3] Wang F, Herzmark P, Weiner OD, Srinivasan S, Servant G, Bourne HR. Lipid products of PI(3)Ks maintain persistent cell polarity and directed motility in neutrophils. *Nature Cell Biology*. 2002;4:513-8.
- [4] Weiner OD, Servant G, Parent CA, Devreotes PN, Bourne HR. Cell polarity in response to chemoattractants. In: Drubin DG, editor. *Cell Polarity: Frontiers in Molecular Biology*. Oxford University Press; Oxford: 2000. p. 201-39.
- [5] Breitman TR, Selonick SE, Collins SJ. Induction of differentiation of the human promyelocytic leukemia cell line (HL-60) by retinoic acid. *Proceedings of the National Academy of Sciences of the United States of America*. 1980;77:2936-40.
- [6] Collins SJ, Ruscetti FW, Gallagher RE, Gallo RC. Normal functional characteristics of cultured human promyelocytic leukemia cells (HL-60) after induction of differentiation by dimethylsulfoxide. *Journal of Experimental Medicine*. 1979;149:969-74.
- [7] Donaldson DD, Wongf GG, Moreau J, Stahl M, Rogers D. Inhibition of pluripotential embryonic stem cell differentiation by purified polypeptides. *Nature*. 1988;336:688-90.
- [8] Phung YT, Bekker JM, Hallmark OG, Black SM. Both neuronal NO synthase and nitric oxide are required for PC12 cell differentiation: a cGMP independent pathway. *Molecular Brain Research*. 1999;64:165-78.
- [9] Wang GX, Poo M. Requirement of TRPC channels in netrin-1-induced chemotropic turning of nerve growth cones. *Nature*. 2005;434:898-904.
- [10] Zheng JQ, Poo M, Connor JA. Calcium and chemotropic turning of nerve growth cones. *Perspectives on Developmental Neurobiology*. 1996;4:205-13.
- [11] Song H, Poo M. Signal transduction underlying growth cone guidance by diffusible factors. *Current Opinion in Neurobiology*. 1999;9:355-63.
- [12] Ming G, Song H, Berninger B, Holt CE, Tessier-Lavigne M, Poo M. cAMP-dependent growth cone guidance by netrin-1. *Neuron*. 1997;19:1225-35.

- [13] Nielson R, Shear JB. Parallel chemical dosing of subcellular targets. *Analytical Chemistry*. 2006;78:5987-93.
- [14] Brody JP, Yager P, Goldstein RE, Austin RH. Biotechnology at low Reynolds numbers. *Biophysical Journal*. 1996;71:3430-41.
- [15] Kamholz AE, Yager P. Theoretical analysis of molecular diffusion in pressure-driven laminar flow in microfluidic channels. *Biophysical Journal*. 2001;80:155-60.
- [16] Moorjani S, Nielson R, Chang XA, Shear JB. Dynamic remodeling of subcellular chemical gradients using a multi-directional flow device. *Lab on a Chip*. 2010;10:2139-46.
- [17] Hauert AB, Martinelli S, Marone C, Niggli V. Differentiated HL-60 cells are a valid model system for the analysis of human neutrophil migration and chemotaxis. *International Journal of Biochemistry & Cell Biology*. 2002;34:838-54.
- [18] Millius A, Weiner OD. Chemotaxis in neutrophil-like HL-60 cells. In: *Methods in Molecular Biology*. New Jersey: 2009;571. p. 167-77.
- [19] Dertinger SKW, Chiu DT, Jeon NL, Whitesides GM. Generation of gradients having complex shapes using microfluidic networks. *Analytical Chemistry*. 2001;73:1240-6.
- [20] Jeon NL, Baskaran H, Dertinger SKW, Whitesides GM, Van de Water L, Toner M. Neutrophil chemotaxis in linear and complex gradients of interleukin-8 formed in a microfabricated device. *Nature Biotechnology*. 2002;20:826-30.
- [21] Jeon NL, Dertinger SKW, Chiu DT, Choi IS, Stroock AD, Whitesides GM. Generation of solution and surface gradients using microfluidic systems. *Langmuir*. 2000;16:8311-6.
- [22] Takayama S, Ostuni E, LeDuc P, Naruse K, Ingber DE, Whitesides GM. Laminar flows: Subcellular positioning of small molecules. *Nature*. 2001;411:1016.
- [23] Takayama S, Ostuni E, LeDuc P, Naruse K, Ingber DE, Whitesides GM. Selective chemical treatment of cellular microdomains using multiple laminar streams. *Chemistry & Biology*. 2003;10:123-30.
- [24] Mannion BA, Weiss J, Elsbach P. Separation of sublethal and lethal effects of the bactericidal/permeability increasing protein on *Escherichia coli*. *Journal of Clinical Investigation*. 1990;85:853-60.

- [25] Lloyd AR, Oppenheim JJ. Poly's lament: the neglected role of the polymorphonuclear neutrophil in the afferent limb of the immune response. *Immunology Today*. 1992;13:169-72.
- [26] Ratcliffe DR, Nolin SL, Cramer EB. Neutrophil interaction with influenza-infected epithelial cells. *Blood*. 1988;72:142-9.
- [27] Gwira JA, Wei F, Ishibe S, Ueland JM, Barasch J, Cantley LG. Expression of neutrophil gelatinase-associated lipocalin regulates epithelial morphogenesis in vitro. *Journal of Biological Chemistry*. 2005;280:7875-82.
- [28] Martin P, Parkhurst SM. Parallels between tissue repair and embryo morphogenesis. *Development*. 2004;131:3021-34.
- [29] Weiss SJ. Tissue destruction by neutrophils. *New England Journal of Medicine*. 1989;320:365-76.
- [30] Smith JA. Neutrophils, host defense, and inflammation: a double-edged sword. *Journal of Leukocyte Biology*. 1994;56:672-86.
- [31] Scaccini C, Jialal I. LDL modification by activated polymorphonuclear leukocytes: a cellular model of mild oxidative stress. *Free Radical Biology and Medicine*. 1994;16:49-55.
- [32] Zerneck A, Bot I, Talab YD, Shagdarsuren E, Bidzhekov K, Meiler S, Krohn R, Schober A, Sperandio M, Soehnlein O. Protective role of CXC receptor 4/CXC ligand 12 unveils the importance of neutrophils in atherosclerosis. *Circulation Research*. 2008;102:209-17.
- [33] Robinson J, Watson F, Bucknall RC, Edwards SW. Activation of neutrophil reactive-oxidant production by synovial fluid from patients with inflammatory joint disease. Soluble and insoluble immunoglobulin aggregates activate different pathways in primed and unprimed cells. *Biochemical Journal*. 1992;286:345-51.
- [34] Ricevuti G, Mazzone A, Pasotti D, Servi S, Specchia G. Role of granulocytes in endothelial injury in coronary heart disease in humans. *Atherosclerosis*. 1991;91:1-14.
- [35] McCord JM. Oxygen-derived radicals: a link between reperfusion injury and inflammation. *Federation Proceedings*. 1987;46:2402-6.
- [36] Coussens LM, Werb Z. Inflammation and cancer. *Nature*. 2002;420:860-7.

- [37] Opdenakker G, Van Damme J. Cytokines and proteases in invasive processes: molecular similarities between inflammation and cancer. *Cytokine*. 1992;4:251-8.
- [38] Weitzman SA, Gordon LI. Inflammation and cancer: role of phagocyte-generated oxidants in carcinogenesis. *Blood*. 1990;76:655-63.
- [39] Ang KH, Chong G, Li Y. PID control system analysis, design, and technology. *IEEE Transactions on Control Systems Technology*. 2005;13:559-76.
- [40] Lee Y, Park S, Lee M, Brosilow C. PID controller tuning for desired closed-loop responses for SI/SO systems. *American Institute of Chemical Engineers Journal*. 1998;44:106-15.
- [41] Rivera DE, Morari M, Skogestad S. Internal model control: PID controller design. *Industrial & Engineering Chemistry Process Design and Development*. 1986;25:252-65.
- [42] Luyben WL. Tuning proportional-integral-derivative controllers for integrator/deadtime processes. *Industrial & Engineering Chemistry Research*. 1996;35:3480-3.
- [43] Visioli A. In: *Practical PID Control*. Springer-Verlag; London: 2006;1.
- [44] Åström KJ, Hägglund T. In: *PID Controllers: Theory, Design, and Tuning*. Instrument Society of America; North Carolina: 1995;2.
- [45] Åström KJ, Hägglund T. In: *Automatic Tuning of PID Controllers*. Instrument Society of America; North Carolina: 1988.
- [46] Armani MD, Chaudhary SV, Probst R, Shapiro B. Using feedback control of microflows to independently steer multiple particles. *Journal of Microelectromechanical Systems*. 2006;15:945-56.

Chapter 5: Multiple Dosing Agents within Laminar Flow Devices

5.1 INTRODUCTION

The previous chapters of this dissertation described strategies for on-the-fly control of chemical gradients, offering unparalleled spatial and temporal precision for dynamic interactions with cells [1, 2]. The multi-directional flow devices presented in these chapters overcome most of the limitations of the Whitesides' method [3-7] and offer important new chemical dosing capabilities. These capabilities were exploited in Chapter 3 for investigating cellular reorientation mechanisms adopted by neutrophil-like HL-60 cells during chemoattractant gradient switches, a step towards solving the mysteries of gradient sensing and directed migration. Cell motility and chemotaxis [8-15] play an important role in many biological processes, including inflammation [16-18], wound healing [19-22], and cancer metastasis [23-26]. Ultimately, unraveling chemotactic gradient sensing mechanisms has the promise for finding new approaches to combat acute and chronic inflammation in human disease.

Despite the advantages of the multi-directional chemical dosing devices, limitations exist with respect to the number of dosants. The flow devices presented in the previous chapters are designed to supply only a single dosing solution, *i.e.*, all reagent streams emerging through pores ablated in polymer membranes are necessarily of identical composition. Supplying the same dosing solution to multiple, highly resolved sites have enabled important insights into chemotactic responses (Chapter 3). However, far more detailed characterizations would be possible by selectively dosing subcellular

regions with distinct solutions. For example, by dosing one site with a chemoattractant and a second site with an inhibitor, properties of signal integration between the two pathways could be evaluated. Furthermore, a tunable mixture of these two cellular effectors could be supplied through ablated pores. Cellular responses under such diverse conditions could provide valuable insights into the interactions between various signaling pathways that effectively allow cell navigation inside chemical gradients.

This chapter reports two strategies for adapting the flow devices to a multiple-reagent format. The first method relies on incorporation of confluent parallel laminar streams in the reagent chamber, a design similar to the Whitesides' approach [3]. By incorporating different signal transduction effectors in the parallel reagent streams, and moving the interfacial boundaries created between them, the composition of streams emerging through ablated pores can be controlled. A multi-directional flow chamber (similar to the designs described in Chapters 2 and 4) will be used to form the cell-dosing compartment, which in conjunction with the multi-reagent flow chamber, will allow for creation and rapid reorientation of steep gradients of more than one chemical species, thus permitting parallel dosing of selected subcellular regions with different effector molecules. Also, laminar streams containing varying concentrations of a single chemical species can be used to subject cells to a more gradual gradient. A second method discussed in this chapter permits rapid sequential dosing of subcellular sites with multiple reagents, a format which can be extended to generate arbitrary chemical waveforms.

5.2 EXPERIMENTAL METHODS

5.2.1 Device design and fabrication

The basic design of the cell-dosing device—consisting of two stacked laminar flow chambers separated by a 2.5 μm thick Mylar membrane—remained the same. Each flow chamber was composed of a flow cell and its corresponding gasket, as described in Chapter 2. To construct flow cells, channels were cut in 0.12 mm thick adhesive sheets using a laser cutter. The cut adhesives were aligned with plastic coverslips with holes drilled in them to serve as entry and exit ports for fluid flow. The diameter of the holes was set equal to the channel width.

Three types of flow cells were used in this chapter—single-channel, cross-shaped, and multi-stream flow cells. For the single-channel and cross flow cells, 12 – 18 W of laser power with a laser head speed of 4.50 inches per second was used for cutting the adhesive sheets. An intermediate number of PPI (value = 500) with air flow set to 30 psi were used. For cutting the multi-stream flow cells, 30 W of laser power with a laser head speed of 2.25 inches per second and maximum PPI (value = 1000) were used.

The upper flow cell, which contained the cell medium, was composed of either a single 31 mm long x 1 mm wide channel or two intersecting channels of the same dimensions arranged in a cross-shaped geometry. Single-channel and cross flow cells were also used to form the reagent (lower) chamber in some experiments. In addition, multi-stream flow cells—two-stream and four-stream formats—were also used in the reagent chamber. In the two-stream flow cells, the inlet channels were 0.5 mm wide, and in the four-stream design, they were 0.4 mm wide. The main channel, where the reagent streams became confluent, was 1 mm wide in both cases (**Figure 5.1**). PDMS gaskets,

containing access ports for inserting the feed and drain tubes, were used in conjunction with the flow cells to establish flow inside the channels.

Masters for the reagent gasket were created by gluing pieces of polyurethane-coated wires (0.9-mm diameter) to the bottom of a Petri dish using cyanoacrylate in an orientation initially normal to the surface. For fabrication of the cross reagent gasket, four pieces of wires were used to form 2 inlet and 2 outlet ports (*i.e.*, an inlet/outlet pair for each channel). Similarly, for the single-channel reagent gasket, two pieces of wires were used (1 inlet, 1 outlet). For the two-stream and four-stream designs, three pieces (2 inlets, 1 outlet) and five pieces (4 inlets, 1 outlet) of the same wires were used, respectively. At a height of ~2 mm, the wires were bent parallel to the surface of the Petri dish. PDMS, mixed at a 10:1 ratio of monomer to curing agent, was poured into the Petri dish mold, and cured overnight at 60 °C. The hardened polymer was separated from its master by pulling out the wires, and the mold was cut to its final form using a razor. The gasket for the cross cell-dosing chamber was fabricated in a similar fashion except eight pieces of thicker solder wires (1.27-mm diameter) were used to create the masters to form 4 inlet and 4 outlet ports (*i.e.*, two inlet/outlet pairs for each channel). Lastly, the single-channel dosing gasket consisted of 1 inlet and 1 outlet port fabricated using the solder wires.

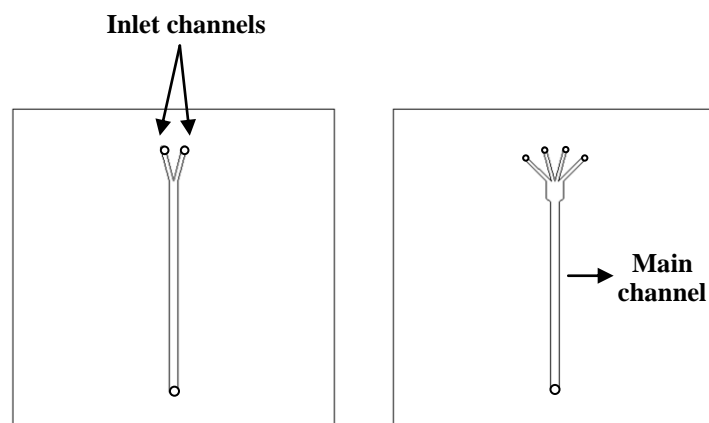


Figure 5.1: Multi-stream reagent flow cells. Two-stream and four-stream flow cells (top view) were used to form the reagent chamber. The flow cells were constructed by aligning channels cut in adhesive sheets with holes drilled in polycarbonate coverslips. In both cases, the main channel, where the laminar streams became confluent, was 1 mm wide.

The entire device, consisting of the membrane sandwiched between the two flow cells with their corresponding gaskets, was assembled on a microscope stage, with the dosing channel (vertical channel in case of cross dosing flow cells) aligned with the reagent channel, which was the main channel in the multi-stream flow cells and the vertical channel when cross flow cells were used to form the reagent chamber. A plexiglass plate with two screws was used to clamp the assembly tightly onto the stage. An intermediate borosilicate glass piece was placed between the upper PDMS gasket and the plexiglass plate. This process yielded two flow chambers separated by the polymer membrane.

Feed and drain tubes were connected to both flow chambers. Solutions were supplied by syringes driven by electro-mechanical pumps. Platinum-cured silicone tubing

(0.8-mm inner diameter) provided fluidic connection between the chambers and syringe pumps on the feed side and on the reagent drain line. The same type of tubing with a larger inner diameter (1.6 mm) was used for the drain lines from the upper chamber, a configuration that resulted in pressure-driven transfer of the reagent into the cell-dosing chamber. In addition, a small diameter tube (~0.4-mm outer diameter) typically was inserted at the end of the reagent drain tube to create additional pressure within the reagent chamber. Separate syringe pumps delivered cell medium to the upper chamber and desired reagents to the lower chamber. For supplying media to the cross cell-dosing chamber, the feed line was split into four lines using a PDMS manifold to deliver solution to the four inlet ports of the dosing chamber.

Four electrically-controlled solenoid pinch valves were used to switch the flow direction in the cross cell-dosing chamber. The pinch valves were interfaced with the computer using a Desktop Connector Block to control the activation of valves using LabView software. Each channel of the cell-dosing chamber was connected to two pinch valves to obtain two flow directions, yielding a total of four flow directions from the two channels of the cross chamber (**Figure 5.2a**). Cross flow chambers were also used to form the lower (reagent) chamber in some experiments. The flow chamber design remained the same, except the PDMS gasket in this case consisted of two inlet and two outlet ports (*i.e.*, a single inlet/outlet pair for each channel), which in conjunction with two pinch valves allowed unidirectional flow in each cross channel (**Figure 5.2b**). This setup was used for delivering two different chemical species, using syringe pumps, to the two cross channels. Lastly, to rapidly switch between the two chemical species, two additional solenoid pinch valves—one per reagent feed line—were incorporated to direct

the reagents to a waste reservoir when they were not delivered to the chamber. With these additional valves, the reagents could be directed either to the chamber or to the waste reservoir with the syringe pumps running at all times (**Figure 5.3**). Although syringe pumps could be used to switch between the two reagents (by simply stopping the pump to prevent flow of the reagent it was supplying), the process took 30 – 40 s due to the slow response times of the pumps. Using the pinch valves, reagents could be switched in less than 1 s. Thus, a total of eight solenoid pinch valves—four in the cell-dosing chamber and four in the reagent chamber—were used when the flow device consisted of two stacked cross chambers. Note that no valves were used with single-channel flow chamber configurations.

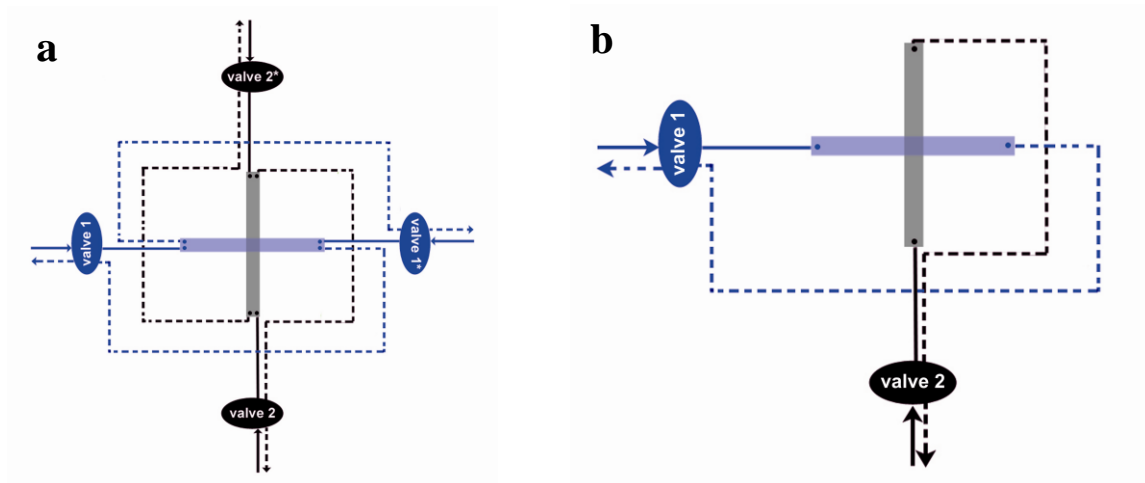


Figure 5.2: Valve schematic for cell-dosing and reagent flow chambers. (a) Four solenoid pinch valves were used to change flow direction in the cross cell-dosing chamber. Each channel was connected to two valves to obtain two flow directions, giving a total of four directions. (b) Solenoid pinch valves were used in the reagent chamber to switch between two different chemical species. Each channel was connected to a pinch valve, thus allowing unidirectional flow in the channels. The solid lines denote the feed tubes and the dashed lines denote drains.

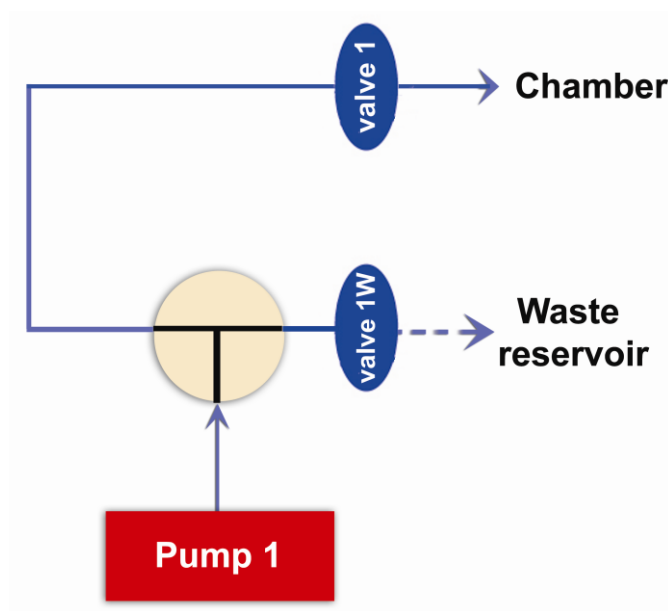


Figure 5.3: Valve schematic for rapid switching between chemical species. Solenoid pinch valves were used to direct a reagent to the lower chamber of the flow device or to a waste reservoir. The incorporation of valves prevented delays arising from the slow response time of syringe pumps and allowed for rapid switching between reagents. Note *valve 1* is the same valve from **Figure 5.2b**. The same setup was also used on the feed side of the second reagent.

Reagents were delivered using syringe pumps (described above) or gravity. For delivery using gravity, syringes (with their plungers removed) were connected to ring stands, using clamps, such that the syringe outlets were at a greater height than the height of the reagent chamber inlets to establish a hydrostatic head. In order to minimize fluidic resistance, the larger diameter silicone tubing (1.6 mm) was used to provide fluidic connection between the syringes and the reagent chamber. Also, 3-way valves, commonly used in intravenous applications, were connected to the syringe outlets to

provide a means to stop flow when needed. Delivery using gravity was typically used when multi-stream flow cells (**Figure 5.1**) formed the reagent chamber.

Lastly, all solutions were vacuum degassed for 2 – 3 h before introduction into the flow chambers to minimize formation of air bubbles.

5.2.2 Chemicals and reagents

In addition to the chemicals and reagents used in previous chapters, two fluorescent dyes, fluorescein (Acros Organics, 119241000; Fairlawn, NJ) and rhodamine B (Alfa Aesar, A13572; Ward Hill, MA), were used. All chemicals and reagents were used without additional purification.

5.2.3 Cell culture

All culture procedures used for growth, differentiation, and attachment of HL-60 cells are described in Chapter 2.

5.2.4 Membrane ablation

All studies described here were conducted using a frequency-doubled (532 nm), Q-switched Nd:YAG laser, also used in the work reported in previous chapters. Laser powers ranging from 10 – 15 mW (measured before the back aperture of the objective) were used for ablation of pores.

In the studies described in previous chapters, micron-sized pores were typically ablated with an empty reagent chamber by focusing the laser beam at desired positions, typically near the top surface of Mylar membranes, and irradiating the membranes with a train of 10 exposures of 5 ms each, spaced by 50 ms intervals. For production of pores in the presence of aqueous solutions in both the upper and lower chambers, the reagent

solution was replaced with air or ethanol before performing ablations, an approach that required re-introduction of the reagent solution after pores were ablated.

The studies described in this chapter and on-going experiments with multiple reagents often require rapid ablation of pores and creation of reagent streams in the presence of aqueous solutions in both flow chambers. Ablations performed with an air-filled or ethanol-filled lower chamber, in addition to being cumbersome and time-consuming due to multiple fluid exchanges (between air/ethanol and dosant solution), often caused membrane flexing. This was especially prevalent with an air-filled lower chamber, resulting in formation of air bubbles in the dosing chamber and consequent detachment of cells. Ablations performed with an ethanol-filled lower chamber posed other issues. BSA solutions, typically used in the reagent chamber, precipitate in ethanol, requiring flow of an intermediate buffer solution (*e.g.*, PBS) between BSA and ethanol[†]. This process often required several minutes for ablation of pores and creation of laminar flow streams, a solution that was impractical for targeting motile cells that often migrated away before introduction of the reagent streams in the dosing chamber.

[†]The procedure consisted of first introducing the buffer solution in the reagent chamber to remove the BSA, then flowing ethanol and performing ablations, followed by flow of buffer again to remove the ethanol, and then re-introduction of the BSA solution in the reagent chamber.

To overcome some of these limitations, other strategies were explored in these studies for ablation of pores in the presence of aqueous solutions in both chambers of the flow device. A range of ablation parameters was tested, such as varying the pressure gradient across membranes, increasing the length of laser exposures and/or reducing the delay between exposures, and positioning of the laser focus within membranes. It was found that 10 exposures of 5 ms each, spaced by 10 ms intervals resulted in more regularly sized pores compared to the other investigated parameters. The reduction in delay (compared to the 50 ms delay used in ablations with an empty reagent chamber) possibly prevented dissipation of heat between exposures that allowed for dielectric breakdown to occur resulting in pore formation.

Solution flow through pores, and resultant formation of laminar reagent streams, were monitored visually using solutions in the two chambers that had different refractive indices (*e.g.*, by dissolving 3 – 6% BSA in one of the solutions) or by flowing a fluorescent dye in the reagent chamber.

5.3 RESULTS AND DISCUSSION

5.3.1 Rapid switching between two chemical species

To rapidly change the chemical species emerging through pores ablated in Mylar membranes, a reagent chamber composed of a four-ported cross flow cell and a corresponding PDMS gasket, containing two inlet and two outlet ports (*i.e.*, an inlet/outlet pair per channel), was designed (**Figure 5.2b**). Syringe pumps were used to deliver two different reagents to the two perpendicular channels of the cross chamber (to have a reagent per channel). Each reagent feed line was split using a PDMS T-splitter, and computer-controlled solenoid pinch valves were used to direct solutions to either the reagent chamber or to a waste reservoir (**Figure 5.3**). Rapid switching between the two reagents occurred by opening a given reagent valve (with its waste valve closed) in conjunction with opening the second waste valve (and closing the corresponding reagent valve). **Figure 5.4** is an overlay of fluorescein and rhodamine B streams emerging through the same pore into the cell-dosing chamber. In these studies, a cross flow chamber, similar to the reagent chamber but with two additional inlet and outlet ports, was used to form the dosing chamber (**Figure 5.2a**). Note that the reagent stream orientations are determined by the flow direction of the cross cell-dosing chamber and are independent of the flow direction in the reagent chamber. The reagent chamber, on the other hand, serves as a reservoir for the fluorescent dyes and determines which chemical species emerges through the ablated pores.

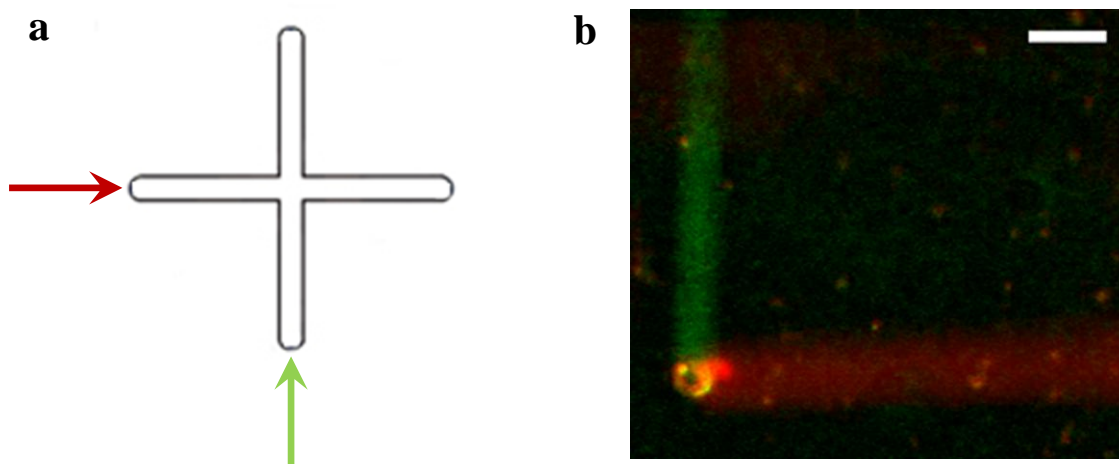


Figure 5.4: Switching orientation and composition of laminar streams. (a) Delivery of solutions to the reagent chamber. Two fluorescent dyes, fluorescein and rhodamine B, were flowed in the reagent chamber (a dye through each channel). (b) Processed overlay of two images—each consisting of a single dye stream—acquired by flowing fluorescein and rhodamine B sequentially through separate channels of the cross reagent chamber. The stream orientations were obtained by changing the flow direction in the dosing chamber and the composition of the streams was determined by the flow conditions of the reagent chamber. Both dyes were flowed at 0.15 mL min^{-1} . DPBS was flowed in the cell-dosing chamber at the same volumetric flow rate. Scale bar, $20 \text{ }\mu\text{m}$.

The plot of **Figure 5.5** shows that the composition of reagent streams can be changed in less than 500 ms. This assessment was made by initially flowing only rhodamine B in the reagent chamber and then switching to fluorescein by closing the valve directing fluorescein to the waste reservoir (and opening the fluorescein chamber valve) in conjunction with opening the valve that directed rhodamine to the waste reservoir (and closing the rhodamine chamber valve). The plot shows fluorescein

intensity values measured 15 μm downstream from the pore. The reagents could be switched within a single frame of the 2 Hz time-lapse acquisition.

Since the reagent channels were primed before the start of the time-lapse acquisition, the reagent switching time should depend on the reagent dead volume, which is the volume of the central mating region of the cross channels, the reagent flow rate, and the time taken by the reagent stream to travel 15 μm downstream from the pore. At a nominal cell-dosing flow rate of 0.15 mL min^{-1} (which corresponds to $\sim 2 \text{ mm s}^{-1}$ calculated 2 μm above the membrane) and at an equal reagent volumetric flow rate, this switching time was calculated to be $\sim 60 \text{ ms}$, almost an order of magnitude smaller than the duration of a single frame period. The switching time can be slowed by experimental factors, such as the response time of the solenoid pinch valves used to switch between the reagents and delays from the LabView software used to control the activation of valves. Faster imaging (*e.g.*, using a video CCD) should provide more accurate measurements of reagent switching times.

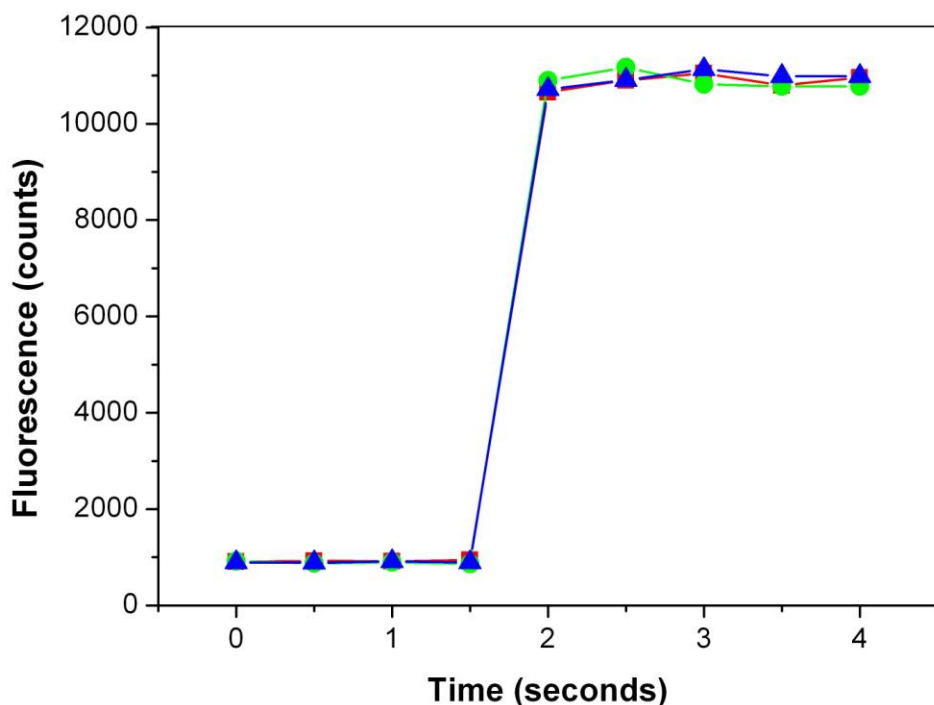


Figure 5.5: Subsecond switching of composition of reagent streams. Reagent switching times were assessed by first flowing rhodamine B in one of the cross channels followed by flowing fluorescein in the other channel (and stopping rhodamine flow). The time plot shows fluorescein intensity data acquired from 3 switching cycles, inside the same flow-cell device, using a CCD camera at 2 Hz. The fluorescein intensity values were measured 15 μm downstream from the pore. Both dyes were flowed at 0.15 mL min^{-1} . DPBS was flowed in the cell-dosing chamber at the same volumetric flow rate.

Lastly, the two dyes can also be flowed simultaneously in the reagent chamber. By incorporating the motorized pinch clamp, discussed in Chapter 4, to control reagent flow rates, it may be possible to generate tunable mixtures, containing varying proportions of the two reagents, which can then be supplied to the cell-dosing chamber via ablated pores. Future work will involve modeling and/or experimentally evaluating

the mixing conditions inside the mating area between the cross channels to generate predictable reagent concentrations inside tuned mixtures.

5.3.2 Simultaneous dosing of cells with two different chemical species

In this dissertation, several examples of dosing HL-60 cells, a neutrophil precursor cell line [9, 27-29], with chemoattractant molecules have been demonstrated. In all these chemical dosing instances, only one selected subcellular region was dosed at a time. Often the dosing sites were switched between two cellular regions (*e.g.*, the leading and trailing edges of cells), but once again, only a single subcellular site was chemically stimulated at a given time. Out of a lab “brainstorming” session came the idea of dual chemical stimulation of cells, *i.e.*, parallel dosing of two subcellular regions (on the same cell) with chemoattractant streams. Such experiments would provide insights into how long-range communication works in neutrophils and if “bipolarity” is possible in this cell type.

Figure 5.6 shows chemoattractant streams dosing two sites on an HL-60 cell. In these studies, differentiated HL-60 cells were attached to fibronectin-coated Mylar membranes mounted inside the flow-cell device. After formation of two pores, 100 nM of fMLP, a bacterially-derived chemoattractant, was flowed in the reagent chamber, producing two chemotactic laminar flow streams in the cell-dosing chamber targeted to selected subcellular regions. Initially, the HL-60 cell showed ruffling on both subcellular sites that were inside the chemotactic streams, followed by a stage during which it appeared that the cell exhibited bipolarity, showing protrusions and pseudopod-like features on both the dosed sites, a stage that lasted for ~3 min (2nd panel of the figure).

This was followed by a gradual thinning of the left (dosed) edge of the cell and development of a defined polarity—the right edge forming the front of the cell and the left forming its tail—with the cell ultimately migrating into the right stream.

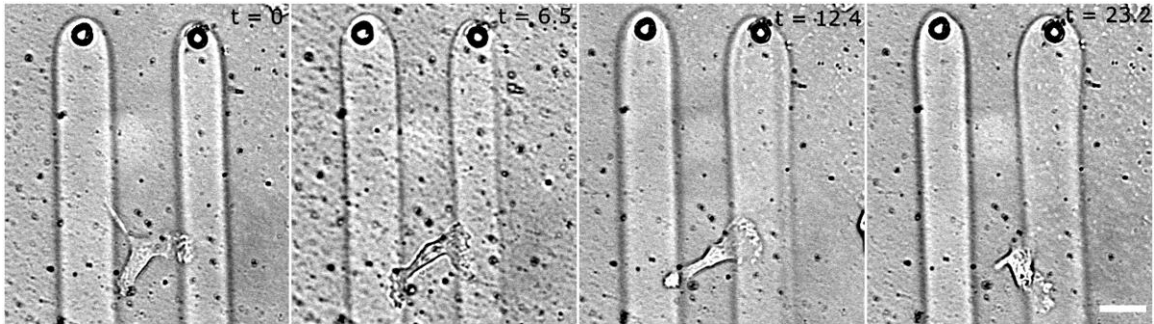


Figure 5.6: Parallel dosing of subcellular sites of an HL-60 cell. Time sequence showing an HL-60 cell changing its polarization in response to 100 nM fMLP streams emerging through two pores ablated in Mylar membrane. Time in minutes (from the 26-min time-lapse video) is denoted as t . In these studies, single-channel flow chambers formed both the upper and lower chambers of the flow device. Throughout dosing, Gey's medium with 0.5% BSA was flowed in the cell-dosing chamber at 0.15 mL min^{-1} and fMLP was flowed in the reagent chamber at 0.20 mL min^{-1} . 3% BSA was added for visualization of the fMLP streams. A heated microscope stage was used to maintain cells at $\sim 37^\circ\text{C}$. Scale bar, $20 \mu\text{m}$.

This data provides insights into how HL-60 cells respond when they are faced with similar gradient conditions on opposing sides of their bodies. Other dosing experiments, such as parallel dosing with two chemo-inhibitor streams or with a chemoattractant and an inhibitor or two chemoattractant streams of different concentrations, can be easily envisioned. Also, introducing the second stream after a short delay would provide insights into whether the first activated site establishes dominance or only the current levels of stimulation affect cellular responses[†]. The capabilities presented thus far in this dissertation do not allow for parallel dosing with two different reagents. The flow devices presented in the previous chapters were designed to supply only a single dosing solution, *i.e.*, all reagent streams emerging through pores ablated in polymer membranes were necessarily of identical composition. Development of methodologies to achieve parallel dosing with two different reagents is the last topic of this dissertation.

Simultaneous dosing with multiple cellular effectors requires a means to introduce and arbitrarily change the individual locations of multiple components in the reagent flow chamber to selectively deliver the reagents through different pores to distinct regions of a cell or to a group of cells. To achieve this end, a simple and versatile solution has been devised, which involves incorporating a previously described chamber design by Whitesides and coworkers. In the Whitesides' chamber, multiple reagents are supplied through separate inlet channels that converge into a main channel. Due to laminar flow conditions inside the main channel, the reagent streams flow adjacent to each other with

[†]Such experiments will require rapid ablation of pores and creation of reagent streams in the presence of aqueous solutions in both the upper and lower chambers of the flow device. This was achieved by manipulation of laser ablation parameters (see Experimental Methods).

mixing limited to the small amount of diffusional transport across the boundaries between the streams [26, 28, 33]. By incorporating this confluent channel design to form the reagent chamber of the flow device described in previous chapters and maintaining a reasonably high chamber flow rate (*e.g.*, 4 – 8 mm s⁻¹), diffusional mixing can be minimized over the several millimeter distance that the streams flow adjacent to each other. By ablating pores on opposing sides of the sharp solution boundaries, reagent streams of different compositions can be introduced in the cell-dosing chamber via the pores (**Figure 5.7a**). Moreover, it is possible to move the position of the boundaries by changing the relative flow rates of the two supply lines, thus permitting dynamic targeting of subcellular regions with different effector molecules, achieved by combining the capabilities developed in this dissertation with previously described microfluidic dosing technologies.

In preliminary studies, the feasibility of this approach has been confirmed in two reagent chamber designs—two-pronged and four-pronged Ys (**Figure 5.1**)—housing two and four reagent streams, respectively. Distinct interfaces were seen between adjacent streams (**Figure 5.7b**), with the width of the interface being a function of the flow rate in the reagent chamber. By controlling the volumetric rates of the syringe pumps supplying the reagents, interfaces between streams could be moved (**Figure 5.8**) to control the chemical composition of reagent streams emerging through ablated pores.

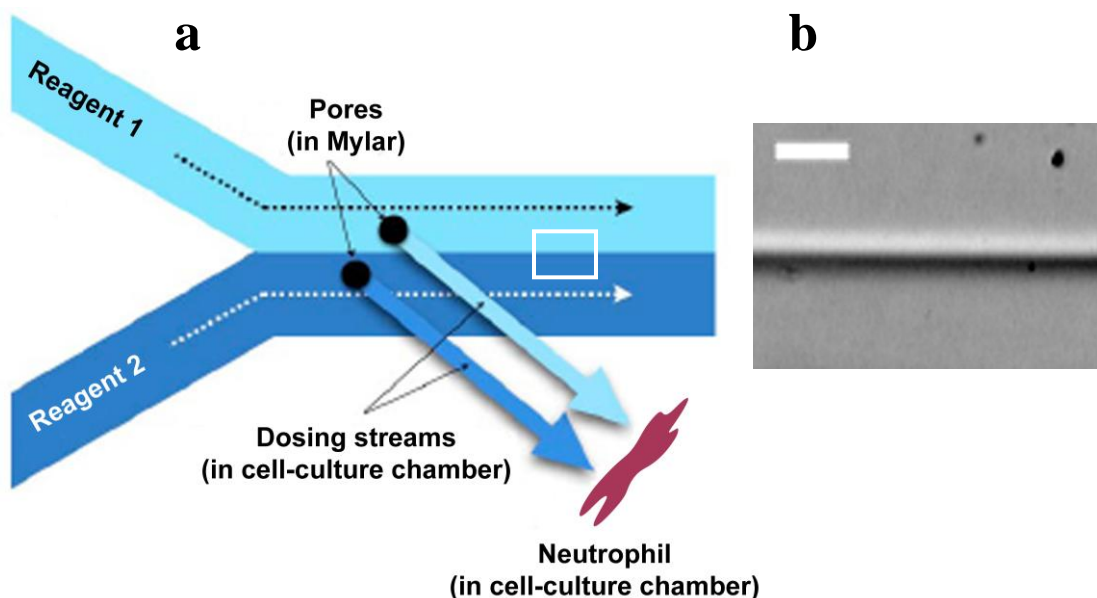


Figure 5.7: Dosing distinct subcellular microdomains with different chemical species. (a) Schematic illustrating subcellular dosing by delivery of two reagents to the inlet channels of a Y-shaped reagent chamber. The reagent streams flow adjacent to each other separated by a sharp interfacial boundary. By ablating pores on opposing sides of the boundary, combined with the capability of changing the directionality of the reagent streams emerging through these pores, distinct regions of a cell can be dosed with two different chemical species. Adapted from illustration made by J. B. Shear. (b) Image of the boundary region (boxed region in (a)) showing the interface between DPBS and 6% BSA streams. DPBS was flowed at 0.03 mL min^{-1} and BSA was flowed at 0.10 mL min^{-1} in the reagent chamber. Scale bar, $100 \text{ }\mu\text{m}$.

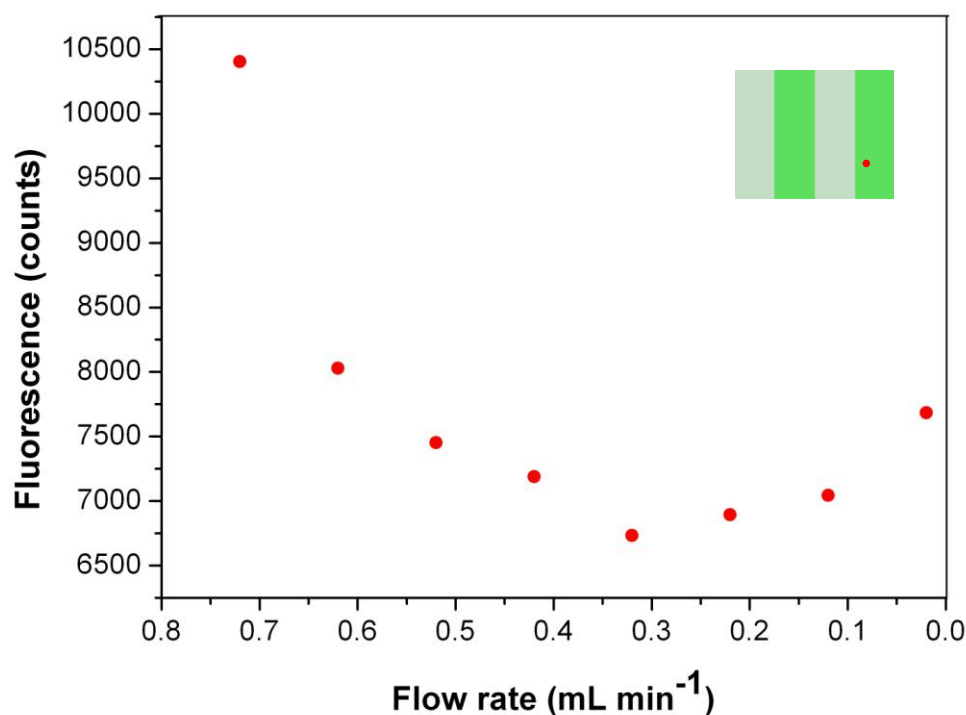


Figure 5.8: Moving interfaces between laminar flow streams. Fluorescein streams of two different concentrations—0.75 μM (light green) and 1.50 μM (dark green)—were flowed in an alternating manner in the main channel of a four-stream reagent chamber (plot inset). Shown are the fluorescence intensity values of a given coordinate (red circle in inset) that initially fell inside the rightmost (1.50 μM fluorescein) stream. In these studies, the flow rate of 0.75 μM fluorescein was maintained at a constant value and the flow rate of 1.5 μM fluorescein was incrementally decreased, which caused a gradual widening of the 0.75 μM fluorescein streams, with movement of the interfaces towards the right. The intensity at the shown coordinate, initially inside the 1.50 μM fluorescein stream, reduced as the adjacent 0.75 μM fluorescein stream widened and the interfaces moved to the right. The increase in intensity as the flow rate of 1.50 μM fluorescein was further decreased is due to movement of the middle interface to the right, with the shown coordinate gradually falling inside the middle interfacial region. This data was extracted from a fluorescence time-lapse video. Throughout the experiment, 0.75 μM fluorescein was flowed at 0.10 mL min⁻¹.

The interfaces in our experiments can undergo lateral movement of up to 15 μm in both the two-stream and four-stream configurations. Pulsations arising from the stepper motor-driven syringe pumps used to deliver reagents could be contributing to interfacial instability, a common problem encountered in microfluidic systems [30, 31]. Notably, in these studies, the middle interface in the four-stream configuration was found to be very stable with interfacial movement less than 1 μm (possibly a result of the out-of-sync syringe pump pulsations cancelling out). The mean interfacial movement of the middle interface was found to be $0.9 \pm 1.8 \mu\text{m}$ (mean \pm standard deviation) measured over nine 15-min observation periods from 3 independent experiments. Each experiment was conducted on a different day with new flow cells outfitted with fresh pieces of Mylar membranes. More experiments need to be done to improve the interfacial stability of the other interfaces. Possible solutions include delivery of reagents using gravity (see Experimental Methods), which is an ongoing investigation showing promising early results.

5.4 CONCLUSION

The chemical dosing devices presented in previous chapters were fundamentally limited in that the reagent chamber was capable of supplying only a single dosing solution. This chapter described two approaches for incorporation of multiple reagents. A multi-reagent format would significantly enhance the utility and versatility of this chemical dosing platform, increasing its appeal to the biological community.

The first approach relied on the use of a multi-channel flow chamber to house distinct chemical species in different channels. In these studies, subsecond switching

between chemical species was demonstrated, which would allow for rapid sequential delivery of different effector molecules to selected subcellular regions. This approach also offers promise for generation of reagent mixtures containing varying proportions of individual components. By incorporating tunable mixtures in laminar streams emerging through ablated pores, dynamically changing chemical signals could be presented to adherent cells in a temporally-defined manner.

The second approach presented in this chapter used multiple parallel laminar-flow streams of different compositions in the reagent chamber. By judicious selection of relative position of pores and reagent stream orientation, this approach should allow for simultaneous delivery of different chemical species to distinct selected regions on the same cell or on a group of cells.

These studies provide a foundation for a highly versatile chemical dosing platform that may enable currently inaccessible problems in neutrophil biology to be addressed. For instance, the ability to dose two edges of a cell in a differential manner, *e.g.*, with a chemoattractant and an inhibitor, is an important step towards understanding how long range communication works in motile cells. Current strategies for defining chemical interactions *in vitro* largely rely on pre-fabricated gradient generators. By providing what is essentially a static cell-reagent interaction, ‘pre-determined’ gradient generator technologies are unable to achieve the temporal and spatial dexterity offered by the flow devices described in this dissertation. Such capabilities are necessary for dynamic interactions with cells undergoing migration.

Finally, fabrication of the flow devices discussed in this dissertation using alternative approaches, such as PDMS molding technologies, can be envisioned. This will

permit integration of “on-chip” valves and pumps [32-34]. Such future developments will allow device miniaturization, reduction in cost and bulkiness, and easier dissemination in the biological community.

5.5 REFERENCES

- [1] Moorjani S, Nielson R, Chang XA, Shear JB. Dynamic remodeling of subcellular chemical gradients using a multi-directional flow device. *Lab on a Chip*. 2010;10:2139-46.
- [2] Nielson R, Shear JB. Parallel chemical dosing of subcellular targets. *Analytical Chemistry*. 2006;78:5987-93.
- [3] Jeon NL, Dertinger SKW, Chiu DT, Choi IS, Stroock AD, Whitesides GM. Generation of solution and surface gradients using microfluidic systems. *Langmuir*. 2000;16:8311-6.
- [4] Takayama S, Ostuni E, LeDuc P, Naruse K, Ingber DE, Whitesides GM. Selective chemical treatment of cellular microdomains using multiple laminar streams. *Chemistry & Biology*. 2003;10:123-30.
- [5] Takayama S, Ostuni E, LeDuc P, Naruse K, Ingber DE, Whitesides GM. Laminar flows: Subcellular positioning of small molecules. *Nature*. 2001;411:1016.
- [6] Dertinger SKW, Chiu DT, Jeon NL, Whitesides GM. Generation of gradients having complex shapes using microfluidic networks. *Analytical Chemistry*. 2001;73:1240-6.
- [7] Jeon NL, Baskaran H, Dertinger SKW, Whitesides GM, Van de Water L, Toner M. Neutrophil chemotaxis in linear and complex gradients of interleukin-8 formed in a microfabricated device. *Nature Biotechnology*. 2002;20:826-30.
- [8] Bourne HR, Weiner OD. A chemical compass. *Nature*. 2002;419:21.
- [9] Millius A, Weiner OD. Chemotaxis in neutrophil-like HL-60 cells. In: *Methods in Molecular Biology*. New Jersey: 2009;571. p. 167-77.
- [10] Servant G, Weiner OD, Herzmark P, Balla T, Sedat JW, Bourne HR. Polarization of chemoattractant receptor signaling during neutrophil chemotaxis. *Science*. 2000;287:1037-40.
- [11] Wang F, Herzmark P, Weiner OD, Srinivasan S, Servant G, Bourne HR. Lipid products of PI(3)Ks maintain persistent cell polarity and directed motility in neutrophils. *Nature Cell Biology*. 2002;4:513-18.
- [12] Weiner OD. Regulation of cell polarity during eukaryotic chemotaxis: the chemotactic compass. *Current Opinion in Cell Biology*. 2002;14:196-202.

- [13] Weiner OD, Servant G, Parent CA, Devreotes PN, Bourne HR. Cell polarity in response to chemoattractants. In: Drubin DG, editor. *Cell Polarity: Frontiers in Molecular Biology*. Oxford University Press; Oxford: 2000. p. 201-39.
- [14] Weiner OD, Marganski WA, Wu LF, Altschuler SJ, Kirschner MW. An actin-based wave generator organizes cell motility. *Public Library of Science Biology*. 2007;5:2053-63.
- [15] Weiner OD, Servant G, Welch MD, Mitchison TJ, Sedat JW, Bourne HR. Spatial control of actin polymerization during neutrophil chemotaxis. *Nature Cell Biology*. 1999;1:75-81.
- [16] Yang XD, Corvalan JR, Wang P, Roy CM, Davis CG. Fully human anti-interleukin-8 monoclonal antibodies: potential therapeutics for the treatment of inflammatory disease states. *Journal of Leukocyte Biology*. 1999;66:401-10.
- [17] Lloyd AR, Oppenheim JJ. Poly's lament: the neglected role of the polymorphonuclear neutrophil in the afferent limb of the immune response. *Immunology Today*. 1992;13:169-72.
- [18] Ratcliffe DR, Nolin SL, Cramer EB. Neutrophil interaction with influenza-infected epithelial cells. *Blood*. 1988;72:142-9.
- [19] Maheshwari G, Wells A, Griffith LG, Lauffenburger DA. Biophysical integration of effects of epidermal growth factor and fibronectin on fibroblast migration. *Biophysical Journal*. 1999;76:2814-23.
- [20] Gillitzer R, Goebeler M. Chemokines in cutaneous wound healing. *Journal of Leukocyte Biology*. 2001;69:513-21.
- [21] Singer AJ, Clark RAF. Cutaneous wound healing. *New England Journal of Medicine*. 1999;341:738-46.
- [22] Martin P. Wound healing--Aiming for perfect skin regeneration. *Science*. 1997;276:75-81.
- [23] Wells A, Kassis J, Solava J, Turner T, Lauffenburger DA. Growth factor-induced cell motility in tumor invasion. *Acta Oncologica*. 2002;41:124-30.
- [24] Coussens LM, Werb Z. Inflammation and cancer. *Nature*. 2002;420:860-7.
- [25] Opdenakker G, Van Damme J. Cytokines and proteases in invasive processes: molecular similarities between inflammation and cancer. *Cytokine*. 1992;4:251-8.

- [26] Weitzman SA, Gordon LI. Inflammation and cancer: role of phagocyte-generated oxidants in carcinogenesis. *Blood*. 1990;76:655-63.
- [27] Breitman TR, Selonick SE, Collins SJ. Induction of differentiation of the human promyelocytic leukemia cell line (HL-60) by retinoic acid. *Proceedings of the National Academy of Sciences of the United States of America*. 1980;77:2936-40.
- [28] Collins SJ, Ruscetti FW, Gallagher RE, Gallo RC. Normal functional characteristics of cultured human promyelocytic leukemia cells (HL-60) after induction of differentiation by dimethylsulfoxide. *Journal of Experimental Medicine*. 1979;149:969-74.
- [29] Hauert AB, Martinelli S, Marone C, Niggli V. Differentiated HL-60 cells are a valid model system for the analysis of human neutrophil migration and chemotaxis. *International Journal of Biochemistry & Cell Biology*. 2002;34:838-54.
- [30] Atencia J, Beebe DJ. Controlled microfluidic interfaces. *Nature*. 2004;437:648-55.
- [31] Green R, Vanapalli SA. Chips & Tips: Quick assessment of the stability of flow generated by a syringe pump in a microfluidic device. *Lab on a Chip*. 2009.
- [32] Fu AY, Chou HP, Spence C, Arnold FH, Quake SR. An integrated microfabricated cell sorter. *Analytical Chemistry*. 2002;74:2451-7.
- [33] Thorsen T, Maerkl SJ, Quake SR. Microfluidic large-scale integration. *Science*. 2002;298:580-4.
- [34] Unger MA, Chou HP, Thorsen T, Scherer A, Quake SR. Monolithic microfabricated valves and pumps by multilayer soft lithography. *Science*. 2000;288:113-6.

Appendix: List of Abbreviations

cAMP: cyclic adenosine monophosphate

DIOC₆: 3,3'-dihexyloxacarbocyanine iodide

HL-60: human promyelocytic leukemia

fMLP: *N*-formyl-methionyl-leucyl-phenylalanine

BSA: bovine serum albumin

MPE: multiphoton excitation

Ti:S: titanium-sapphire

NA: numerical aperture

Nd:YAG: neodymium yttrium aluminum garnet

CCD: charge-coupled device

SEM: scanning electron microscopy

IL-8: interleukin-8

LTB₄: leukotriene-B₄

PI3K: phosphatidylinositol 3-kinase

PIP₃: phosphatidylinositol 3,4,5-triphosphate

dHL-60: differentiated human promyelocytic leukemia

MEMS: micro-electromechanical systems

PDMS: polydimethylsiloxane

PPI: pulses per inch

CFM: cubic feet per minute

FBS: fetal bovine serum

DMSO: dimethyl sulfoxide

PBS: phosphate-buffered saline

DAQ: data acquisition

PID: proportional-integral-derivative

DPBS: Dulbecco's phosphate-buffered saline

LUT: look-up table

Bibliography

- Abramoff MD, Magelhaes PJ, Ram SJ. Image processing with ImageJ. *Biophotonics International*. 2004;11:36-42.
- Adler J. Chemotaxis in bacteria. *Science*. 1966;153:708-16.
- Albini A, Iwamoto Y, Kleinman HK, Martin GR, Aaronson SA, Kozlowski JM, McEwan RN. A rapid in vitro assay for quantitating the invasive potential of tumor cells. *Cancer Research*. 1987;47:3239-45.
- Allan RB, Wilkinson PC. A visual analysis of chemotactic and chemokinetic locomotion of human neutrophil leucocytes. Use of a new chemotaxis assay with *Candida albicans* as gradient source. *Experimental Cell Research*. 1978;111:191-203.
- Allen R, Nielson R, Wise D, Shear JB. Catalytic three-dimensional protein architectures. *Analytical Chemistry* 2005;77:5089-95.
- Andresen JL, Ehlers N. Chemotaxis of human keratocytes is increased by platelet-derived growth factor-BB, epidermal growth factor, transforming growth factor- α , acidic fibroblast growth factor, insulin-like growth factor-I, and transforming growth factor- β . *Current Eye Research*. 1998;17:79-87.
- Andresen JL, Ledet T, Ehlers N. Keratocyte migration and peptide growth factors: the effect of PDGF, bFGF, EGF, IGF-I, aFGF and TGF- β on human keratocyte migration in a collagen gel. *Current Eye Research*. 1997;16:605-13.
- Ang KH, Chong G, Li Y. PID control system analysis, design, and technology. *IEEE Transactions on Control Systems Technology*. 2005;13:559-76.
- Armani MD, Chaudhary SV, Probst R, Shapiro B. Using feedback control of microflows to independently steer multiple particles. *Journal of Microelectromechanical Systems*. 2006;15:945-56.
- Aström KJ, Hägglund T. In: *Automatic Tuning of PID Controllers*. Instrument Society of America; North Carolina: 1988.
- Aström KJ, Hägglund T. In: *PID Controllers: Theory, Design, and Tuning*. Instrument Society of America; North Carolina: 1995;2.
- Atencia J, Beebe DJ. Controlled microfluidic interfaces. *Nature*. 2004;437:648-55.

- Beg AA, Baltimore D. An essential role for NF-kappa B in preventing TNF-alpha-induced cell death. *Science*. 1996;274:782-4.
- Beta C, Wyatt D, Rappel WJ, Bodenschatz E. Flow photolysis for spatiotemporal stimulation of single cells. *Analytical Chemistry*. 2007;79:3940-4.
- Bevilacqua MP, Pober JS, Wheeler ME, Cotran RS, Gimbrone Jr MA. Interleukin 1 acts on cultured human vascular endothelium to increase the adhesion of polymorphonuclear leukocytes, monocytes, and related leukocyte cell lines. *Journal of Clinical Investigation*. 1985;76:2003-11.
- Birge RR. One-photon and two-photon excitation spectroscopy. In: Kliger DS, editor. *Ultrasensitive Laser Spectroscopy*. Academic Press; New York: 1983. p. 109-74.
- Boucsein C, Nawrot M, Rotter S, Aertsen A, Heck D. Controlling synaptic input patterns in vitro by dynamic photo stimulation. *Journal of Neurophysiology*. 2005;94:2948-58.
- Bourne HR, Weiner OD. A chemical compass. *Nature*. 2002;419:21.
- Boyden S. The chemotactic effect of mixtures of antibody and antigen on polymorphonuclear leucocytes. *Journal of Experimental Medicine*. 1962;115:453-66.
- Breitman TR, Selonick SE, Collins SJ. Induction of differentiation of the human promyelocytic leukemia cell line (HL-60) by retinoic acid. *Proceedings of the National Academy of Sciences of the United States of America*. 1980;77:2936-40.
- Brody JP, Yager P, Goldstein RE, Austin RH. Biotechnology at low Reynolds numbers. *Biophysical Journal*. 1996;71:3430-41.
- Brown A. Slow axonal transport: stop and go traffic in the axon. *Nature Reviews Molecular Cell Biology*. 2000;1:153-6.
- Brown EB, Shear JB, Adams SR, Tsien RY, Webb WW. Photolysis of caged calcium in femtoliter volumes using two-photon excitation. *Biophysical Journal*. 1999;76:489-99.
- Brown MJ, Loew LM. Electric field-directed fibroblast locomotion involves cell surface molecular reorganization and is calcium independent. *Journal of Cell Biology*. 1994;127:117-28.
- Burgi DS, Chien RL. Optimization in sample stacking for high-performance capillary electrophoresis. *Analytical Chemistry*. 1991;63:2042-7.

- Burgreen D, Nakache FR. Electrokinetic Flow in Ultrafine Capillary Slits. *Journal of Physical Chemistry*. 1964;68:1084-91.
- Callaway EM, Yuste R. Stimulating neurons with light. *Current Opinion in Neurobiology*. 2002;12:587-92.
- Chen S, Springer TA. An automatic braking system that stabilizes leukocyte rolling by an increase in selectin bond number with shear. *Journal of Cell Biology*. 1999;144:185-200.
- Chen S, Sulik KK. Free radicals and ethanol-induced cytotoxicity in neural crest cells. *Alcoholism: Clinical and Experimental Research*. 1996;20:1071-6.
- Chen SY, Yang B, Jacobson K, Sulik KK. The membrane disordering effect of ethanol on neural crest cells in vitro and the protective role of GM1 ganglioside. *Alcohol*. 1996;13:589-95.
- Chichkov BN, Momma C, Nolte S, Von Alvensleben F, Tünnermann A. Femtosecond, picosecond and nanosecond laser ablation of solids. *Applied Physics A: Materials Science & Processing*. 1996;63:109-15.
- Clark P, Connolly P, Curtis AS, Dow JA, Wilkinson CD. Topographical control of cell behaviour. I. Simple step cues. *Development*. 1987;99:439-48.
- Clark P, Connolly P, Curtis AS, Dow JA, Wilkinson CD. Cell guidance by ultrafine topography in vitro. *Journal of Cell Science*. 1991;99:73-7.
- Collins SJ, Ruscetti FW, Gallagher RE, Gallo RC. Normal functional characteristics of cultured human promyelocytic leukemia cells (HL-60) after induction of differentiation by dimethylsulfoxide. *Journal of Experimental Medicine*. 1979;149:969-74.
- Contestabile A, Ciani E. Role of nitric oxide in the regulation of neuronal proliferation, survival and differentiation. *Neurochemistry International*. 2004;45:903-14.
- Costerton JW, Stewart PS, Greenberg EP. Bacterial biofilms: A common cause of persistent infections. *Science*. 1999;284:1318-22.
- Coussens LM, Werb Z. Inflammation and cancer. *Nature*. 2002;420:860-7.
- Cremers DA, Radziemski LJ. In: *Handbook of Laser-Induced Breakdown Spectroscopy*. John Wiley & Sons Ltd; London: 2006.

- Dertinger SKW, Chiu DT, Jeon NL, Whitesides GM. Generation of gradients having complex shapes using microfluidic networks. *Analytical Chemistry*. 2001;73:1240-6.
- Donaldson DD, Wongf GG, Moreau J, Stahl M, Rogers D. Inhibition of pluripotential embryonic stem cell differentiation by purified polypeptides. *Nature*. 1988;336:688-90.
- Elston TC. Probing pathways periodically. *Science Signaling*. 2008;1:47.
- Eriksson C, Nygren H. Polymorphonuclear leukocytes in coagulating whole blood recognize hydrophilic and hydrophobic titanium surfaces by different adhesion receptors and show different patterns of receptor expression. *Journal of Laboratory and Clinical Medicine*. 2001;137:296-302.
- Ewald SJ, Shao H. Ethanol increases apoptotic cell death of thymocytes in vitro. *Alcoholism: Clinical and Experimental Research*. 1993;17:359-65.
- Ferguson GJ, Milne L, Kulkarni S, Sasaki T, Walker S, Andrews S, Crabbe T, Finan P, Jones G, Jackson S. PI(3)K γ has an important context-dependent role in neutrophil chemokinesis. *Nature Cell Biology*. 2006;9:86-91.
- Foxman EF, Campbell JJ, Butcher EC. Multistep navigation and the combinatorial control of leukocyte chemotaxis. *Journal of Cell Biology*. 1997;139:1349-60.
- Foxman EF, Kunkel EJ, Butcher EC. Integrating Conflicting Chemotactic Signals. *Journal of Cell Biology*. 1999;147:577-88.
- Friedman GB, Taylor CT, Parkos CA, Colgan SP. Epithelial permeability induced by neutrophil transmigration is potentiated by hypoxia: Role of intracellular cAMP. *Journal of Cell Physiology*. 1998;176:76-84.
- Fu AY, Chou HP, Spence C, Arnold FH, Quake SR. An integrated microfabricated cell sorter. *Analytical Chemistry*. 2002;74:2451-7.
- Furuta T, Noguchi K. Controlling cellular systems with Bhc-caged compounds. *Trends in Analytical Chemistry*. 2004;23:511-9.
- Gail MH, Boone CW. The locomotion of mouse fibroblasts in tissue culture. *Biophysical Journal*. 1970;10:980-93.
- Gillitzer R, Goebeler M. Chemokines in cutaneous wound healing. *Journal of Leukocyte Biology*. 2001;69:513-21.

- Göppert-Mayer M. Elementary processes with two quantum jumps. In: *Annalen der Physik*. Berlin, Germany. 1931;9. p. 273-94.
- Gostkowski ML, Shear JB. Sub-attomole fluorescence determination of catecholamines in capillary electrophoresis effluent streams. *Journal of the American Chemical Society*. 1998;120:12966-7.
- Goulpeau J, Lonetti B, Trouchet D, Ajdari A, Tabeling P. Building up longitudinal concentration gradients in shallow microchannels. *Lab on a Chip*. 2007;7:1154-61.
- Green R, Vanapalli SA. Chips & Tips: Quick assessment of the stability of flow generated by a syringe pump in a microfluidic device. *Lab on a Chip*. 2009.
- Greenwood JC. Silicon in mechanical sensors. *Journal of Physics E: Scientific Instruments*. 1988;21:1114-28.
- Grotendorst GR, Seppä HE, Kleinman HK, Martin GR. Attachment of smooth muscle cells to collagen and their migration toward platelet-derived growth factor. *Proceedings of the National Academy of Sciences of the United States of America*. 1981;78:3669-72.
- Gwira JA, Wei F, Ishibe S, Ueland JM, Barasch J, Cantley LG. Expression of neutrophil gelatinase-associated lipocalin regulates epithelial morphogenesis in vitro. *Journal of Biological Chemistry*. 2005;280:7875-82.
- Hannah S, Mecklenburgh K, Rahman I, Bellingan GJ, Greening A, Haslett C, Chilvers ER. Hypoxia prolongs neutrophil survival in vitro. *Federation of European Biochemical Societies Letters*. 1995;372:233-7.
- Hannigan M, Zhan L, Li Z, Ai Y, Wu D, Huang CK. Neutrophils lacking phosphoinositide 3-kinase show loss of directionality during N-formyl-Met-Leu-Phe-induced chemotaxis. *Proceedings of the National Academy of Sciences of the United States of America*. 2002;99:3603-8.
- Hauert AB, Martinelli S, Marone C, Niggli V. Differentiated HL-60 cells are a valid model system for the analysis of human neutrophil migration and chemotaxis. *International Journal of Biochemistry & Cell Biology*. 2002;34:838-54.
- Haug E, Nakel W. In: *The Elementary Process of Bremsstrahlung*. World Scientific; Singapore: 2004.
- Hersen P, McClean MN, Mahadevan L, Ramanathan S. Signal processing by the HOG MAP kinase pathway. *Proceedings of the National Academy of Sciences of the United States of America*. 2008;105:7165-70.

- Hill R, Lyon J, Allen R, Stevenson K, Shear JB. Microfabrication of three-dimensional bioelectronic architectures. *Journal of the American Chemical Society*. 2005;127:10707-11.
- Ho CM, Tai YC. Micro-electro-mechanical-systems (MEMS) and fluid flows. *Annual Review of Fluid Mechanics*. 1998;30:579-612.
- Honn KV, Tang DG, Crissman JD. Platelets and cancer metastasis: a causal relationship? *Cancer Metastasis Reiew*. 1992;11:325-51.
- Ingber DE. Mechanical signaling and the cellular response to extracellular matrix in angiogenesis and cardiovascular physiology. *Circulation Research*. 2002;91:877-87.
- Ingber DE. Mechanosensation through integrins: cells act locally but think globally. *Proceedings of the National Academy of Sciences of the United States of America*. 2003;100:1472-4.
- Irimia D, Geba DA, Toner M. Universal microfluidic gradient generator. *Analytical Chemistry*. 2006;78:3472-7.
- Irimia D, Liu SY, Tharp WG, Samadani A, Toner M, Poznansky MC. Microfluidic system for measuring neutrophil migratory responses to fast switches of chemical gradients. *Lab on a Chip*. 2006;6:191-8.
- Ismagilov RF, Stroock AD, Kenis PJA, Whitesides GM, Stone HA. Experimental and theoretical scaling laws for transverse diffusive broadening in two-phase laminar flows in microchannels. *Applied Physics Letters*. 2000;76:2376-8.
- Ito H, Nomoto H, Furukawa Y, Furukawa S. Neurotrophins facilitate synthesis of choline acetyltransferase and tyrosine hydroxylase in cultured mouse neural stem cells independently of their neuronal differentiation. *Neuroscience Letters*. 2003;339:231-4.
- Jeon NL, Baskaran H, Dertinger SKW, Whitesides GM, Van de Water L, Toner M. Neutrophil chemotaxis in linear and complex gradients of interleukin-8 formed in a microfabricated device. *Nature Biotechnology*. 2002;20:826-30.
- Jeon NL, Dertinger SKW, Chiu DT, Choi IS, Stroock AD, Whitesides GM. Generation of solution and surface gradients using microfluidic systems. *Langmuir*. 2000;16:8311-6.
- Ji D, Lape R, Dani JA. Timing and location of nicotinic activity enhances or depresses hippocampal synaptic plasticity. *Neuron*. 2001;31:131-41.

- Joglekar AP, Liu H, Meyhöfer E, Mourou G, Hunt AJ. Optics at critical intensity: Applications to nanomorphing. *Proceedings of the National Academy of Sciences of the United States of America*. 2004;101:5856-61.
- Joglekar AP, Liu H, Spooner GJ, Meyhöfer E, Mourou G, Hunt AJ. A study of the deterministic character of optical damage by femtosecond laser pulses and applications to nanomachining. *Applied Physics B: Lasers and Optics*. 2003;77:25-30.
- Jones DA, Smith CW, McIntire LV. Effects of fluid shear stress on leukocyte adhesion to endothelial cells. In: Granger DN, Schmid-Schonbein GW, editors. *Physiology and Pathophysiology of Leukocyte Adhesion*. Oxford University Press; New York: 1995. p. 148–68.
- Jones GE, Prigmore E, Calvez R, Hogan C, Dunn GA, Hirsch E, Wymann MP, Ridley AJ. Requirement for PI 3-kinase γ in macrophage migration to MCP-1 and CSF-1. *Experimental Cell Research*. 2003;290:120-31.
- Kaehr B, Allen R, Javier DJ, Currie J, Shear JB. Guiding neuronal development with in situ microfabrication. *Proceedings of the National Academy of Sciences of the United States of America*. 2004;101:16104-8.
- Kaiser W, Garrett CGB. Two-Photon Excitation in CaF₂: Eu²⁺. *Physical Review Letters*. 1961;7:229-31.
- Kamholz AE, Yager P. Theoretical analysis of molecular diffusion in pressure-driven laminar flow in microfluidic channels. *Biophysical Journal*. 2001;80:155-60.
- Karten B, Hayashi H, Campenot RB, Vance DE, Vance JE. Neuronal models for studying lipid metabolism and transport. *Methods*. 2005;36:117-28.
- Kataoka M, Fukura Y, Shinohara Y, Baba Y. Analysis of mitochondrial membrane potential in the cells by microchip flow cytometry. *Electrophoresis*. 2005;26:3025-31.
- Keller HU, Niggli V. Colchicine-induced stimulation of PMN motility related to cytoskeletal changes in actin, alpha-actinin, and myosin. *Cell Motility and the Cytoskeleton*. 1993;25:10-8.
- Kenis PJA, Ismagilov RF, Whitesides GM. Microfabrication inside capillaries using multiphase laminar flow patterning. *Science*. 1999;285:83-5.
- Kim YJ, Borsig L, Varki NM, Varki A. P-selectin deficiency attenuates tumor growth and metastasis. *Proceedings of the National Academy of Sciences of the United States of America*. 1998;95:9325-30.

- Kinzer JA, Olesik JW, Olesik SV. Effect of laminar flow in capillary electrophoresis: model and experimental results on controlling analysis time and resolution with inductively coupled plasma mass spectrometry detection. *Analytical Chemistry*. 1996;68:3250-7.
- Koning AJ, Lum PY, Williams JM, Wright R. DiOC6 staining reveals organelle structure and dynamics in living yeast cells. *Cell motility and the Cytoskeleton*. 1993;25:111-28.
- Kritikou E. Chemical detectors or polarity cues? *Nature Reviews Molecular Cell Biology*. 2007;8:93.
- Kumral A, Uysal N, Tugyan K, Sonmez A, Yilmaz O, Gokmen N, Kiray M, Genc S, Duman N, Koroglu TF. Erythropoietin improves long-term spatial memory deficits and brain injury following neonatal hypoxia-ischemia in rats. *Behavioural Brain Research*. 2004;153:77-86.
- LaPlaca MC, Thibault LE. An in vitro traumatic injury model to examine the response of neurons to a hydrodynamically-induced deformation. *Annals of Biomedical Engineering*. 1997;25:665-77.
- Latour I, Gee CE, Robitaille R, Lacaille JC. Differential mechanisms of Ca^{2+} responses in glial cells evoked by exogenous and endogenous glutamate in rat hippocampus. *Hippocampus*. 2001;11:132-45.
- Leclerc E, Sakai Y, Fujii T. Cell culture in 3-dimensional microfluidic structure of PDMS (polydimethylsiloxane). *Biomedical Microdevices*. 2003;5:109-14.
- Leclerc E, Sakai Y, Fujii T. Microfluidic PDMS (polydimethylsiloxane) bioreactor for large-scale culture of hepatocytes. *Biotechnology Progress*. 2004;20:750-5.
- Lecoeur H, Melki MT, Saïdi H, Gougeon ML. Analysis of Apoptotic Pathways by Multiparametric Flow Cytometry: Application to HIV Infection. *Methods in Enzymology*. 2008;442:51-82.
- Lee SW, Yamamoto T, Noji H, Fujii T. Chemical delivery microsystem for single-molecule analysis using multilaminar continuous flow. *Enzyme and Microbial Technology*. 2006;39:519-25.
- Lee Y, Park S, Lee M, Brosilow C. PID controller tuning for desired closed-loop responses for SI/SO systems. *American Institute of Chemical Engineers Journal*. 1998;44:106-15.
- Li GC, Shiu EC, Hahn GM. Similarities in cellular inactivation by hyperthermia or by ethanol. *Radiation Research*. 1980;82:257-68.

- Lin F, Nguyen CMC, Wang SJ, Saadi W, Gross SP, Jeon NL. Effective neutrophil chemotaxis is strongly influenced by mean IL-8 concentration. *Biochemical and Biophysical Research Communications*. 2004;319:576-81.
- Lin F, Nguyen CMC, Wang SJ, Saadi W, Gross SP, Jeon NL. Neutrophil migration in opposing chemoattractant gradients using microfluidic chemotaxis devices. *Annals of Biomedical Engineering*. 2005;33:475-82.
- Lloyd AR, Oppenheim JJ. Poly's lament: the neglected role of the polymorphonuclear neutrophil in the afferent limb of the immune response. *Immunology Today*. 1992;13:169-72.
- Luyben WL. Tuning proportional-integral-derivative controllers for integrator/deadtime processes. *Industrial & Engineering Chemistry Research*. 1996;35:3480-3.
- Maheshwari G, Wells A, Griffith LG, Lauffenburger DA. Biophysical integration of effects of epidermal growth factor and fibronectin on fibroblast migration. *Biophysical Journal*. 1999;76:2814-23.
- Malech HL, Root RK, Gallin JI. Structural analysis of human neutrophil migration: Centriole, microtubule, and microfilament orientation and function during chemotaxis. *Journal of Cell Biology*. 1977;75:666-93.
- Mannion BA, Weiss J, Elsbach P. Separation of sublethal and lethal effects of the bactericidal/permeability increasing protein on *Escherichia coli*. *Journal of Clinical Investigation*. 1990;85:853-60.
- Martin P. Wound healing--Aiming for perfect skin regeneration. *Science*. 1997;276:75-81.
- Martin P, Parkhurst SM. Parallels between tissue repair and embryo morphogenesis. *Development*. 2004;131:3021-34.
- Martinez AW, Phillips ST, Whitesides GM, Carrilho E. Diagnostics for the developing world: Microfluidic paper-based analytical devices. *Analytical Chemistry*. 2010;82:3-10.
- Martinez AW, Phillips ST, Whitesides GM. Three-dimensional microfluidic devices fabricated in layered paper and tape. *Proceedings of the National Academy of Sciences of the United States of America*. 2008;105:19606-11.
- Mato JM, Konijn TM. Chemotaxis and binding of cyclic AMP in cellular slime molds. *Biochimica et Biophysica Acta-General Subjects*. 1975;385:173-9.

- Mato JM, Losada A, Nanjundiah V, Konijn TM. Signal input for a chemotactic response in the cellular slime mold *Dictyostelium discoideum*. *Proceedings of the National Academy of Sciences of the United States of America*. 1975;72:4991-3.
- Matsushima K, Morishita K, Yoshimura T, Lavu S, Kobayashi Y, Lew W, Appella E, Kung HF, Leonard EJ, Oppenheim JJ. Molecular cloning of a human monocyte-derived neutrophil chemotactic factor (MDNCF) and the induction of MDNCF mRNA by interleukin 1 and tumor necrosis factor. *Journal of Experimental Medicine*. 1988;167:1883-93.
- Matsuzaki M, Ellis-Davies GCR, Nemoto T, Miyashita Y, Iino M, Kasai H. Dendritic spine geometry is critical for AMPA receptor expression in hippocampal CA1 pyramidal neurons. *Nature Neuroscience*. 2001;4:1086-92.
- McCord JM. Oxygen-derived radicals: a link between reperfusion injury and inflammation. *Federation Proceedings*. 1987;46:2402-6.
- McCray JA, Trentham DR. Properties and uses of photoreactive caged compounds. *Annual Review of Biophysics and Biophysical Chemistry*. 1989;18:239-70.
- Mettetal JT, Muzzey D, Gomez-Uribe C, van Oudenaarden A. The frequency dependence of osmo-adaptation in *Saccharomyces cerevisiae*. *Science*. 2008;319:482-84.
- Miller C, Jeftinija S, Mallapragada S. Micropatterned Schwann cell-seeded biodegradable polymer substrates significantly enhance neurite alignment and outgrowth. *Tissue Engineering*. 2001;7:705-15.
- Millius A, Dandekar SN, Houk AR, Weiner OD. Neutrophils establish rapid and robust WAVE complex polarity in an actin-dependent fashion. *Current Biology*. 2009;19:253-9.
- Millius A, Weiner OD. Chemotaxis in neutrophil-like HL-60 cells. In: *Methods in Molecular Biology*. New Jersey: 2009;571. p. 167-77.
- Ming G, Song H, Berninger B, Holt CE, Tessier-Lavigne M, Poo M. cAMP-dependent growth cone guidance by netrin-1. *Neuron*. 1997;19:1225-35.
- Moorjani S, Nielson R, Chang XA, Shear JB. Dynamic remodeling of subcellular chemical gradients using a multi-directional flow device. *Lab on a Chip*. 2010;10:2139-46.
- Nahen K, Vogel A. Plasma Formation in Water by Picosecond and Nanosecond Nd:YAG Laser Pulses—Part II: Transmission, Scattering, and Reflection. *IEEE Journal of Selected Topics in Quantum Electronics*. 1996;2:861-71.

- Nakamura H, Herzenberg LA, Bai J, Araya S, Kondo N, Nishinaka Y, Yodoi J. Circulating thioredoxin suppresses lipopolysaccharide-induced neutrophil chemotaxis. *Proceedings of the National Academy of Sciences of the United States of America*. 2001;98:15143-8.
- Nathan C, Xie QW, Halbwachs-Mecarelli L, Jin WW. Albumin inhibits neutrophil spreading and hydrogen peroxide release by blocking the shedding of CD43 (sialophorin, leukosialin). *Journal of Cell Biology*. 1993;122:243-56.
- Nielson R, Shear JB. Parallel chemical dosing of subcellular targets. *Analytical Chemistry*. 2006;78:5987-93.
- Nishimura KY, Isseroff RR, Nuccitelli R. Human keratinocytes migrate to the negative pole in direct current electric fields comparable to those measured in mammalian wounds. *Journal of Cell Science*. 1996;109:199-207.
- Nishio M, Watanabe K, Sasaki J, Taya C, Takasuga S, Iizuka R, Balla T, Yamazaki M, Watanabe H, Itoh R. Control of cell polarity and motility by the PtdIns(3,4,5)P3 phosphatase SHIP1. *Nature Cell Biology*. 2006;9:36-44.
- Noack J, Vogel A. Laser-induced plasma formation in water at nanosecond to femtosecond time scales: calculation of thresholds, absorption coefficients, and energy density. *IEEE Journal of Quantum Electronics*. 1999;35:1156-67.
- Nossal R, Zigmond SH. Chemotropism indices for polymorphonuclear leukocytes. *Biophysical Journal*. 1976;16:1171-82.
- Oatley CW, Nixon WC, Pease RFW. Scanning electron microscopy. *Advances in Electronics and Electron Physics*. 1966;21:181-247.
- Olofsson J, Bridle H, Sinclair J, Granfeldt D, Sahlin E, Orwar O. A chemical waveform synthesizer. *Proceedings of the National Academy of Sciences of the United States of America*. 2005;102:8097-102.
- Olofsson J, Pihl J, Sinclair J, Sahlin E, Karlsson M, Orwar O. A microfluidics approach to the problem of creating separate solution environments accessible from macroscopic volumes. *Analytical Chemistry*. 2004;76:4968-76.
- Opdenakker G, Van Damme J. Cytokines and proteases in invasive processes: molecular similarities between inflammation and cancer. *Cytokine*. 1992;4:251-8.
- Petersen KE. Silicon as a mechanical material. *Proceedings of the IEEE*. 1982;70:420-57.

- Phung YT, Bekker JM, Hallmark OG, Black SM. Both neuronal NO synthase and nitric oxide are required for PC12 cell differentiation: a cGMP independent pathway. *Molecular Brain Research*. 1999;64:165-78.
- Pirrung MC, Drabik SJ, Ahamed J, Ali H. Caged chemotactic peptides. *Bioconjugate Chemistry*. 2000;11:679-81.
- Postlethwaite AE, Seyer JM, Kang AH. Chemotactic attraction of human fibroblasts to type I, II, and III collagens and collagen-derived peptides. *Proceedings of the National Academy of Sciences of the United States of America*. 1978;75:871-5.
- Rainger GE, Buckley CD, Simmons DL, Nash GB. Neutrophils sense flow-generated stress and direct their migration through $\alpha_v\beta_3$ -integrin. *American Journal of Physiology*. 1999;276:H858-64.
- Ramsey WS. Analysis of individual leucocyte behavior during chemotaxis. *Experimental Cell Research*. 1972;70:129-39.
- Ratcliffe DR, Nolin SL, Cramer EB. Neutrophil interaction with influenza-infected epithelial cells. *Blood*. 1988;72:142-9.
- Ricevuti G, Mazzone A, Pasotti D, Servi S, Specchia G. Role of granulocytes in endothelial injury in coronary heart disease in humans. *Atherosclerosis*. 1991;91:1-14.
- Rivera DE, Morari M, Skogestad S. Internal model control: PID controller design. *Industrial & Engineering Chemistry Process Design and Development*. 1986;25:252-65.
- Robinson J, Watson F, Bucknall RC, Edwards SW. Activation of neutrophil reactive-oxidant production by synovial fluid from patients with inflammatory joint disease. Soluble and insoluble immunoglobulin aggregates activate different pathways in primed and unprimed cells. *Biochemical Journal*. 1992;286:345-51.
- Roca-Cusachs P, Almendros I, Sunyer R, Gavara N, Farré R, Navajas D. Rheology of passive and adhesion-activated neutrophils probed by atomic force microscopy. *Biophysical Journal*. 2006;91:3508-18.
- Rosen G. Chemotactic transport theory for neutrophil leukocytes. *Journal of Theoretical Biology*. 1976;59:371-80.
- Saadi W, Wang SJ, Lin F, Jeon NL. A parallel-gradient microfluidic chamber for quantitative analysis of breast cancer cell chemotaxis. *Biomedical Microdevices*. 2006;8:109-18.

- Scaccini C, Jialal I. LDL modification by activated polymorphonuclear leukocytes: a cellular model of mild oxidative stress. *Free Radical Biology and Medicine*. 1994;16:49-55.
- Schaffer CB, Brodeur A, Mazur E. Laser-induced breakdown and damage in bulk transparent materials induced by tightly focused femtosecond laser pulses. *Measurement Science and Technology*. 2001;12:1784-94.
- Schaffer CB, Jamison AO, Garcia JF, Mazur E. Structural changes induced in transparent materials with ultrashort laser pulses. In: Sucha G, editor. *Ultrafast Lasers*. Marcel Dekker, Inc.; New York: 2003. p. 395-418.
- Senior RM, Griffin GL, Huang JS, Walz DA, Deuel TF. Chemotactic activity of platelet alpha granule proteins for fibroblasts. *Journal of Cell Biology*. 1983;96:382-5.
- Sepaniak MJ, Yeung ES. Laser two-photon excited fluorescence detection for high pressure liquid chromatography. *Analytical Chemistry*. 1977;49:1554-6.
- Servant G, Weiner OD, Herzmark P, Balla T, Sedat JW, Bourne HR. Polarization of chemoattractant receptor signaling during neutrophil chemotaxis. *Science*. 2000;287:1037-40.
- Seveau S, Eddy RJ, Maxfield FR, Pierini LM. Cytoskeleton-dependent membrane domain segregation during neutrophil polarization. *Molecular Biology of the Cell*. 2001;12:3550-62.
- Shear JB. Multiphoton-excited fluorescence in bioanalytical chemistry. *Analytical Chemistry*. 1999;71:598-605.
- Shen YR. In: *The Principles of Nonlinear Optics*. Wiley; New York: 1984.
- Shigeri Y, Tatsu Y, Yumoto N. Synthesis and application of caged peptides and proteins. *Pharmacology and Therapeutics*. 2001;91:85-92.
- Shirk MD, Molian PA. A review of ultrashort pulsed laser ablation of materials. *Journal of Laser Applications*. 1998;10:18-28.
- Singer AJ, Clark RAF. Cutaneous wound healing. *New England Journal of Medicine*. 1999;341:738-46.
- Smith CW, Hollers JC, Patrick RA, Hassett C. Motility and adhesiveness in human neutrophils: Effects of chemotactic factors. *Journal of Clinical Investigation*. 1979;63:221-9.

- Smith JA. Neutrophils, host defense, and inflammation: a double-edged sword. *Journal of Leukocyte Biology*. 1994;56:672-86.
- Song H, Poo M. Signal transduction underlying growth cone guidance by diffusible factors. *Current Opinion in Neurobiology*. 1999;9:355-63.
- Srinivasan S, Wang F, Glavas S, Ott A, Hofmann F, Aktories K, Kalman D, Bourne HR. Rac and Cdc42 play distinct roles in regulating PI(3,4,5)P₃ and polarity during neutrophil chemotaxis. *Journal of Cell Biology*. 2003;160:375-85.
- Stuart BC, Feit MD, Rubenchik AM, Shore BW, Perry MD. Laser-induced damage in dielectrics with nanosecond to subpicosecond pulses. *Physical Review Letters*. 1995;74:2248-51.
- Stump RF, Robinson KR. *Xenopus* neural crest cell migration in an applied electrical field. *Journal of Cell Biology*. 1983;97:1226-33.
- Suire S, Condcliffe AM, Ferguson G, Ellson CD, Guillou H, Davidson K, Welch H, Coadwell J, Turner M, Chilvers ER. G β γ s and the Ras binding domain of p110 are both important regulators of PI3K γ signalling in neutrophils. *Nature Cell Biology*. 2006;8:1303-9.
- Takayama S, McDonald JC, Ostuni E, Liang MN, Kenis PJA, Ismagilov RF, Whitesides GM. Patterning cells and their environments using multiple laminar fluid flows in capillary networks. *Proceedings of the National Academy of Sciences of the United States of America*. 1999;96:5545-8.
- Takayama S, Ostuni E, LeDuc P, Naruse K, Ingber DE, Whitesides GM. Laminar flows: Subcellular positioning of small molecules. *Nature*. 2001;411:1016.
- Takayama S, Ostuni E, LeDuc P, Naruse K, Ingber DE, Whitesides GM. Selective chemical treatment of cellular microdomains using multiple laminar streams. *Chemistry & Biology*. 2003;10:123-30.
- Takayama S, Ostuni E, Qian X, McDonald JC, Jiang X, LeDuc P, Wu MH, Ingber DE, Whitesides GM. Topographical micropatterning of poly (dimethylsiloxane) using laminar flows of liquids in capillaries. *Advanced Materials*. 2001;13:570-4.
- Thorsen T, Maerkl SJ, Quake SR. Microfluidic large-scale integration. *Science*. 2002;298:580-4.
- Tien AC, Backus S, Kapteyn H, Murnane M, Mourou G. Short-pulse laser damage in transparent materials as a function of pulse duration. *Physical Review Letters*. 1999;82:3883-6.

- Truskey GA, Yuan F, Katz DF. In: *Transport Phenomena in Biological Systems*. Pearson/Prentice Hall; New Jersey: 2003.
- Unger MA, Chou HP, Thorsen T, Scherer A, Quake SR. Monolithic microfabricated valves and pumps by multilayer soft lithography. *Science*. 2000;288:113-6.
- Van Damme J, Van Beeumen J, Opdenakker G, Billiau A. A novel, NH₂-terminal sequence-characterized human monokine possessing neutrophil chemotactic, skin-reactive, and granulocytosis-promoting activity. *Journal of Experimental Medicine*. 1988;167:1364-76.
- Van den Berg HR, Ten Seldam CA, Van der Gulik PS. Compressible laminar flow in a capillary. *Journal of Fluid Mechanics*. 2006;246:1-20.
- Vicente-Manzanares M, Sancho D, Yanez-Mo M, Sanchez-Madrid F. The leukocyte cytoskeleton in cell migration and immune interactions. *International Review of Cytology*. 2002;216:233-89.
- Visioli A. In: *Practical PID Control*. Springer-Verlag; London: 2006;1.
- Wang F, Herzmark P, Weiner OD, Srinivasan S, Servant G, Bourne HR. Lipid products of PI(3)Ks maintain persistent cell polarity and directed motility in neutrophils. *Nature Cell Biology*. 2002;4:513-18.
- Wang GX, Poo M. Requirement of TRPC channels in netrin-1-induced chemotropic turning of nerve growth cones. *Nature*. 2005;434:898-904.
- Weigl BH, Yager P. Microfluidics: microfluidic diffusion-based separation and detection. *Science*. 1999;283:346-7.
- Weiner OD. Regulation of cell polarity during eukaryotic chemotaxis: the chemotactic compass. *Current Opinion in Cell Biology*. 2002;14:196-202.
- Weiner OD, Marganski WA, Wu LF, Altschuler SJ, Kirschner MW. An actin-based wave generator organizes cell motility. *Public Library of Science Biology*. 2007;5:2053-63.
- Weiner OD, Neilsen PO, Prestwich GD, Kirschner MW, Cantley LC, Bourne HR. A PtdInsP₃-and Rho GTPase-mediated positive feedback loop regulates neutrophil polarity. *Nature Cell Biology*. 2002;4:509-13.
- Weiner OD, Servant G, Parent CA, Devreotes PN, Bourne HR. Cell polarity in response to chemoattractants. In: Drubin DG, editor. *Cell Polarity: Frontiers in Molecular Biology*. Oxford University Press; Oxford: 2000. p. 201-39.

- Weiner OD, Servant G, Welch MD, Mitchison TJ, Sedat JW, Bourne HR. Spatial control of actin polymerization during neutrophil chemotaxis. *Nature Cell Biology*. 1999;1:75-81.
- Weiss SJ. Tissue destruction by neutrophils. *New England Journal of Medicine*. 1989;320:365-76.
- Weitzman SA, Gordon LI. Inflammation and cancer: role of phagocyte-generated oxidants in carcinogenesis. *Blood*. 1990;76:655-63.
- Wells A, Kassis J, Solava J, Turner T, Lauffenburger DA. Growth factor-induced cell motility in tumor invasion. *Acta Oncologica*. 2002;41:124-30.
- Wetzel R, Becker M, Behlke J, Billwitz H, Böhm S, Ebert B, Hamann H, Krumbiegel J, Lassmann G. Temperature behaviour of human serum albumin. *European Journal of Biochemistry*. 1980;104:469-78.
- Wilkinson PC. Assays of leukocyte locomotion and chemotaxis. *Journal of Immunological Methods*. 1998;216:139-53.
- Wise K. Integrated sensors, MEMS, and microsystems: Reflections on a fantastic voyage. *Sensors and Actuators A: Physical*. 2007;136:39-50.
- Wood JG, Johnson JS, Mattioli LF, Gonzalez NC. Systemic hypoxia increases leukocyte emigration and vascular permeability in conscious rats. *Journal of Applied Physiology*. 2000;89:1561-8.
- Xu C, Zipfel W, Shear JB, Williams RM, Webb WW. Multiphoton fluorescence excitation: new spectral windows for biological nonlinear microscopy. *Proceedings of the National Academy of Sciences of the United States of America*. 1996;93:10763-8.
- Xu J, Wang F, Van Keymeulen A, Herzmark P, Straight A, Kelly K, Takuwa Y, Sugimoto N, Mitchison T, Bourne HR. Divergent signals and cytoskeletal assemblies regulate self-organizing polarity in neutrophils. *Cell*. 2003;114:201-14.
- Yang XD, Corvalan JR, Wang P, Roy CM, Davis CG. Fully human anti-interleukin-8 monoclonal antibodies: potential therapeutics for the treatment of inflammatory disease states. *Journal of Leukocyte Biology*. 1999;66:401-10.
- Yoshimura T, Matsushima K, Tanaka S, Robinson EA, Appella E, Oppenheim JJ, Leonard EJ. Purification of a human monocyte-derived neutrophil chemotactic factor that has peptide sequence similarity to other host defense cytokines.

- Proceedings of the National Academy of Sciences of the United States of America. 1987;84:9233-7.
- Zadeh AD, Keller H. Chemotactically directed redistribution of α -actinin precedes morphological polarization and reversal of polarity in human polymorphonuclear leucocytes (PMNs). *European Journal of Cell Biology*. 2003;82:93-6.
- Zernecke A, Bot I, Talab YD, Shagdarsuren E, Bidzhekov K, Meiler S, Krohn R, Schober A, Sperandio M, Soehnlein O. Protective role of CXC receptor 4/CXC ligand 12 unveils the importance of neutrophils in atherosclerosis. *Circulation Research*. 2008;102:209-17.
- Zhao M, Song B, Pu J, Wada T, Reid B, Tai G, Wang F, Guo A, Walczysko P, Gu Y. Electrical signals control wound healing through phosphatidylinositol-3-OH kinase and PTEN. *Nature*. 2006;442:457-60.
- Zhelev DV, Alteraifi A. Signaling in the motility responses of the human neutrophil. *Annals of Biomedical Engineering*. 2002;30:356-70.
- Zheng JQ, Poo M, Connor JA. Calcium and chemotropic turning of nerve growth cones. *Perspectives on Developmental Neurobiology*. 1996;4:205-13.
- Zicha D, Dunn G, Jones G. Analyzing chemotaxis using the Dunn direct-viewing chamber. *Methods in Molecular Biology*. 1997;75:449-58.
- Zicha D, Dunn GA, Brown AF. A new direct-viewing chemotaxis chamber. *Journal of Cell Science*. 1991;99:769-75.
- Zigmond SH. Orientation chamber in chemotaxis. *Methods in Enzymology*. 1988;162:65-72.
- Zigmond SH. Mechanisms of sensing chemical gradients by polymorphonuclear leukocytes. *Nature*. 1974;249:450-2.
- Zigmond SH. Ability of polymorphonuclear leukocytes to orient in gradients of chemotactic factors. *Journal of Cell Biology*. 1977;75:606-16.
- Zigmond SH. Recent quantitative studies of actin filament turnover during cell locomotion. *Cell Motility and the Cytoskeleton*. 1993;25:309-16.
- Zigmond SH, Levitsky HI, Kreel BJ. Cell polarity: an examination of its behavioral expression and its consequences for polymorphonuclear leukocyte chemotaxis. *Journal of Cell Biology*. 1981;89:585-92.

Zipfel WR, Williams RM, Webb WW. Nonlinear magic: multiphoton microscopy in the biosciences. *Nature Biotechnology*. 2003;21:1369-77.

Vita

Samira Gian Moorjani was born in Mumbai, India on May 25, 1978 to Gian and Neena Moorjani. She completed her secondary education at Bhavan's College, Mumbai in 1996, followed by a Bachelor of Engineering degree in Biomedical Engineering from Thadomal Shahani Engineering College, affiliated with the University of Mumbai (2001). In 2001, she joined the Bioengineering graduate program at Pennsylvania State University, where she earned a Master of Science (2003). In the fall of 2005, she enrolled in the Biomedical Engineering graduate program at the University of Texas at Austin.

Permanent address: A/1, No. 2, Mom Apts, Yari Road, Versova, Mumbai 400061, India

Email: samira.moorjani@gmail.com

This dissertation was typed by the author.